UNIVERSITY OF SOUTHAMPTON

FACULTY OF ENGINEERING, SCIENCE AND MATHEMATICS

School of Mathematics

Gravitational Waves from Deformed Rotating Neutron Stars

by

Brynmor Dylan Luigi Haskell

Thesis for the degree of Doctor of Philosophy

March 2007

UNIVERSITY OF SOUTHAMPTON

ABSTRACT

FACULTY OF ENGINEERING, SCIENCE AND MATHEMATICS
SCHOOL OF MATHEMATICS

Doctor of Philosophy

Gravitational Waves from Deformed Rotating Neutron Stars

by Brynmor Dylan Luigi Haskell

This thesis is devoted to studying gravitational waves from "mountains" on neutron stars. It is, in fact, well known that a non-axisymmetric deformation of a rotating neutron star will lead to a time varying quadrupole and thus to gravitational wave emission. We shall consider first of all the case of the LMXBs, as it has been suggested that the spin equilibrium period of these systems cannot be explained by accretion physics alone, but is dictated by gravitational wave emission. We present a more refined accretion model, which can explain the observations without gravitational waves. This means that, to model the gravitational wave emission of these systems, one needs a more detailed picture of the emission mechanisms at work. We, therefore, move on to discuss the "maximum mountain" that a neutron star can sustain. To do these we develop a perturbation formalism to study a star with a fluid core and an elastic crust which is gradually deformed until the crust cracks. We apply the formalism to the case of a neutron star, both with an accreted and a non accreted crust. We find that a non accreted crust can support a slightly larger mountain. Finally we consider magnetic deformations of neutron stars. It is, in fact, well known that a magnetic star cannot be spherical, and if the rotation and magnetic axis are not aligned we can, once again, have a time varying quadrupole. We consider the case of a dipolar field which is compatible with a constant density star and with an $n = 1$ polytrope; in both cases one finds that it is impossible to have a purely toroidal field, but one must always have a dipolar component. We then calculate the deformations due to the field and find that the star is oblate when the field is poloidal and becomes prolate as the toroidal component increases in strength. Having determined the deformed configuration, we then use it as a background to write the equations for a general mode of oscillation.

Contents

List of Tables

List of Figures

Acknowledgements

I would like to thank my supervisor Nils Andersson for inspiration and support during my whole PhD. I would also like to thank the whole Southampton Relativity group for all their help and for the fact that there has always been someone ready to listen to my questions and, at times, even answer them. Special thanks go to Ian Jones, Kostas Glampedakis and Lars Samuelsson. I am also grateful to all the students that have passed through the group during my stay and especially to Ian Hinder, Mina Maniopoulou, David Hilditch and Trevor Sidery for all their support, both scientific and personal.

Finally I thank my wife, Marina, for all her encouragement and patience, and my parents, for always being there for me, even though they are far away.

Introduction

Gravitational Waves are one of the most important and exciting predictions of Einstein's theory of General Relativity (GR). The idea that a perturbation of the gravitational field should propagate as a wave is, in some sense, intuitive. Let us consider the electromagnetic case. It is well known that, in electrodynamics, electromagnetic waves carry information about the dynamics of a charged system. In a similar way, when a mass-energy distribution evolves in space-time, the information about its dynamics and evolution should propagate in the form of waves. There is, however, one main difference: in the case of e.m. waves the field is a *vector* field and the waves are intrinsically *dipolar*. Within the framework of GR, on the other hand, the waves take the form of metric waves because the gravitational potential and the space-time curvature are both expressed in terms of the metric tensor $g_{\alpha\beta}$; the waves are therefore intrinsically *quadrupolar*. In fact the gravitational monopole and dipole cannot radiate because they represent conserved quantities, the total mass and momentum of the system.

Einstein himself realised that such phenomena arose from his theory and, together with Infeld and Hoffmann, studied the effects of gravitational radiation on the dynamics of a binary star system. However, the computation of the decay of the orbital period, due to the energy loss in Gravitational Waves, led Einstein to the conclusion that 'the effect is too small to be measured'. The extraordinary experimental effort carried out in recent years, however, is such that not only is the effect no longer 'too small to be measured', but there is also hope that gravitational radiation will be **directly** detected in the near future.

The first **indirect** evidence of the existence of gravitational waves has come from the measurement of the decay of the orbital period of the binary pulsar PSR B1913 + 16 by Hulse and Taylor [55]. In this system, the orbital period decays due to the loss of orbital energy and angular momentum produced by the emission of gravitational waves; this is associated to the time dependent mass-quadrupole of the system. The

observations of the orbital decay of PSR B1913 + 16, now spanning a 25-year baseline, are in agreement with the theoretical predictions of GR, within the experimental errors. Today the experimental effort is mainly devoted to the task of direct gravitational wave detection. There are two main types of detectors: resonant-mass antennas (ALLEGRO, AURIGA, EXPLORER and NAUTILUS) and ground-based interferometers (LIGO,VIRGO,GEO600,TAMA and AIGO). There is also a project, approved by the European (ESA) and American (NASA) space agencies, for a space-based interferometer (LISA). These two kinds of detectors, however, work on the same principle: when gravitational waves propagate they produce a local disturbance in the geometry of space-time, and thus a variation of the proper distance between two points on a geodesic. This is exactly the quantity that one should measure. In the case of a resonant mass detector, a periodic variation of the proper distance within the antenna can excite the normal modes of the bar; while in the case of an interferometer, the changing length of the arms can be measured by monitoring the interference pattern of a laser beam propagating in the arms themselves. Some of these detectors are now entering into the commissioning phase, while others are already collecting data of astrophysical relevance. At the moment the best strategy for data analysis seems to be that of using a theoretical model of the signal to be detected, to enable us to extract the signal itself from the detector noise (matched filtering technique). It is in this aspect that theoretical work can play a crucial role, producing as much information as possible about the signals that we can expect, and about the astrophysical sources that could produce them. The theoretical predictions may then be used, in the experimental search for gravitational waves, as the templates required for extracting the signal from the noise of the detectors with a higher signal to noise ratio.

One of the most promising sources for present, and future, detectors are gravitational waves emitted by rapidly rotating neutron stars. A particularly interesting class of these stars are found in accreting binary systems, such as the Low Mass X-ray binaries. I will describe issues relating to modelling the spin-equilibrium of neutron stars in LMXBs in chapters 3 and 4, where I shall present work published in [9]. In this work I performed most of the calculations, in collaboration with K.Glampedakis. N.Andersson produced the first draft of the paper and A.Watts helped supply the data. Chapter 2 will be devoted to describing the structure of a Neutron star, and in chapter 5 I will present some work on the maximum size of a "mountain" a Neutron star can sustain, and what implications this has on the gravitational emission of such a rotating

star, as published in [50]. In this work I performed all the calculations and produced the first draft of the paper. Finally in chapter 6 I will discuss magnetic deformations of neutron stars and in chapter 7 I will present the equations for oscillations of a deformed magnetised neutron star. Before describing my work in more detail I will however give a breif overview of the kind of gravitational wave emission one could expect from binary systems and from rotating neutron stars.

Chapter 1

Gravitational wave sources

Gravitational waves originate from energetic astrophysical events such as the coalescence of massive compact objects, gravitational collapse to form neutron stars or black holes, rotating neutron stars, etc.. Gravitational waves interact so weakly with surrounding matter that we can expect them to pass through it with substantial impunity. This differs from electromagnetic radiation, which is easily absorbed and scattered, and even from neutrinos which, although they easily penetrate ordinary matter, would scatter thousands of times while leaving, for example, the core of a supernova. These differences make it likely that the eventual observation of Gravitational Waves will create a revolution in our view of the universe, allowing us to study objects and events that would otherwise be 'invisible' to classic astronomy. We will now give a brief description of the basic concepts that are needed in the study of gravitational radiation (cfr. also [94, 151, 93, 15]).

1.1 Introduction to Gravitational Waves

The essence of the theory of General Relativity can be expressed through the Einstein Equations:

$$R_{\alpha\beta} - \frac{1}{2} g_{\alpha\beta} R = 8\pi T_{\alpha\beta} \tag{1.1}$$

that have the following meaning: any mass-energy distribution described by its stress-energy tensor $T_{\alpha\beta}$, induces a non-zero curvature of the space-time, which is described by the Ricci curvature tensor $R_{\alpha\beta}$ and the underlying (symmetric) tensor $g_{\alpha\beta}$. The motion of a free massive particle (and of null particles as well) is determined by the space-time curvature and

takes place along a geodesic of the space-time. The equation of motion of a particle moving with four-velocity U^α is:

$$\frac{dU^\alpha}{d\tau} + \Gamma^\alpha_{\beta\gamma} U^\beta U^\gamma = 0 \tag{1.2}$$

where $\Gamma^\alpha_{\beta\gamma}$ are the affine connections that are related to the metric tensor $g_{\alpha\beta}$ by the relation:

$$\Gamma^\alpha_{\beta\gamma} = \frac{1}{2} g^{\delta\alpha}(g_{\delta\beta,\gamma} + g_{\delta\gamma,\beta} - g_{\beta\gamma,\delta}), \tag{1.3}$$

Gravitational Waves can be studied both as perturbations of a given background space-time, or as exact solutions of the Einstein Equations (1.1). In the first approach the perturbation produced by the Gravitational Wave induces small variations in the gravitational field, and the corresponding metric tensor takes the form:

$$g_{\alpha\beta} = g^{(0)}_{\alpha\beta} + h_{\alpha\beta} \tag{1.4}$$

where $g^{(0)}_{\alpha\beta}$ is the unperturbed background metric tensor (for example the flat Minkowsky metric or the metric generated by a black hole or star) and $h_{\alpha\beta}$ is a small perturbation. In the following all terms which are of second (or higher) order in $h_{\alpha\beta}$ will be systematically neglected. It should be stressed, however, that, as Gravitational Waves are so weak, this approximation scheme suits a vast range of astrophysical situations. If the background metric tensor is that of flat space-time, the Einstein Equations (1.1) can be written in terms of the perturbation as:

$$\Box h_{\alpha\beta} - \left(h^\gamma_{\beta,\gamma\alpha} + h^\gamma_{\alpha,\gamma\beta} - h^\mu_{\mu,\alpha\beta}\right) = -16\pi\left(T_{\alpha\beta} - \frac{1}{2} g_{\alpha\beta} T\right) \tag{1.5}$$

where $\Box = -\partial^2/\partial t^2 + \nabla^2$ and $h = h^\alpha_\alpha$.
However the Einstein Equations do not determine the metric tensor uniquely, only up to an arbitrary coordinate transformation. This allows us to choose the gauge we want to work in. In order to simplify the equations we shall take a gauge, known as the harmonic gauge, such that:

$$h^\alpha_{\beta,\alpha} = \frac{1}{2} h^\mu_{\mu,\beta} \tag{1.6}$$

in this gauge the equations take the form:

$$\Box h_{\alpha\beta} = -16\pi\left(T_{\alpha\beta} - \frac{1}{2} g_{\alpha\beta} T\right) \tag{1.7}$$

(1.8)

or, introducing a new tensor:

$$\overline{h}_{\alpha\beta} = h_{\alpha\beta} - \frac{1}{2} g_{\alpha\beta} h, \tag{1.9}$$

we have:

$$\Box \overline{h}_{\alpha\beta} = -16\pi T_{\alpha\beta}, \quad \text{with the condition :} \quad \overline{h}^{\alpha}_{\beta,\alpha} = 0 \tag{1.10}$$

We can now solve these equations in vacuum, i.e. with $T_{\alpha\beta} = 0$. Thus, from equation (1.10) it is clear that a perturbation of a flat spacetime propagates as a wave travelling at the speed of light. The simplest solution of the wave equation (1.10) in vacuum is a monochromatic plane wave

$$\overline{h}_{\alpha\beta} = A_{\alpha\beta} e^{ik^{\gamma} x_{\gamma}} \tag{1.11}$$

where $A_{\alpha\beta}$ is called polarization tensor, and k^{γ} is the wave vector, satisfying $k^{\alpha} k_{\alpha} = 0$. The 0-component of the wave vector is identified with the frequency ω of the gravitational wave, so that we have

$$k^{\alpha} = (\omega, k^{i}) \ \text{ and, as } k^{\alpha} \text{ is a null-vector } \ \omega = \sqrt{k^{i} k_{i}} \tag{1.12}$$

If we then calculate the phase velocity of the wave we obtain

$$v_{phase} = \frac{\omega}{|\vec{k}|} = 1 \ \text{ the wave travels at the speed of light.} \tag{1.13}$$

In addition the harmonic gauge condition $\overline{h}^{\alpha}_{\beta,\alpha} = 0$ requires that the polarization tensor be orthogonal to the wave vector

$$A_{\alpha\beta} k^{\alpha} = 0 \tag{1.14}$$

that is to say that it requires Gravitational Waves to be **transverse waves**.
Not all the components of $\overline{h}_{\beta\alpha}$, or equivalently $A_{\alpha\beta}$, have a real physical meaning. This is due to the fact that the gauge has not yet been uniquely determined by the harmonic condition. We still have the freedom to make an infinitesimal coordinate transformation:

$$x'^{\alpha} = x^{\alpha} + \xi^{\alpha}(x^{\alpha}), \tag{1.15}$$

which yields for $h_{\alpha\beta}$

$$h_{\alpha\beta} \rightarrow h_{\alpha\beta} + \xi_{\alpha,\beta} + \xi_{\beta,\alpha} \tag{1.16}$$

with the condition that ξ^α satisfies the wave equation in vacuum:

$$\Box\xi_\alpha = 0 \tag{1.17}$$

We can thus choose a coordinate transformation that will outline the components of $A_{\alpha\beta}$ that have true physical meaning. We shall take

$$\xi_\alpha = b_\alpha e^{ik^\gamma x_\gamma} \tag{1.18}$$

where b_α is chosen in such a way as to impose the conditions:

$$\begin{aligned} A^\alpha_\alpha &= 0 \\ A_{\alpha 0} &= 0 \end{aligned} \tag{1.19}$$

This is known as the **Transverse Traceless** gauge, or TT-gauge. Let us assume that the wave is propagating in the z-direction and therefore

$$k^\lambda = (k, 0, 0, k) \tag{1.20}$$

this gives us

$$\begin{gathered} A_{\alpha 0} = A_{\alpha z} = 0 \quad \forall\ \alpha \\ A^\alpha_\alpha = 0 \quad \text{that is} \quad A_{xx} = -A_{yy} \end{gathered} \tag{1.21}$$

$$\begin{pmatrix} A_{11} & A_{12} & 0 \\ A_{12} & -A_{11} & 0 \\ 0 & 0 & 0 \end{pmatrix} = A_{11} \times \begin{pmatrix} 1 & 0 & 0 \\ 0 & -1 & 0 \\ 0 & 0 & 0 \end{pmatrix} + A_{12} \times \begin{pmatrix} 0 & 1 & 0 \\ 1 & 0 & 0 \\ 0 & 0 & 0 \end{pmatrix} \tag{1.22}$$

It follows that a gravitational plane wave propagating along the z-axis is described by two functions h_{xx} and h_{xy}, while the remaining components can be set equal to zero by a suitable choice of the gauge. Thus a Gravitational Wave has only two degrees of freedom, which correspond to its two independent states of polarization, usually indicated as $h_{ii} = h_+$ and $h_{ij} = h_\times$ where i and j are spacial indexes that vary in the plane orthogonal to the direction of propagation.

1.2 Observable effects of gravitational waves

The study of the motion of a single particle does not provide any information about the passage of a gravitational wave. In fact if we consider the metric tensor:

$$g_{\alpha\beta} = g^{(0)}_{\alpha\beta} + h_{\alpha\beta} \tag{1.23}$$

and write out the Christoffel symbols up to the first order in h, we obtain:

$$\Gamma^{\alpha}_{\beta\gamma} = \frac{1}{2} g^{\delta\alpha}_{(0)} (h_{\delta\beta,\gamma} + h_{\delta\gamma,\beta} - h_{\beta\gamma,\delta}), \tag{1.24}$$

let us now insert this expression into the equations of motion (1.2) for a particle initially at rest, i.e. with initial four-velocity $U^{\alpha} = \delta^{\alpha}_{0}$ (this implies no loss of generality, for we can always construct the rest-frame of a massive particle close to the particle itself). The equation of motion therefore becomes:

$$\left(\frac{dU^{\alpha}}{d\tau}\right)_{t=0} = -\Gamma^{\alpha}_{00} = -\frac{1}{2} g^{\alpha\beta}_{(0)} \left(h_{\beta 0,0} + h_{0\beta,0} + h_{00,\beta}\right) = 0, \tag{1.25}$$

where the last equality is due to the properties of $h_{\alpha\beta}$ in the TT-gauge, as previously discussed.
Therefore a particle which is initially at rest remains at rest, even if a gravitational wave is incident on it. This is due to the fact that the position of the particle does not change with respect to our coordinate system. However this does not imply that there is no physical effect at all. To see this effect let us consider two nearby particles, one located at the origin of our reference frame, the other at a certain position x_0 on the x-axis, and both initially at rest. If there is some incident gravitational radiation, the two particles, in view of our previous discussion, will remain at their initial coordinate positions. Accordingly, the coordinate distance between the two will not change, and remain fixed at x_0. However the proper (physical) distance between the two particles, as measured by a meter stick or by radar ranging, also depends on the metric. The proper distance between the two particles is:

$$\Delta l = \int \mid g_{\alpha\beta} dx^{\alpha} dx^{\beta} \mid^{1/2} = \int_0^{x_0} \mid 1 + h^{TT}_{xx} \mid^{1/2} \simeq x_0 + \frac{1}{2} \int_0^{x_0} h^{TT}_{xx} dx \tag{1.26}$$

Thus the proper distance depends on the perturbations of the metric and, if one has, for instance, an incident monochromatic plane wave, it actually oscillates at the frequency of the incoming gravitational wave with an amplitude that is proportional to that of the wave itself.
We can outline this effect even better if we examine the equations of geodesic deviation:

$$\frac{d^2 \xi^{\alpha}}{d\tau^2} = R^{\alpha}_{\mu\beta\nu} \frac{dx^{\beta}}{d\tau} \frac{dx^{\mu}}{d\tau} \xi^{\nu} \tag{1.27}$$

where ξ^{ν} is the distance between the two geodesics. In our case the two test masses are initially at rest and $\frac{dx^{\mu}}{d\tau} = \delta^{\mu}_{\tau}$, while the Riemann tensor

becomes:

$$R^i_{0k0} = \frac{1}{2} h^k_{i,00} = \frac{1}{2} \ddot{h}^k_i \tag{1.28}$$

thus the equation reads:

$$\ddot{\xi}^i = -R^i_{0k0} \xi^k \rightarrow \frac{1}{2} \ddot{h}^i_k \xi^k \tag{1.29}$$

Let us assume that the displacement is small when compared to the initial separation (as is the case with a gravitational wave). This allows us to write:

$$\xi^i = \xi^i_0 + \delta\xi^i \tag{1.30}$$

and the equations become:

$$\ddot{\xi}^i = -\frac{1}{2} \ddot{h}^i_k \left(\xi^k_0 + \delta\xi^k\right) \tag{1.31}$$

or, neglecting orders of $\ddot{h}\delta\xi$,

$$\ddot{\xi}^i = -\frac{1}{2} \ddot{h}^i_k \xi^k_0 \text{ from which } \frac{\delta\xi}{\xi} \simeq h \tag{1.32}$$

We can easily see that the displacement is proportional to the original distance (hence, as we shall see, the length of the arms in the interferometer experiments) and to the amplitude of the wave, and it also oscillates with the same frequency of the wave.

1.2.1 Resonant antennas

The experimental search for gravitational waves began in the early sixties with Joseph Weber, who invented the so-called resonant-mass antennas or bar detectors. The basic concept of gravitational wave detection by a resonant-mass antenna is that expressed by the equation of geodesic deviation. The effect of an incident gravitational wave is to alter the proper distance between two masses with an amplitude proportional to the amplitude of the wave and with the same frequency as the wave. We can, therefore, attempt to amplify this effect by constructing a massive body whose vibration frequencies are very close to the expected frequency of the wave. Let us consider a toy model: two masses connected by a spring. The equation of geodesic deviation becomes:

$$\delta\ddot{\xi}^i = -\frac{1}{2} \ddot{h}^i_k \xi^k_0 - \omega_0^2 \delta\xi^i \tag{1.33}$$

where the frequency ω_0^i is that given by the spring or, in our model, that of the eigen-mode we are considering. From equation (1.33), for a wave of frequency ω, we obtain:

$$\delta\xi^i = \frac{\omega^2 h_k^i \xi_0^k}{2(\omega_0^2 - \omega^2)} \tag{1.34}$$

It is therefore obvious that the normal mode of oscillation will be efficiently excited only by those components of the waves which have a frequency within a narrow band near ω_0. This is why resonant-mass detectors possess good sensitivity around the frequencies of their normal modes but have narrow bandwidths. The vibrations of the resonant-mass have to be amplified and converted (with the aid of a transducer) into electrical signals. The antenna is equipped with a resonant transducer (i.e. a light mass oscillator mechanically coupled to the antenna and electrically coupled to a low noise amplifier) which monitors the amplitude of one, or more, of the antenna's normal modes of oscillation. Obviously, given the small effect, it is necessary to cryogenically cool the bar to a very low temperature (to reduce thermal noise) and to isolate the mass with a series of suspensions (to reduce seismic noise, both natural and man-made). There are five resonant antennas which are currently in operation. They constitute the core of the IGEC, the International Gravitational Event Collaboration, whose main goal is to produce a common analysis of the available data and to make full use of all these detectors to perform coincidence analysis, thus reducing the number of false detections. The antennas currently in operation are ALLEGRO, at Lousiana State University, in Baton Rouge, Lousiana, USA; AURIGA, at the Laboratori Nazionali di Legnaro in Italy; NAUTILUS at the Laboratori Nazionali di Frascati in Italy and EXPLORER at CERN in Geneva, Switzerland, which are operated by the Rome group. A sample sensitivity curve of NAUTILUS is shown in figure 1.1.

1.2.2 Interferometers

Interferometric detectors are based on the concept of Michelson and Morley's interferometer which consists of two arms typically arranged in an L-shaped pattern (with a 90^0 angle between the two). In some detectors, such as VIRGO, at the end of each arm there are two mirrors facing each other to form a Fabry-Perot cavity which traps the laser light for a long period of time and increases the detector sensitivity. The effect of a gravitational wave on the interferometer is that of changing the proper distance between the test masses (the mirrors). It can be shown that

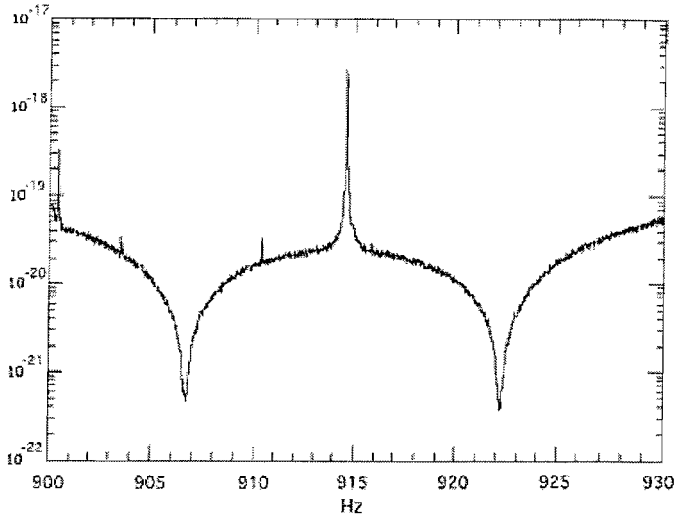

Figure 1.1: Noise spectral amlitude in units of $Hz^{-1/2}$ for Nautilus, the sensitivity at the two resonances is approximately 4 X 10^{-22} $Hz^{-1/2}$. From [12].

if a gravitational wave impinges orthogonally on the interferometer one of the arms is stretched while the other shrinks due to the fact that the radiation is quadrupolar. The changing arm length can be observed by monitoring the relative phase of two laser beams propagating in the arms (i.e. monitoring the interference pattern). As we have previously observed

$$\frac{\delta L}{L} \simeq h \tag{1.35}$$

When one examines the performance of laser interferometry, one sees good prospects of achieving measurement accuracies of $\delta L \approx 10^{-16} \frac{cm}{\sqrt{Hz}}$. Working with such levels of accuracy, an interferometer must have an arm length $L = \frac{\delta L}{h} \approx 1 - 10km$ in order to detect a gravitational wave with an amplitude of $10^{-21} - 10^{-22}$, which is the typical amplitude expected on Earth from the most promising sources. The principle advantage of interferometers is that they are broad-band detectors and thus are sensitive to a greater part of the complete wave form, not only to a limited number of Fourier components, as is the case with bar-detectors. We can expect interferometers to be sensitive to sources emitting gravitational radiation in the frequency range from 10 Hz to several kHz. The sensitivity of ground-based interferometers is limited by a number of noise sources. The most important source of noise are natural or 'culturally induced' seismic waves; this is why the test masses are held in vacuum

and must be isolated using a series of suspensions. At low frequencies, however, seismic noise imposes the limit for detector sensitivity. Above several tens of Hz thermal noise begins to be the dominant source of noise, while in the high frequency band (i.e. above 200 Hz) the sensitivity is limited by photon shot noise (due to fluctuations in the number of photons in the input laser beam).
There are several laser interferometric detectors currently taking data or coming online. A 300 m detector, TAMA, in Tokyo, Japan, and a 600 m British-German interferometer GEO600 in Hannover, Germany, have been taking data for some time now and the two 4km LIGO antennas in Livingston, Louisiana and Hanford, Washington, have now reached design sensitivity, as can be seen in figure 1.2, and are in the process of collecting a one year stretch of data. The French-Italian 3 km antenna, VIRGO, is currently in the commissioning phase. A last interfermoetric antenna, AIGO, is currently under construction in Australia.

Finally, there are plans for a space based interferometric antenna, LISA, which is expected to launch in 2015. LISA will consist of three spacecraft equipped with lasers, freely flying five million kilometers apart in an equilateral triangle. This gives rise to three independent interferometers which, thanks to the large arm length and to the removal of all earth based interference, will allow us to probe the frequency range between 10^{-4} Hz and $1Hz$, thus being complementary to the earth based interferometers.

1.3 Gravitational waves from binary systems: The quadrupole approach

As electromagnetic radiation can be generated by the acceleration of charges, gravitational waves arise from the acceleration of masses. There is, however, a fundamental difference between the two types of radiation. At the lowest order electromagnetic radiation is *dipolar*, while gravitational radiation is *quadrupolar*. Let us then examine the electromagnetic analogy in detail. Let us take two sources s of the field (two charges in the electromagnetic case, two masses in the gravitational one) at a distance d from each other. If the wave-length is such that $\lambda \gg d$, we can expand in multipoles of $\frac{d}{\lambda}$. In electromagnetism we can define the "electric" dipole:

$$\vec{p}_{em} = \sum_a d_a e_a \text{ where } e \text{ is the charge} \tag{1.36}$$

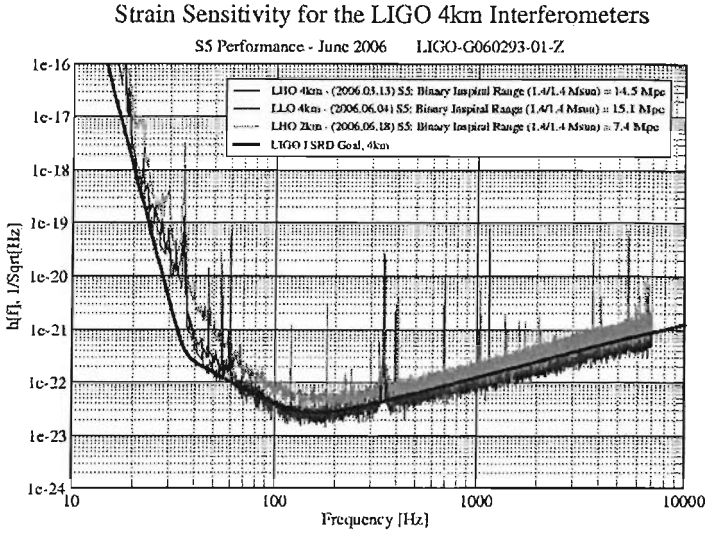

Figure 1.2: The sensitivity curve for the current S5 run, both for the Livingston (LLO) and Hanford (LHO) interferometers, compared to the science goal. From the LIGO Laboratory http://www.ligo.caltech.edu/ jzweizig/distribution/LSC_Data/

and the "magnetic" dipole:

$$\vec{\mu_{em}} = \sum_a e_a \vec{d_a} \wedge \dot{\vec{d}}_a \tag{1.37}$$

By analogy we can extend these definitions to the gravitational case and have a gravitational "electric" dipole:

$$\vec{p}_G = \sum_a d_a m_a \text{where } m \text{ is the mass} \tag{1.38}$$

and a gravitational "magnetic" dipole:

$$\vec{\mu_G} = \sum_a m_a \vec{d_a} \wedge \dot{\vec{d}}_a \tag{1.39}$$

If we examine the radiation emitted by the system at the lowest order we have that:

$$\frac{\partial E}{\partial t} \propto \ddot{\vec{p}} \tag{1.40}$$

In the electromagnetic case, therefore, there is a dipolar emission due to the accelerated motion of the charges; in the gravitational case, on the

other hand:

$$\dot{\vec{p_G}} = \sum_a m_a \dot{d} = \vec{I} \text{ the conserved momentum of the system} \qquad (1.41)$$

there is, therefore, no emission. Similarly, for the magnetic dipole:

$$\dot{\vec{\mu_G}} = \sum_a m_a \vec{d_a} \wedge \dot{\vec{d_a}} = \vec{L} \text{ the angular momentum} \qquad (1.42)$$

Due to angular momentum conservation one has:

$$\ddot{\vec{\mu}} = \ddot{\vec{L}} = 0 \qquad (1.43)$$

In order to obtain gravitational wave emission one has to define the quadrupole:

$$Q^{ik} = \sum_a m_a (d_a^i d_a^k - \frac{1}{3}\delta^{ik} d^2) \qquad (1.44)$$

As we shall see the gravitational wave luminosity is:

$$L_G = \frac{1}{5} \langle \dddot{Q}^{ik} \dddot{Q}_{ik} \rangle \qquad (1.45)$$

The object we have defined in (1.44) is actually the traceless Inertia tensor. This implies that if one has a spherically symmetric perturbation, such as a radial pulsation, this would only modify the trace of the Inertia tensor and:

$$\dddot{Q}^{ik} = 0 \qquad (1.46)$$

However, if the perturbation is non-radial, one can have

$$\dddot{Q}^{ik} \neq 0 \qquad (1.47)$$

There is, therefore, an emission of gravitational waves linked to the time-variation of the quadrupole. There are various methods of calculating the gravitational emission of a binary system. All these methods are, however, based on numerical simulations or on approximation schemes as there is, at the moment, no exact solution to the two body problem in General Relativity. The simplest method is the lowest-order post-Newtonian approximation, known as the quadrupole-formula.
If one solves Einstein's wave equation (1.10) in the case of a source contained in a volume V and for which one can apply the slow-motion weak-field approximation, one obtains a solution of the kind:

$$\begin{cases} \overline{h}^{\mu 0} = 0, \quad \mu = 0, 3 \\ \overline{h}^{ik} = \frac{2}{r} e^{i\omega r} \left[\frac{d^2}{dt^2} q^{ik}(t) \right] \end{cases} \qquad (1.48)$$

where

$$q^{ik}(t) = \int_V T^{00}(t, x^n) x^i x^k dx^3 \tag{1.49}$$

that is we have defined the quadrupole tensor without removing its trace. We now need to pass to the TT-gauge with an infinitesimal coordinate transformation $x'^{\mu} = x^{\mu} + \epsilon^{\mu}$ that does not spoil the harmonic gauge and satisfies the conditions (1.19). If we take a system in the xy plane, in the TT-gauge the wave emitted in the z direction is:

$$\begin{cases} h^{TT}_{\mu 0} = 0, \qquad h^{TT}_{zi} = 0, \\ h^{TT}_{xx} = -h^{TT}_{yy} = \frac{1}{r} e^{i\omega r} \frac{d^2}{dt^2}(Q_{xx} - Q_{yy}), \\ h^{TT}_{xy} = -\frac{2}{r} e^{i\omega r} \frac{d^2}{dt^2} Q_{xy} \end{cases} \tag{1.50}$$

Where Q_{ij} is now the traceless tensor we had previously defined:

$$Q_{ij}(t) = q_{ij} - \frac{1}{3}\delta_{ij} q^k_k \tag{1.51}$$

The energy that flows through a surface perpendicular to the z axis, per unit of time, is:

$$\frac{dE_{GW}}{dt dS} = t^{0z} = \frac{1}{16\pi}\left[\mid \frac{d}{dt} h^{TT}_{xx} \mid^2 + \mid \frac{d}{dt} h^{TT}_{xy} \mid^2 \right] \tag{1.52}$$

To obtain the luminosity one must integrate over the surface and average over the polarizations, thus obtaining:

$$\begin{aligned} L_{GW} &= \frac{1}{5}\left[\mid \frac{d}{dt} h^{TT}_{xx} \mid^2 + \mid \frac{d}{dt} h^{TT}_{xy} \mid^2 \right] \\ &= \frac{1}{5}\left[\dddot{Q}^{ij} \dddot{Q}_{ij} \right] \end{aligned} \tag{1.53}$$

Let us restrict our attention to a binary system of two point masses m_1 and m_2 ($m_1 + m_2 = M$), on a circular orbit of diameter R; for this system we can write the Newtonian equations of motion:

$$\begin{cases} x_1 = \frac{Rm_2}{M} \cos \omega t \\ y_1 = \frac{Rm_2}{M} \sin \omega t \end{cases} \qquad \begin{cases} x_2 = -\frac{Rm_1}{M} \cos \omega t \\ y_2 = -\frac{Rm_1}{M} \sin \omega t \end{cases} \tag{1.54}$$

$$\omega^2 = \frac{M}{R^3} \tag{1.55}$$

$$T^{00} = \sum_{n=1}^{2} m_n \delta(x - x_n)\delta(y - y_n)\delta(z) \tag{1.56}$$

We can therefore compute the components of the quadrupole tensor:

$$\begin{cases} q_{xx} = \mu R^2 \cos^2 \omega t = \frac{1}{2}\mu R^2 \cos 2\omega t + \text{constant}, \\ q_{yy} = \mu R^2 \sin^2 \omega t = -\frac{1}{2}\mu R^2 \cos 2\omega t + \text{constant}, \\ q_{xy} = q_{yx} = \mu R^2 \cos \omega t \sin \omega t = \frac{1}{2}\mu R^2 \sin 2\omega t, \end{cases} \tag{1.57}$$

where μ is the reduced mass $\mu = m_1 m_2 / M$.
The variable part of Q_{ij} is thus:

$$\begin{aligned} Q_{xx} &= -Q_{yy} = \tfrac{R^2}{2}\mu \, \Re(e^{2i\omega(r-t)}) \\ Q_{xy} &= \tfrac{R^2}{2}\mu \, \Im(e^{2i\omega(r-t)}) \end{aligned} \tag{1.58}$$

The radiation is clearly emitted at twice the orbital frequency; therefore, by substituting Q_{ij} in equation (1.50), one obtains, for a wave propagating in the z direction from a source at a distance r:

$$h_{xx}^{TT} = -h_{yy}^{TT} = -\frac{2R^2}{r}\mu(2\omega)^2 \, \Re(e^{2i\omega(r-t)}) \tag{1.59}$$

$$h_{xy}^{TT} = -\frac{2R^2}{r}\mu(2\omega)^2 \, \Im(e^{2i\omega(r-t)}) \tag{1.60}$$

In conclusion:

- The frequency of the gravitational wave is **twice** the orbital frequency
- The radiation is emitted with both polarizations
- Seen as $h_{xx}^{TT} = i\, h_{yy}^{TT}$, it possesses a circular polarization.

The luminosity in gravitational waves (1.53) in this case becomes:

$$L = \frac{32}{5}\frac{M^3\mu^2}{R^5} \tag{1.61}$$

this is for a circular orbit, in the case of an elliptical orbit the Newtonian equations of motion yield, for the stellar separation:

$$R = \frac{a(1 - e^2)}{1 + e\cos(\omega t)} \tag{1.62}$$

where a is the major semi-axis and e is the eccentricity of the orbit. The orbital frequency is given by:

$$\omega = \frac{[Ma(1-e^2)]^{1/2}}{R^2} \tag{1.63}$$

From which, after averaging over a period of the elliptical motion, one finds for the luminosity:

$$< L >= \frac{32}{5} \frac{M^3\mu^2}{a^5(1-e^2)^{7/2}} \left(1 + \frac{73}{24}e^2 + \frac{37}{96}e^4\right) \tag{1.64}$$

As we can see, the radiated power depends strongly on the eccentricity and the orbital separation. The radiated power increases along with increasing accelerations; the two bodies will, thus, radiate the most at their closest point of approach and, for a fixed orbital energy, for a higher value of the eccentricity. Since the emission of gravitational waves continuously carries away energy and angular momentum from the system, the two orbiting masses spiral towards each other, thus increasing their orbital frequency (and consequently that of the wave) and decreasing their orbital period T. Let us concentrate on the circular-orbit case. This is in fact not very restrictive, as in the last stage of coalescence radiation reaction has already circularised the orbits. The total energy of the system is:

$$E = \left(\frac{1}{2}m_1 d_1^2 + \frac{1}{2}m_2 d_2^2\right)\omega^2 - \frac{m_1 m_2}{R} = -\frac{1}{2}\frac{\mu M}{R} \tag{1.65}$$

or, if we substitute the value of ω obtained from Kepler's law $\omega^2 = \frac{M}{R^3}$, and the equations of motion in the centre of mass frame

$$\begin{cases} d_1 = \frac{m_2}{M}R \\ \\ d_2 = \frac{m_1}{M}R \end{cases} \tag{1.66}$$

one obtains:

$$E = -\frac{\mu M^{2/3}\omega^{2/3}}{2} \tag{1.67}$$

If we now take the logarithm and derive with respect to time

$$(\ln E)_{,t} = -(\frac{2}{3}\ln\omega + \text{const})_{,t} \tag{1.68}$$

from which:

$$\frac{1}{E}\frac{dE}{dt} = -\frac{2}{3}\frac{1}{\omega}\frac{d\omega}{dt} = \frac{2}{3}\frac{1}{T}\frac{dT}{dt} \tag{1.69}$$

where T is the orbital period.
If we now assume that the system's only loss of energy is that due to the emission of gravitational waves, we find:

$$\frac{dE}{dt} = -L_{GW} \tag{1.70}$$

and therefore:

$$\frac{1}{T}\frac{dT}{dt} = -\frac{3}{2}\frac{1}{E}L_{GW} = -\frac{96}{5}\frac{\mu M^2}{R^4} \tag{1.71}$$

In the case of the binary pulsar PSR B1913 + 16 (Hulse and Taylor [55]) the variation of the orbital period has been measured with great accuracy. The prediction based on General Relativity (taking into account the eccentricity of the orbit $e \simeq 0.617$ and other orbital parameters that have been measured) is $\dot{T}_{th} = -2.4 \cdot 10^{-12}$, while the value measured by Hulse and Taylor is $\dot{T}_{obs} = -(2.3 \pm 0.22) \cdot 10^{-12}$, thus confirming the theoretical prediction within the experimental errors. This was the first indirect evidence of the existence of gravitational waves. Today many more such measurements have been carried out, most spectacularly of all on the double pulsar PSR J0737-3039 in which both components are visible as pulsars, thus allowing us to test general relativity to an unprecedented level of precision [69].

1.3.1 Time evolution

As we have seen, the system loses energy due to the emission of gravitational waves:

$$L_{GW} = -\frac{dE}{dt} \tag{1.72}$$

This leads to an increase of the orbital frequency and a decrease in the orbital period. Let us make a rough estimate of how the orbit evolves in time. If we once again take a system of two masses m_1 and m_2 on a circular orbit at a distance R we have:

$$E = -\frac{1}{2}\frac{\mu M}{R} \tag{1.73}$$

$$\frac{1}{E}\frac{dE}{dt} = -\frac{1}{R}\frac{dR}{dt} \tag{1.74}$$

and therefore from equation (1.72):

$$\frac{dE}{dt} = -L_{GW} = \frac{32}{5}\frac{M^3\mu^2}{R^5} \tag{1.75}$$

for the separation between the two stars we have:

$$\frac{1}{R}\frac{dR}{dt} = -\frac{2R}{\mu M}\frac{32}{5}\frac{M^3\mu^2}{R^5} \tag{1.76}$$

$$\frac{dR}{dt} = -\frac{64}{5}\frac{M^2}{R^3}\mu \tag{1.77}$$

This is, therefore, a differential equation for the temporal evolution of R. If we assume that at $t = 0$ the initial radius is R_0, we find:

$$R(t) = R_0\left[1 - \frac{t}{t_{coal}}\right]^{1/4} \tag{1.78}$$

where we assume t_{coal} to be the coalescence time, i.e the time at which the orbital separation would reduce to 0 (we must remember that in this approach the two stars are considered to be point-like)

$$t_{coal} = \frac{5}{256}\frac{R_0^4}{M^2\mu} \tag{1.79}$$

As the orbital separation decreases, so does the orbital period and consequently that of the gravitational wave, leading to an increase of the frequency:

$$\Omega = \sqrt{\frac{M}{R^3}} = \Omega_0\left[1 - \frac{t}{t_{coal}}\right]^{-3/8} \tag{1.80}$$

Also the amplitude of the gravitational wave varies with R, we can easily estimate the trend if we consider the relation

$$L_{GW} \propto |\, A_{GW}\,|^2 |\,\Omega\,|^2 \tag{1.81}$$

and from the expression for L_{GW} one obtains that:

$$A_{GW} = A_0\left[1 - \frac{t}{t_{coal}}\right]^{-2/8} \tag{1.82}$$

This behaviour of the signal, notably the increase of the frequency and of the amplitude, is typical of the coalescence of binary systems and is known as a chirp.

1.4 Gravitational waves from rotating neutron stars

There are various mechanisms by which a rotating neutron star could emit gravitational waves, and some of them will be presented in chapter

3. The most simple, which can be studied in the quadrupole approach, is however that of a small 'mountain' forming on the star. In fact as soon as a neutron star cools roughly below $10^{10}K$ its outer layers will begin to crystallize and form a crust. The crust can now sustain shear stresses and could therefore sustain a mountain. If the star is rotating, this would lead to a time varying quadrupole and thus a gravitational wave emission at twice the spin frequency. Let us then consider a neutron star spinning around the z-axis. We shall assume that the star has principal moments of inertia I_x,I_y and I_z. If there is a small asymmetry we will have $I_x \neq I_y$ and the star will radiate gravitationally. In order to calculate the emission in the inertial frame we first need to translate the moments of inertia to this frame from the rotating frame of the star. If we define $\phi = \omega t$ where ω is the angular velocity of the star, the rotation matrix is

$$R = \begin{pmatrix} \cos\phi & \sin\phi & 0 \\ -\sin\phi & \cos\phi & 0 \\ 0 & 0 & 1 \end{pmatrix} \tag{1.83}$$

and therefore

$$I_{inertial} = R^T I_{body} R \tag{1.84}$$

Explicitly we find (in the inertial frame) that:

$$I_{xx} = -I_{yy} = \frac{1}{2}(I_x - I_y)\cos 2\phi \tag{1.85}$$

$$I_{xy} = I_{yx} = \frac{1}{2}(I_x - I_y)\sin 2\phi \tag{1.86}$$

where we have omitted all constant contributions, as we will have to take derivatives in the following. We also have that

$$I_j^j = I_x + I_y + I_z = constant \tag{1.87}$$

The difference between the moment of inertia and the reduced quadrupole moment is thus a constant, and we can use our expression in the quadrupole formula. This gives us:

$$\frac{dE}{dt} = \frac{G}{5c^5}\langle \dddot{I}_{xx}^2 + 2\dddot{I}_{xy}^2 + \dddot{I}_{yy}^2 \rangle = \frac{32G}{5c^5}(I_x - I_y)^2\omega^6 \tag{1.88}$$

Let us now assume that the star is a homogeneous ellipsoid with semiaxes a,b and c. Then

$$I_x = \frac{1}{5}M(b^2 + c^2) \qquad I_y = \frac{1}{5}M(a^2 + c^2) \qquad I_z = \frac{1}{5}M(a^2 + b^2) \tag{1.89}$$

If we assume that the difference between a and b is small we can write

$$I_x - I_y = \frac{2\epsilon M(a+b)^2}{5} \approx \frac{2\epsilon MR^2}{5} = \epsilon I_0 \tag{1.90}$$

where $\epsilon = \frac{b-a}{2(a+b)}$ and $I_0 = 2MR^2/5$ is the moment of inertia of a uniform density sphere. In this approximation the gravitational wave luminosity is

$$\frac{dE}{dt} \approx \frac{32G}{5c^5}\epsilon^2 I_0^2 \omega^6 \tag{1.91}$$

We can at this point try to constrain the size of the mountains, i.e. the ellipticity, by comparing with observations. For example, if we assume that the spin down of the Crab pulsar is uniquely due to gravitational waves, we can compare the observed value to the predicted one. We have that

$$\frac{\dot{P}}{P} = -\frac{\dot{E}}{2E} = -\frac{32G}{5c^5}\epsilon^2 I_0 \omega^4 \tag{1.92}$$

where we have assumed that $E = I_0\omega^2/2$. If we now evaluate this for the Crab pulsar, i.e. we use $P = 33ms$, $M = 1.4M_\odot$ and $R = 10km$, we find that

$$\dot{P}_{GW} \approx -8 \times 10^{-7}\epsilon^2 \quad \text{while} \quad \dot{P}_{obs} \approx -4.2 \times 10^{-13} \tag{1.93}$$

This means we would need to have $\epsilon \approx 7 \times 10^{-4}$ to explain the observation.This mountain would be unrealistically large as the physical upper limits, based on the deformation that the crust could actually sustain and derived in chapter 5 of this thesis, are closer to $\epsilon \approx \times 10^{-6}$.

Chapter 2

Neutron Star Physics

In this chapter I review briefly some of the main elements of neutron star physics, including how to build equilibrium models and details of the structure which will be needed for the subsequent developments. More details can be found in many books, for example [94] and [125].

2.1 What is a Neutron star?

A neutron star is the collapsed core of a massive star, which has reached the point where it has a radius of $\approx$ 10 km, a mass of $\approx 1.4 M_\odot$ with internal densities of about 10^{14}g/cm^3 (approximately nuclear density) and strong magnetic fields (up to $\approx 10^{15}$G). The typical way of picturing this is thinking of an object of the mass of the sun, the size of Chicago, and which could possibly be spinning 100 times a second. It is then quite natural to ask how such extreme objects could form, and how can we be sure they exist at all? We will attempt to answer the second question first. The existence of Neutron stars had been postulated by Baade and Zwicky in 1934, shortly after the discovery of the neutron. However they remained just a possibility until 1967 when Jocelyn Bell and her supervisor Antony Hewish observed the first radio pulsar. A number of pulsars were discovered shortly after, and it soon became clear that the regular pulsed signals were in fact the signature of rapidly rotating neutron stars. If a source varies over some time t, then its size must be less then the distance that light can travel in that time, ct, or the variation would be happening faster than the speed of light. If we then take the period of Bell's pulsar, 0.033 seconds, we obtain that the object must be less than 10,000 km in size. This allows only white dwarfs, neutron stars and black hole (and possibly some more exotic candidate). White dwarfs

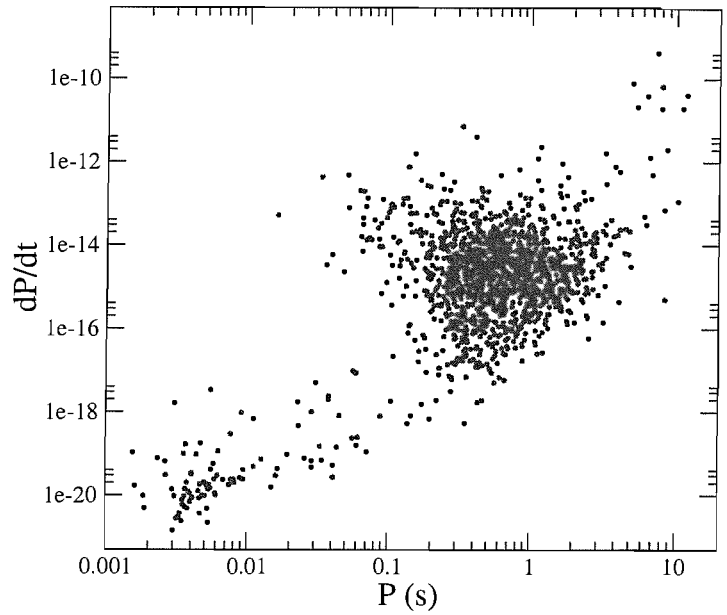

Figure 2.1: A plot of period versus period derivative for spinning down pulsar, from [76]. Downloaded from the ATNF pulsar catalogue http://www.atnf.csiro.au/research/pulsar/psrcat/.

are large enough that their maximum pulsational, rotational or orbital frequencies are more than a second, so they can be ruled out. Black holes on the other hand have no surface on which to attach a beacon, so this leaves us either with a rotating neutron star, or a black hole-neutron star binary. In the case of a binary the system would emit gravitational waves, the two stars would spiral in toward each other and we would observe the period decreasing. But pulsars are observed to **spin down** (except for some very notable exceptions which shall be discussed later), so the period must increase. This leaves us with the standard picture of a radio pulsar being a rotating neutron star spinning down due to magneto-dipole radiation. Today, as we can see from figure 2.1, more than 1500 pulsars have been discovered, leading to even more refined observations of these objects in this strong gravity environment.

2.1.1 Evolution

Let us now try to answer the first question: How are neutron stars born? Neutron stars are believed to form in the explosion of supernovae. Although the picture is not completely clear, the basic concept is that when the central part of the star fuses its way down to iron (Fe^{56}) it cannot

go any farther, as at low densities this is the most energetically favored state, so an Iron core begins to accumulate. As the pressure gets higher the electrons begin to form a Fermi gas and at pressures of $\approx 10^5$ g/cm^3 electron degeneracy pressure dominates and the compressibility index Γ defined as

$$\Gamma = \frac{\rho c^2 + p}{p} \frac{dp}{d\rho c^2} \tag{2.1}$$

is 5/3, the value for a non relativistic Fermi gas. Between 10^5 and 10^7 g/cm^3 the electrons become relativistic and Γ approaches 4/3. If the original mass of the supernova is less than 15 $M_\odot$ it is thought that the evolution will end here and the star will end its life as a white dwarf. If on the other hand the initial mass was somewhere between 15 and 30 $M_\odot$ the iron core can reach the Chandrasekhar mass and the collapse can continue past the point where electron degeneracy pressure no longer supports the star. In fact above 1.4×10^7 g/cm^3 the rest mass of 62 Fe^{56}_{26} nuclei plus the rest mass of 44 electrons and their kinetic energy, exceeds the rest mass of 56 Ni^{62}_{28} nuclei. Thus the reaction

$$62Fe^{56}_{26} + 44e^- \longrightarrow 56Ni^{62}_{28} \tag{2.2}$$

goes to its endpoint with a release of energy. As compression continues the rising Fermi energy of the electrons induces more nuclear reactions involving different nuclei. These reactions lead to the capture of more and more electrons to form neutron rich nuclei. When the density reaches 3×10^{11} g/cm^3 the nuclei become so neutron rich (Y^{122}_{39}) that it is energetically favorable for neutrons to drip out of them, and at 4×10^{11} g/cm^3 there are enough free neutrons that their degeneracy pressure exceeds that of the electrons. Further compression to $\approx 10^{13}$ g/cm^3 completely disintegrates the nuclei and leaves a sample of nearly pure neutrons sustaining the star, with just enough electrons to maintain charge neutrality with the protons. Further compression pushes matter to nuclear densities where the behaviour of matter is only poorly understood. If the original supernova was massive enough (more than 30 $M_\odot$) then the collapse will continue and eventually a black hole will form.

2.1.2 Neutron Star Structure

It is important to understand that the processes described in the previous section do not happen all at once throughout the star. They are more like the description of what would happen to an element of cold catalysed matter as it gets pushed deeper and deeper inside the star. Let us then

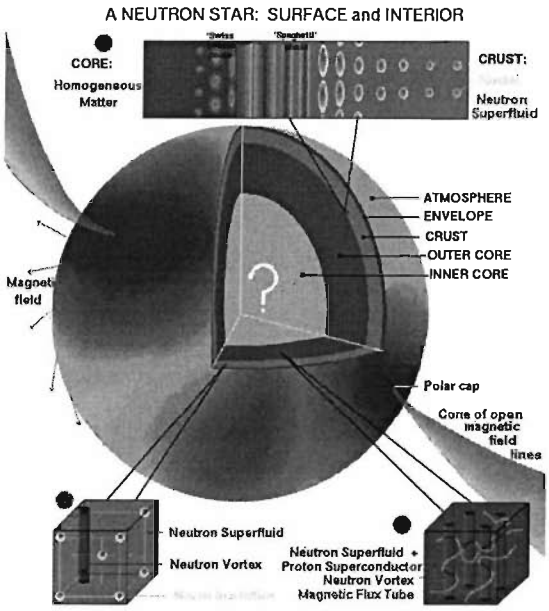

Figure 2.2: Composition of a Neutron Star, from http://www.lsw.uni-heidelberg.de/users/mcamenzi/NS_Mass.html

see what the cross section of a neutron star would look like. Close to the surface the density is still quite low and we have regular nuclei which form a lattice that gives rise to a crust, i.e. an ordered structure that can support shear stresses. We shall describe the crust in more detail later on. So as we have said close to the surface we expect to find mainly Fe^{56} and as we go further down the equilibrium atomic weight rises and we find more and more neutron rich nuclei. Eventually we reach the neutron drip layer at 4×10^{11} g/cm^3 and after that the main contribution to the equation of state comes from the degenerate neutron gas. Towards the base of the crust, at $\approx 10^{14}$ g/cm^3 the surface energy of the nuclei becomes comparable to their Coulomb energy, and it becomes energetically favourable for the nuclei to form rods or plates. Further down we have the liquid core of the neutron star. It should be noted that the protons and neutrons are expected to be superfluid. Now, if the central density exceeds the nuclear density 2.8×10^{14} g/cm^3 by a factor of 2 or 3 we can have a central core with exotic states of matter, such as pion condensates or hyperons, which may also form rods and plates which, as we shall see, could have interesting consequences.

2.2 Neutron Star Crusts

The upper layers of a Neutron star are comprised by a solid crust which separates the stellar interior from the photosphere, from which X-ray radiation is emitted. Even though its mass is only $\approx 1\%$ of the total mass and its thickness is less than one tenth of the stellar radius, the crust still has important observational consequences. The transport of heat from the core to the surface, through the crust, is crucial in determining the relation between the temperature of the bulk of the star and the X-ray flux. The fact that the crust is solid also allows the star to sustain toroidal modes, which would have zero frequency in a purely fluid star; and the boundary conditions at the crust core interface are important for determining the properties of non-radial modes. The coupling between the superfluid and the crust is also assumed to be the cause of the observed "glitches" in many pulsars. It is in fact thought that as the crust is spun down the superfluid core lags behind, until the difference in velocities is too great and there is a rapid exchange of angular momentum. Last but not least the crust, as it is solid, can support shearing and can thus support a deviation from axisymmetry which would give a rotating neutron star a time varying quadrupole and make it a very interesting source of gravitational waves.

2.2.1 Formation of the crust

When a neutron star forms in the collapse of a supernova it is initially very hot ($\approx 10^{11}$K). As it cools down the envelope of this hot neutron star will become the crust. The hot envelope is a mixture of heavy and light nuclei, neutrons, protons, electrons and photons, and at temperatures above 10^{10} K most nuclei are completely evaporated. As the crust cools (at 10^{10} K matter is now transparent to neutrinos) the fraction of free neutrons and α particles decreases until at 10^9 K thermal effects are mostly negligible (as is the number of free neutrons at densities below neutron drip) and the $T = 0$ approximation becomes quite accurate. At this point the composition "freezes in" and no longer changes with decreasing temperature. The crust will eventually solidify when the temperature decreases below the melting point corresponding to the local density and composition. This means that we can assume matter in the crust of an "old" neutron star (with typical temperatures of $\approx 10^8$ K) to be in its ground state (complete thermodynamic equilibrium, cold catalysed matter) and we will assume that it forms a perfect crystal of a single species (number of nucleons A, number of protons Z).

2.2.2 Composition of the crust

The problem of determining the composition of the upper layers of the crust, where all neutrons are bound in nuclei (densities below neutron drip) was first studied by Baym, Pethick and Sutherland [14] and consists, basically, in minimising the Gibbs Energy per nucleon.

$$g = (E + P)/n_b \tag{2.3}$$

where E is the energy density, P the pressure and n_b is the baryon density. If we divide matter into electrically neutral cells (Wigner-Seitz) containing one nucleus, we can write the Gibbs Energy per cell, which will in general be of the form:

$$G_{\text{cell}}(A, Z) = G_{\text{nucleus}} + G_{\text{lattice}} + G_{\text{electrons}} \tag{2.4}$$

Minimising this expression with respect to A and Z (with the input of the ground state atomic masses) allows us to compute the composition at a given density. Recent results can be found in [28], and are summarised in table 2.1.

The problem becomes much more complicated beyond neutron drip, as we now have to deal with nuclei immersed in a neutron gas. At this point there are many approximations that can be used to deal with the many-body problem and to determine an effective Hamiltonian for the system. The results one obtains obviously depend slightly on the scheme one chooses to follow, details can be found in the review article by Haensel [48]. The approximation scheme in fact also determines the behaviour of matter close to the edge of the crust. In fact at densities of $\approx 10^{14}$ g/cm^3, depending on the calculation, the surface energy of the nuclei becomes comparable with their Coulomb Energy and the spherical state is no longer the preferred state. If we define the volume of a Wigner-Seitz cell as

$$V_c = 1/n_n \tag{2.5}$$

$$n_n = n_b/A \quad \text{nucleon density} \tag{2.6}$$

then we can define the volume fraction occupied by the nuclear phase as

$$w = V_p/V_c = (\text{if nuclei are spherical})(r_p/r_c)^3 \tag{2.7}$$

where r_p is the radius of the proton, defined so that

$$\frac{4\pi}{3} r_p^3 n_p = Z \tag{2.8}$$

Table 2.1: Structure and composition of the inner neutron-star crust (ground state) calculated within the Compressible Liquid Drop Model with SLy effective nucleon-nucleon interaction. X_n is the fraction of nucleons in the neutron gas outside nuclei. The upper part with $X_n = 0$ corresponds to a shell of the outer crust, just above the neutron drip surface in the neutron-star interior, calculated within the same model. We also have the Wigner-Seitz cell radius and fraction of volume occupied by nuclear matter (equal to that occupied by protons) w. From Douchin and Haensel (2001) [28].

n_b (fm^{-3})	Z	A	X_n	R_{cell} (fm)	w (%)
1.2126 E-4	42.198	130.076	0.0000	63.503	0.063
1.6241 E-4	42.698	135.750	0.0000	58.440	0.084
1.9772 E-4	43.019	139.956	0.0000	55.287	0.102
2.0905 E-4	43.106	141.564	0.0000	54.470	0.107
2.2059 E-4	43.140	142.161	0.0247	54.032	0.110
2.3114 E-4	43.163	142.562	0.0513	53.745	0.113
2.6426 E-4	43.215	143.530	0.1299	53.020	0.118
3.0533 E-4	43.265	144.490	0.2107	52.312	0.123
3.5331 E-4	43.313	145.444	0.2853	51.617	0.129
4.0764 E-4	43.359	146.398	0.3512	50.937	0.135
4.6800 E-4	43.404	147.351	0.4082	50.269	0.142
5.3414 E-4	43.447	148.306	0.4573	49.615	0.148
6.0594 E-4	43.490	149.263	0.4994	48.974	0.155
7.6608 E-4	43.571	151.184	0.5669	47.736	0.169
1.0471 E-3	43.685	154.094	0.6384	45.972	0.193
1.2616 E-3	43.755	156.055	0.6727	44.847	0.211
1.6246 E-3	43.851	159.030	0.7111	43.245	0.239

Table 2.2: Structure and composition of the inner neutron-star crust - continued. The last line corresponds to the bottom edge of the inner crust, at a density of approximately 0.7 times nuclear density.

n_b (fm^{-3})	Z	A	X_n	R_{cell} (fm)	u (%)
2.0384 E-3	43.935	162.051	0.7389	41.732	0.271
2.6726 E-3	44.030	166.150	0.7652	39.835	0.320
3.4064 E-3	44.101	170.333	0.7836	38.068	0.377
4.4746 E-3	44.155	175.678	0.7994	36.012	0.460
5.7260 E-3	44.164	181.144	0.8099	34.122	0.560
7.4963 E-3	44.108	187.838	0.8179	32.030	0.706
9.9795 E-3	43.939	195.775	0.8231	29.806	0.923
1.2513 E-2	43.691	202.614	0.8250	28.060	1.159
1.6547 E-2	43.198	211.641	0.8249	25.932	1.566
2.1405 E-2	42.506	220.400	0.8222	24.000	2.115
2.4157 E-2	42.089	224.660	0.8200	23.106	2.458
2.7894 E-2	41.507	229.922	0.8164	22.046	2.967
3.1941 E-2	40.876	235.253	0.8116	21.053	3.585
3.6264 E-2	40.219	240.924	0.8055	20.128	4.337
3.9888 E-2	39.699	245.999	0.7994	19.433	5.058
4.4578 E-2	39.094	253.566	0.7900	18.630	6.146
4.8425 E-2	38.686	261.185	0.7806	18.038	7.202
5.2327 E-2	38.393	270.963	0.7693	17.499	8.470
5.6264 E-2	38.281	283.993	0.7553	17.014	10.011
6.0219 E-2	38.458	302.074	0.7381	16.598	11.914
6.4183 E-2	39.116	328.489	0.7163	16.271	14.323
6.7163 E-2	40.154	357.685	0.6958	16.107	16.606
7.0154 E-2	42.051	401.652	0.6699	16.058	19.501
7.3174 E-2	45.719	476.253	0.6354	16.213	23.393
7.5226 E-2	50.492	566.654	0.6038	16.557	26.996
7.5959 E-2	53.162	615.840	0.5898	16.772	28.603

(n_p is the proton number density) and r_c is the radius of a spherical cell of volume V_c. At low densities $r_p/r_c << 1$ and from a Compressible Liquid Drop Model we can expect the spherical shape to minimise the energy, which includes the shape dependent contribution $E_{\text{surface}} + E_{\text{Coulomb}}$. However at $\rho \approx 10^{14}$ g/cm^3 we have $r_p/r_c \approx 0.5$ and it is no longer obvious that the preferred shape is the spherical one. In fact Ravenhall et al. [115] found that matter can undergo a series of phase transitions and form first rods ("spaghetti"), then plates ("lasagna"), and eventually turn inside out and form "bubbles" inside dense nuclear matter ("swiss cheese"). The filling factor will then be given by

$$w = (r_p/r_c)^d \tag{2.9}$$

where d is the dimensionality of the phase (3 for spherical nuclei and spherical bubbles, 2 for rods and cylindrical bubbles and 1 for plates). These structures could potentially be very interesting as they have the elastic properties of liquid crystals and could thus support shearing and have some influence on the shear modulus of the crust and on the maximum quadrupole one could build on a neutron star. Even more interesting is the possibility that such structures may be present in the dense core of the star in some exotic scenarios. This would allow for a "mountain" in the very dense regions at the centre of the star, and thus potentially to a strong source of gravitational waves [47]. For example the shear modulus of a solid pion-condensate core has been estimated in [140, 106] to be $\mu \approx 10^{35} dyne/cm^2$. However it is interesting to ask what the breaking strain would be for a liquid crystal core. It would appear that in laboratory conditions the breaking stress P_{br} for such a liquid crystal can go from a few to a few thousand Pa (compared to a few thousand MPa for ordinary crystals) [5]. We are interested in the strain, so in the quantity

$$\sigma_{br} = \frac{P_{br}}{\mu} \tag{2.10}$$

To have an estimate of this we can work on the assumption that the ratio μ/ρ is constant in our neutron star (as will be shown to be a reasonable approximation later in the chapter). So if we assume $\mu \approx 10^{35} dyne/cm^2$ for a density of $\rho \approx 10^{15} g/cm^2$ close to the centre, we have, at earth densities of $\rho \approx 1 g/cm^3$ that $\mu \approx 10^{20} dyne/cm^2$. If we now assume that the maximum breaking strain for a liquid crystal is $P_{br} \approx 10^4 Pa \approx 10^5 dyne/cm^2$ we have a yield strain of

$$\sigma_{br} = 10^{-15} \tag{2.11}$$

As we can see this value is very small, and even if it is a rough estimate it is still several orders of magnitude too small for the core to build up a significant quadrupole, even though the shear modulus is quite large. Returning to our description, most models predict this kind of behaviour and then eventually find a transition to a uniform neutron, proton and electron liquid at densities of approximately 1.5×10^{14} g/cm^3. This transition is weakly first order, as it takes place at constant pressure with a small density discontinuity. Once we have chosen the effective nuclear Hamiltonian we can also calculate the equation of state for cold catalysed matter. In reality after neutron drip this will essentially be due only to the neutron gas. An equation of state for a crust of cold catalysed matter is presented in table 2.3, again from [28].

2.3 Accreted Crusts

Up to now we have considered a crust composed of cold catalysed matter, which was formed at the birth of the neutron star. However this is not always the case. Many neutron stars are in binary systems and can undergo prolonged periods of accretion (as we will see in chapter 4). For example, if a neutron star is accreting at a rate of 10^{-10}M$_\odot$/yr, which is well below the Eddington limit, the original crust, made of nuclei in their ground state embedded in an electron gas, will be replaced by a new, non-catalysed one, in $\approx 10^5$ yr. At this point the temperature of the star does not exceed 10^8 K and in these conditions the only reactions that can take place as the matter sinks inwards are electron captures, neutron emission and absorption and, at high density, pycnonuclear fusion. This means that the new matter is not at equilibrium, as at these temperatures the reactions which would take it to its ground state may be much slower compared to others (for example they may involve double electron captures, which are much slower than single electron captures, which therefore proceed first). Non equilibrium processes thus lead to a different composition for an accreted crust, in which the very neutron rich nuclei of cold catalysed matter do not form. This, we shall see, has important consequences for the shear modulus of the crust.

The composition of an accreted crust and the equation of state has been calculated in [46] and is presented in tables 2.5 and 2.4. It is worth mentioning two things here however. First of all that the composition of the accreted crust is calculated only up to $\rho \approx 1.2 \times 10^{13}$g/cm^3, because at this point 80% of nucleons form a neutron gas outside of nuclei, and thus the equation of state is simply that of a neutron gas. However, the

Table 2.3: Equation of state of the inner crust. The first line corresponds to the neutron drip point, as calculated within the Compressible Liquid Drop Model. The last line corresponds to the bottom edge of the crust. $\Gamma = \frac{\rho c^2 + p}{p} \frac{dp}{d\rho c^2}$ is the compressibility index. From [28]

n_b (fm^{-3})	ρ (g cm^{-3})	P (erg cm^{-3})	Γ
2.0905 E-4	3.4951 E11	6.2150 E29	1.177
2.2059 E-4	3.6883 E11	6.4304 E29	0.527
2.3114 E-4	3.8650 E11	6.5813 E29	0.476
2.6426 E-4	4.4199 E11	6.9945 E29	0.447
3.0533 E-4	5.1080 E11	7.4685 E29	0.466
3.5331 E-4	5.9119 E11	8.0149 E29	0.504
4.0764 E-4	6.8224 E11	8.6443 E29	0.554
4.6800 E-4	7.8339 E11	9.3667 E29	0.610
5.3414 E-4	8.9426 E11	1.0191 E30	0.668
6.0594 E-4	1.0146 E12	1.1128 E30	0.726
7.6608 E-4	1.2831 E12	1.3370 E30	0.840
1.0471 E-3	1.7543 E12	1.7792 E30	0.987
1.2616 E-3	2.1141 E12	2.1547 E30	1.067
1.6246 E-3	2.7232 E12	2.8565 E30	1.160
2.0384 E-3	3.4178 E12	3.7461 E30	1.227
2.6726 E-3	4.4827 E12	5.2679 E30	1.286
3.4064 E-3	5.7153 E12	7.2304 E30	1.322
4.4746 E-3	7.5106 E12	1.0405 E31	1.344
5.7260 E-3	9.6148 E12	1.4513 E31	1.353
7.4963 E-3	1.2593 E13	2.0894 E31	1.351
9.9795 E-3	1.6774 E13	3.0720 E31	1.342
1.2513 E-2	2.1042 E13	4.1574 E31	1.332
1.6547 E-2	2.7844 E13	6.0234 E31	1.322
2.1405 E-2	3.6043 E13	8.4613 E31	1.320
2.4157 E-2	4.0688 E13	9.9286 E31	1.325
2.7894 E-2	4.7001 E13	1.2023 E32	1.338
3.1941 E-2	5.3843 E13	1.4430 E32	1.358
3.6264 E-2	6.1153 E13	1.7175 E32	1.38
3.9888 E-2	6.7284 E13	1.9626 E32	1.416
4.4578 E-2	7.5224 E13	2.3024 E32	1.45
5.2327 E-2	8.8350 E13	2.9261 E32	1.536
5.6264 E-2	9.5022 E13	3.2756 E32	1.576
6.0219 E-2	1.0173 E14	3.6505 E32	1.615
6.4183 E-2	1.0845 E14	4.0509 E32	1.650
6.7163 E-2	1.1351 E14	4.3681 E32	1.672
7.0154 E-2	1.1859 E14	4.6998 E32	1.68
7.3174 E-2	1.2372 E14	5.0462 E32	1.685
7.5226 E-2	1.2720 E14	5.2856 E32	1.662
7.5959 E-2	1.2845 E14	5.3739 E32	1.644

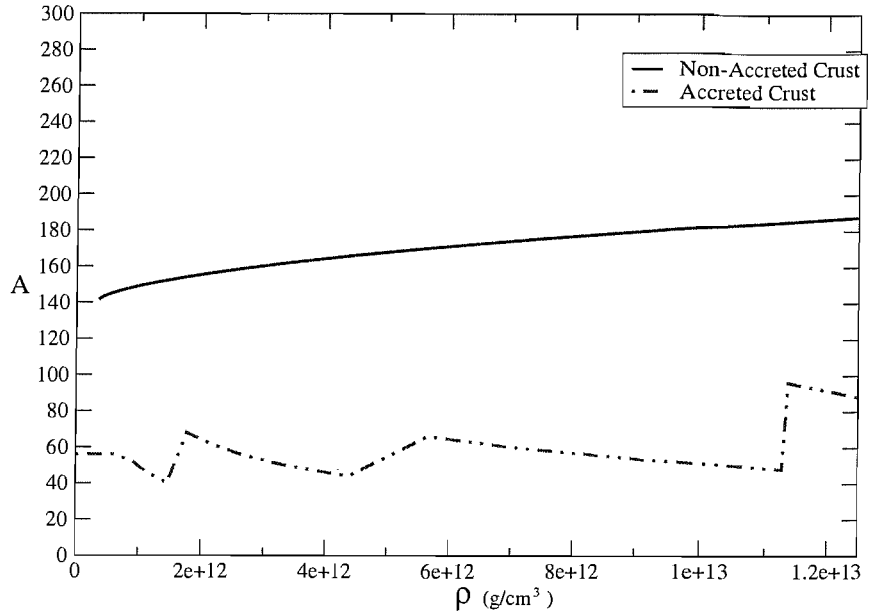

Figure 2.3: Comparison of the atomic number A in an accreted and a non-accreted crust.

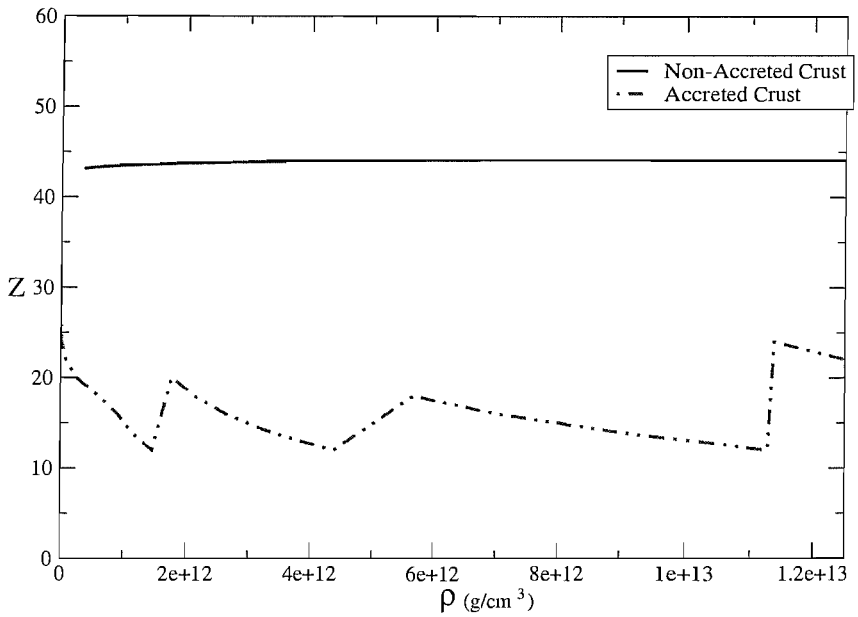

Figure 2.4: Comparison of the atomic number Z in an accreted and a non-accreted crust.

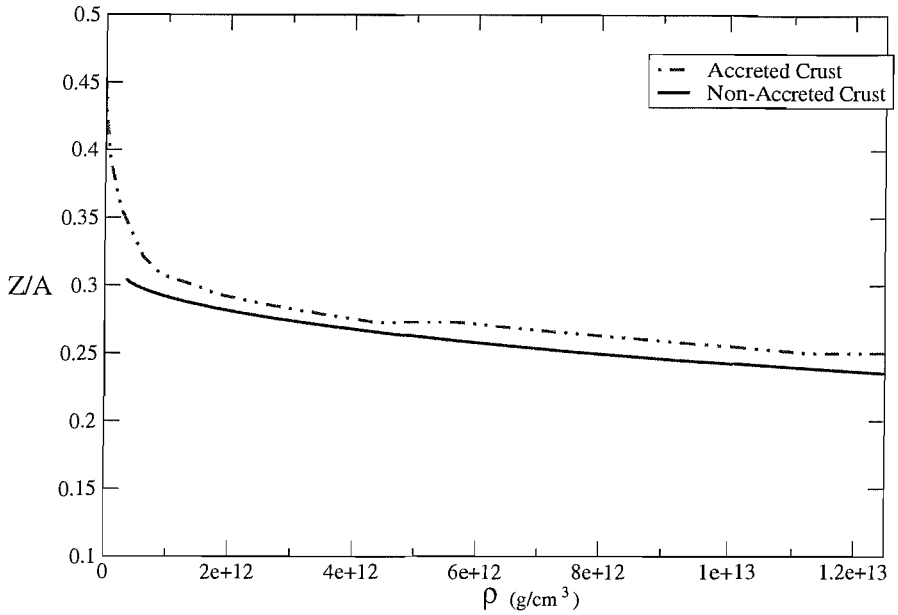

Figure 2.5: Comparison of the ratio Z/A in an accreted and a non-accreted crust.

composition is quite different as we have Z<20 compared to Z=40-50 in cold catalysed matter, and A is about 60, compared to 200 for a regular crust, even though the ratio Z/A does not vary much in the two cases. The second remark is that the equation of state is not as soft as in the catalysed case, and this leads to a crust that is about 20% thicker than for a standard crust built of catalysed matter.

2.4 Elastic properties of the crust

As we have seen, the core of a neutron star consists of a lattice of nuclei. It can therefore sustain an elastic strain. As a neutron star is a relativistic object we should describe elastic effects in the crust with a relativistic theory of elasticity. Such a theory has indeed been developed (see [65] and references therein), however in the following we shall deal only with Newtonian elasticity. This is mainly for simplicity, but is to some extent justified by the fact that at the relatively low densities of the crust Newtonian theory is quite adequate. In particular it is adequate to describe elastic forces, which are much smaller than those of gravity and pressure. We will use the standard procedure of Landau and Lifshitz [70] for studying the continuous displacements of nuclei from their

Table 2.4: Equation of state for an accreted crust. From [46].

ρ (g cm^{-3})	P (erg cm^{-3})	$n_{\rm b}$ (cm^{-3})	ρ (g cm^{-3})	P (erg cm^{-3})	$n_{\rm b}$ (cm^{-3})
3.207E7	3.833E24	1.933E31	7.580E10	1.100E29	4.547E34
6.401E7	1.006E25	3.858E31	1.048E11	1.495E29	6.284E34
1.277E8	2.604E25	7.6965E31	1.320E11	2.033E29	7.913E34
2.549E8	6.676E25	1.536E32	1.587E11	2.597E29	9.507E34
3.109E8	8.738E25	1.873E32	1.720E11	2.892E29	1.031E35
4.928E8	1.629E26	2.969E32	1.895E11	3.290E29	1.135E35
7.811E8	3.029E26	4.704E32	2.387E11	4.473E29	1.429E35
9.836E8	4.129E26	5.923E32	3.225E11	4.816E29	1.930E35
1.140E9	5.036E26	6.866E32	4.056E11	7.890E29	2.426E35
1.436E9	6.860E26	8.644E32	4.7845E11	9.831E29	2.861E35
2.462E9	1.272E27	1.482E33	5.620E11	1.218E30	3.359E35
3.903E9	2.356E27	2.348E33	6.990E11	1.399E30	4.176E35
6.188E9	4.362E27	3.722E33	7.869E11	1.638E30	4.700E35
7.522E9	5.662E27	4.524E33	8.970E11	1.950E30	5.356E35
9.472E9	7.702E27	5.696E33	1.436E12	2.592E30	8.570E35
1.2995E10	1.048E28	7.812E33	2.471E12	3.506E30	1.474E36
1.636E10	1.425E28	9.833E33	3.688E12	4.771E30	2.199E36
2.060E10	1.938E28	1.238E34	5.237E12	6.481E30	3.122E36
2.496E10	2.503E28	1.4995E34	6.773E12	8.748E30	4.036E36
3.143E10	3.404E28	1.888E34	8.679E12	1.170E31	5.170E36
3.958E10	4.628E28	2.377E34	1.194E13	1.695E31	7.111E36
4.779E10	5.949E28	2.869E34	1.462E13	2.209E31	8.706E36
6.018E10	8.089E28	3.6115E34			

Table 2.5: Composition of an accreted crust. The maximum pressure and density at which the nuclide is present are listed. X_n is the fraction of neutrons outside of nuclei. From [46].

$\rho_{\max}$ (g cm^{-3})	P_{max} (erg cm^{-3})	$n_{\rm b}$ (fm^{-3})	Z	A	X_n
1.494E09	7.235E26	8.994E-7	26	56	0.
1.1145E10	9.569E27	6.701E-6	24	56	0.
7.848E10	1.152E29	4.708E-5	22	56	0.
2.496E11	4.747E29	1.494E-4	20	56	0.
6.110E11	1.361E30	3.651E-4	18	56	0.
9.075E11	1.980E30	5.418E-4	16	52	0.07
1.131E12	2.253E30	6.748E-4	14	46	0.18
1.455E12	2.637E30	8.682E-4	12	40	0.29
1.766E12	2.771E30	1.054E-3	20	68	0.39
2.134E12	3.216E30	1.273E-3	18	62	0.45
2.634E12	3.825E30	1.571E-3	16	56	0.50
3.338E12	4.699E30	1.990E-3	14	50	0.55
4.379E12	6.044E30	2.610E-3	12	44	0.61
5.665E12	7.233E30	3.377E-3	18	66	0.70
7.041E12	9.2385E30	4.196E-3	16	60	0.73
8.980E12	1.228E31	5.349E-3	14	54	0.76
1.127E13	1.602E31	6.712E-3	12	48	0.79
1.137E13	1.613E31	6.769E-3	24	96	0.79
1.253E13	1.816E31	7.464E-3	22	88	0.80

equilibrium position to a new position

$$\bar{r}' = \bar{r} + \bar{\xi}(r) \tag{2.12}$$

where r points to the lattice sites of the bcc (body-centered-cubic) lattice and is a continuous field obtained by averaging over many lattice sites, as is ξ. A non zero displacement gives rise to an elastic strain which is described by the strain tensor, which to first order in ξ is

$$t_{ik} = t_{ki} = \frac{1}{2}\left(\frac{\partial \xi_i}{\partial x_k} + \frac{\partial \xi_k}{\partial x_i}\right) \tag{2.13}$$

and can be split into a compression and a shear term

$$\begin{aligned} t_{ik} &= t_{ik}^{\text{comp}} + t_{ik}^{\text{shear}} \\ t_{ik}^{\text{comp}} &= \frac{1}{3}\delta_{ik}\nabla^j \xi_j \\ t_{ik}^{\text{shear}} &= t_{ik} - \frac{1}{3}\delta_{ik}\nabla^j \xi_j \end{aligned} \tag{2.14}$$

After deformation the volume of a matter element changes according to

$$dV' = dV(1 + \nabla^j \xi_j) \tag{2.15}$$

This means that pure compression changes the volume of a matter element, but not the shape, while pure shear does not change the volume, as it is divergence free. To lowest order the deformation energy is quadratic in the deformation tensor, and takes the form

$$\varepsilon = \frac{1}{2}\lambda_{iklm} t_{ik} t_{lm} \tag{2.16}$$

where the linearly independent components of λ_{iklm} are known as elastic moduli, and general symmetry considerations reduce their number to 21. Their number becomes smaller as we increase the symmetry of the medium, and is only 3 in the case of a bcc lattice. The simplest case we can consider is that of an isotropic solid. In this case we have only two elastic moduli and the deformation energy can be written as

$$\varepsilon = \frac{1}{2}K(\nabla^j \xi_j)^2 + \mu(t_{ik} - \delta_{ik}\frac{1}{3}\nabla^j \xi_j)(t^{ik} - \frac{1}{3}\delta^{ik}\nabla^j \xi_j) \tag{2.17}$$

where K is known as the *compression modulus* and μ as the *shear modulus*. The elastic stress tensor is defined as

$$\sigma_{ik} = \frac{\partial \varepsilon}{\partial t_{ik}} \tag{2.18}$$

This takes a particularly simple form if we consider an **isotropic** solid:

$$\sigma_{ik} = K\nabla^j\xi_j\delta_{ik} + 2\mu\left(t_{ik} - \frac{1}{3}\delta_{ik}\nabla^j\xi_j\right) \tag{2.19}$$

if we consider pure uniform compression we find that

$$K = n_b\frac{\partial P}{\partial n_b} = \Gamma P \tag{2.20}$$

where Γ is the adiabatic index $\Gamma = \frac{n_b}{P}\frac{\partial P}{\partial n_b}$ and n_b is the number density of nuclei in the latice. This means that the shear stress tensor is simply

$$\sigma_{ik}^{\text{shear}} = 2\mu t_{ik} \tag{2.21}$$

The simplicity of these expressions make it desirable to treat the neutron star crust as an isotropic solid. However, as we believe a bcc crystal to be a better description, we have to define some sort of 'average' shear modulus from the three elastic moduli we have. In reality it is sufficient to consider two if we only consider shearing (volume preserving deformations). Note, however, that this is not the only possibility and there have even been suggestions that the crust may be an amorphous substance [59].

For volume preserving deformations of a bcc crystal the energy takes the form

$$\varepsilon = b_{11}(t_{xx}^2 + t_{yy}^2 + t_{zz}^2) + c_{44}(t_{xy}^2 + t_{xz}^2 + t_{yz}^2) \tag{2.22}$$

Ogata and Ichimaru [104] performed directional averages over the rotations of the Cartesian axes and obtained at $T = 0$

$$\begin{aligned}\mu(0) &= \frac{1}{5}(2b_{11} + 3c_{44}) = 0.1194\frac{n_n(Ze)^2}{r_c} \\ &= 0.1194\left(\frac{3}{4\pi}\right)^{1/3}\left(\frac{1-X_n}{A}n_b\right)^{4/3}(Ze)^2\end{aligned} \tag{2.23}$$

The dependence of μ on temperature was studied in [135] where the authors find that their results can be represented by the formula

$$\mu(T) = \frac{\mu(0)}{1 + 1.781(100/\gamma)^2} \tag{2.24}$$

where $\gamma = Z^2e^2/(r_cK_bT)$ contains the temperature dependence. As expected the shear modulus decreases with increasing temperature. The authors also find that the $T = 0$ approximation is a good one throughout

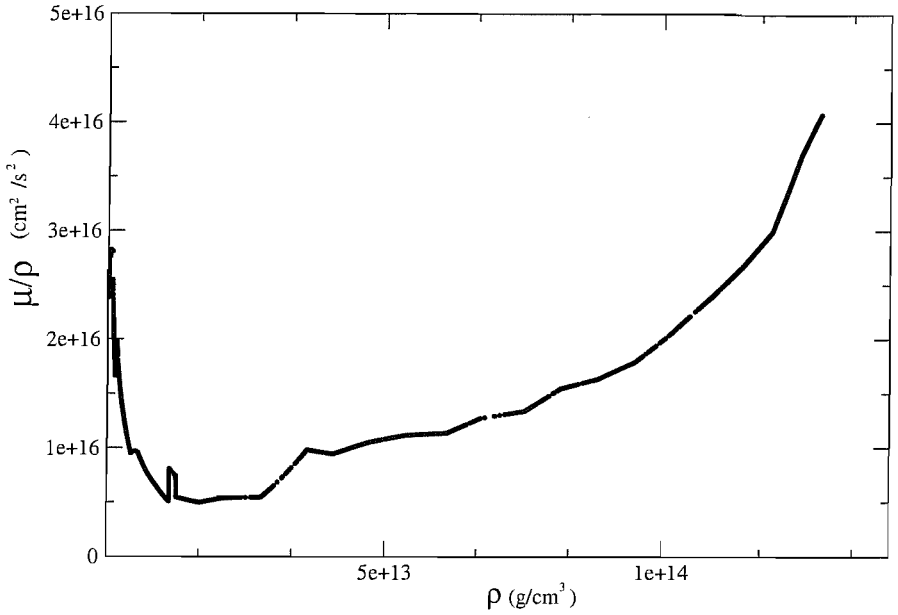

Figure 2.6: The ratio of μ/ρ in the crust. This figure is for the case of an accreted crust, but the situation is substantially the same for an accreted crust.

most of the crust. As is obvious from the above expressions the shear modulus depends on the composition of the crust, and is thus different in an accreted crust and a non-accreted crust. One last remark that is important to make is that if one looks at the graph of μ/ρ it appears that this quantity remains nearly constant in the crust, only varying of factors of a few close to the base of the crust and close to the surface, as can be seen in figure 5.3. This allows us to simplify the problem even more and make the approximation

$$\frac{\mu}{\rho} \approx \text{constant} = 10^{16}\ \text{cm}^2\ /\ \text{s}^2 \tag{2.25}$$

We now have a basic understanding of the composition and equation of state of a neutron star crust, both in the accreted and non accreted case. We also have described how to study elastic effects in the crust. In order to study the consequences of these effects (e.g. how large a deformation a star could sustain) we now need to 'build' an equilibrium model for a neutron star. Let us therefore concentrate on constructing a stellar model.

2.5 Newtonian Equilibrium Configurations

Once we have chosen an equation of state, for example one of those presented above for the crust, we need to calculate the equilibrium configuration of our neutron star. As we want an *equilibrium* state we shall consider the star to be stationary (we shall see how to include the effects of slow rotation later) and spherically symmetric. If we proceed in Newtonian theory the relevant equations are those of hydrostatic equilibrium, given by balancing the forces of gravity and pressure:

$$\frac{dP(r)}{dr} = -\rho(r)\frac{Gm(r)}{r^2} \tag{2.26}$$

where G is Newton's gravitational constant, $P(r)$ and $\rho(r)$ are the pressure and density at a given radius r and $m(r)$ is the mass contained within this radius:

$$\frac{dm(r)}{dr} = 4\pi r^2 \rho(r) \tag{2.27}$$

It is convenient to combine these equations by dividing the first by ρ and then taking it's divergence (which, as we are in polar coordinates, is the operator $\frac{1}{r^2}\frac{d}{dr}r^2$). By then using the continuity equation we have:

$$\frac{1}{r^2}\frac{d}{dr}\left(\frac{r^2}{\rho}dPdr\right) = -4\pi G\rho \tag{2.28}$$

Let us choose a polytropic equation of state:

$$P = K\rho^{1+1/n} \tag{2.29}$$

this gives us

$$\frac{1}{r^2}\frac{d}{dr}\frac{r^2}{\rho}K\frac{n+1}{n}\rho^{1/n}\frac{d\rho}{dr} = -4\pi G\rho \tag{2.30}$$

We can now make the change of variables

$$\begin{aligned} r &= \xi\alpha \\ \rho &= \Theta^n\rho_c \end{aligned} \tag{2.31}$$

where ρ_c is the central density and

$$\alpha^2 = K\frac{(n+1)}{4\pi G}\rho_c^{\frac{1-n}{n}} \tag{2.32}$$

this leaves us with what is known as the Lane-Emden equation

$$\frac{1}{\xi^2}\frac{d}{d\xi}\left(\xi^2\frac{d\Theta}{d\xi}\right) = -\Theta^n \tag{2.33}$$

with boundary conditions

$$\begin{aligned} \Theta(0) &= 1 \\ \Theta'(0) &= 0 \end{aligned} \tag{2.34}$$

which select the regular solution and give us, as expected, the maximum of $\rho(r)$ at the centre. We must integrate to the surface, i.e. to the point where $\Theta(\xi) = 0$.

2.5.1 n=1 polytrope

We will take the polytropic index to be $n = 1$. This is mainly because, as we are about to see, this case allows for a simple solution. However it is also a reasonably good approximation for more realistic equations of state because, as we can see also in table 2.3, the compressibility index Γ is quite close to 2 (the value for an $n = 1$ polytrope) throughout most of the star. Our equation of state is then

$$P = K\rho^2 \tag{2.35}$$

the Lane-Emden equation takes the form

$$\frac{1}{\xi^2}\frac{d}{d\xi}\left(\xi^2\frac{d\theta}{d\xi}\right) = -\theta \tag{2.36}$$

with the substitution $\theta = \psi(\xi)/\xi$ the equation becomes that of a harmonic oscillator $\psi''(\xi) = -\psi(\xi)$. This gives us a solution of the form

$$\theta(\xi) = \frac{\sin\xi}{\xi} \quad \longrightarrow \quad \rho(\xi) = \rho_c\frac{\sin\xi}{\xi} \tag{2.37}$$

this passes through 0 for the first time when $\xi = \pi$, which corresponds to the stellar surface. We thus have

$$R = \pi\alpha \longrightarrow \alpha = \frac{R}{\pi} \longrightarrow \xi = \frac{r}{\alpha} = \pi\frac{r}{R} \tag{2.38}$$

If we now impose that the density remain 0 after the first node, we have

$$\rho(r) = \rho_c\frac{\sin(\pi r/R)}{r\pi} \qquad r < R \tag{2.39}$$

$$P(r) = K\rho(r)^2 \tag{2.40}$$

This solution depends only on two parameters, ρ_c and K, so we might as well express it in terms of M and R. The central density is given by

$$\rho_c = \frac{\pi M}{4R^3} \tag{2.41}$$

and the coefficient of the equation of state is

$$K = \frac{2GR^2}{\pi}. \tag{2.42}$$

If we choose our neutron star to have a mass $M = 1.4M_\odot$ and a radius $R = 10$ km, then we have

$$\begin{aligned} \rho_c &= 2.2 \times 10^{15} \mathrm{g/cm^3} \\ K &= 4.25 \times 10^4 \mathrm{g^{-1} cm^5 s^{-2}} \end{aligned} \tag{2.43}$$

Note that in general, for a given n, the solution to the Lane-Emden equation can be written in terms of *three* parameters, usually chosen to be M, R and ρ_c. The $n = 1$ case is peculiar as the radius does not depend on the mass or central density of the star

$$R = \pi\alpha = \pi \left(K \frac{2}{4\pi G} \right)^{1/2} \tag{2.44}$$

which allows us to express the solution in terms of only *two* parameters. A similar thing happens for the $n = 3$ case, relevant for white dwarfs, in which the mass does not depend on the central density.

2.5.2 Slow Rotation

I will briefly present a method to obtain the equilibrium shape of a uniformly rotating configuration, known as the Clairaut-Legendre expansion [141]. As we are considering a purely fluid star (no elastic forces) the equations of equilibrium are simply those we have already seen

$$\frac{1}{\rho}\frac{dP}{dr} = -\frac{d\Phi}{dr} \tag{2.45}$$

where we have however defined an effective potential

$$\Phi = V - \frac{1}{2}\Omega^2 r^2 \sin\theta^2 \tag{2.46}$$

with Ω the rotation rate and V the gravitational potential. As is clear from equation (2.45) the level surfaces of Φ coincide with the isobaric (and thus isopycnic if we have $\rho = \rho(p)$) surfaces, we can thus define a new variable a that label such surfaces and describes the deformed shape that the star has when it is rotating

$$a(r) = r\left[1 - \epsilon(r) P_2(\cos\theta)\right] \tag{2.47}$$

The form of the centrifugal potential justifies our choice of angular dependence in the definition. One can now carry out a linear analysis in ϵ (i.e. slow rotation approximation, effectively assuming that the centrifugal forces are much smaller than the gravitational forces) and impose that Φ should be a function of a only (no extra angular dependence). Omitting the details which can be found in [141], we can obtain an integral equation for ϵ of the form:

$$\left(a^2\frac{d\epsilon}{da}+2a\epsilon\right)\int_0^a \rho(a')da' - a^4\int_a^{a_s}\rho(a')\frac{d}{da'}[\epsilon(a')]da' = \frac{5}{12}\frac{\Omega^2}{\pi G}a^4 \tag{2.48}$$

dividing this by a^4 and differentiating we can obtain a second order differential equation for ϵ

$$a^2\frac{d^2\epsilon}{da^2}+6\frac{\rho(a)}{\rho_m(a)}\left(a\frac{d\epsilon}{da}+\epsilon\right)=6\epsilon \tag{2.49}$$

where

$$\rho_m(a)=\frac{3}{a^3}\int_0^a \rho(a')a'^2da' \tag{2.50}$$

which must be solved by choosing the regular solution at the centre of the star (the form of which obviously depends on the equation of state) and the shape at the surface, which depends on the rotation rate and is given from equation (2.48)

$$a\frac{d\epsilon}{da}+2\epsilon=\frac{5}{12}\frac{\Omega^2}{4\pi^2GM}a^3 \tag{2.51}$$

Finally we can introduce the variable

$$\eta(a)=\frac{a}{\epsilon}\frac{d\epsilon}{da} \tag{2.52}$$

this allows us to write equation (2.49) as

$$a\frac{d\eta}{da}+6\frac{\rho(a)}{\rho_m(a)}(\eta+1)+\eta(\eta-1)=6. \tag{2.53}$$

From this equation we can see that $\eta(0)=0$, which is the boundary condition we need to solve the equation. We can then reconstruct ϵ from equations (2.52) and (2.48). All the above expressions are derived in chapter 5 of [141]. As our analysis is first order in ϵ, we can ignore the difference between r and a in these expressions. We can thus solve

for $\epsilon(r)$, and the reconstruct the value of the pressure for example by assuming that to first order we have

$$P(a) = P(r) + \delta p(r) P_2(\cos\theta) \tag{2.54}$$

where

$$\delta p(r) = -\epsilon(r) r \frac{dP}{dr}(r) \tag{2.55}$$

2.5.3 Constant density star

Let us now consider an incompressible star rotating with angular velocity Ω. For this simple case equation (2.53) reduces to:

$$a\frac{d\eta}{da} + 5\eta + \eta^2 = 0 \tag{2.56}$$

for which the only solution that satisfies the boundary condition $\eta(0) = 0$ is the trivial one. We thus have, from equation (2.52) that

$$\frac{d\epsilon}{da} = 0 \tag{2.57}$$

ϵ is thus a constant and for simplicity we can obtain its value at the surface directly from equation (2.48), which reduces to:

$$2\frac{\epsilon(R)}{R}\frac{M}{4\pi} = \frac{5}{12}\frac{\Omega^2}{G\pi}R^2 \tag{2.58}$$

giving us

$$\epsilon(R) = \frac{5}{6}\frac{\Omega^2 R^3}{GM} \tag{2.59}$$

We can also obtain this result with a different method, similar to the Chandrasekhar-Milne expansion [141]. We still perturb the background model, which is given for example in [131]

$$\begin{aligned} p &= 2\pi G\rho^2 \frac{1}{3}(R^2 - r^2) \\ \phi &= -2\pi G\rho(R^2 - \frac{r^2}{3}) \end{aligned} \tag{2.60}$$

and impose that the new bounding surface is of the form

$$x = r(1 + \sum_l \epsilon^l(r) P_l(\theta)) \tag{2.61}$$

where P_l is a Legendre polynomial. We also impose that the mass of the star remain constant. This gives us the condition for the mass obtained for the new shape

$$\begin{aligned} M_\epsilon &= \rho \int_0^R (1+\epsilon^l P_l) r^2 d\Omega = M \\ M_\epsilon &= M + \int \epsilon^l P_l d\Omega \end{aligned} \tag{2.62}$$

which gives us the condition that

$$\epsilon^0 = 0 \tag{2.63}$$

as for $l \neq 0$ the integral over the angles vanishes. We can now consider the perturbed Euler equations

$$\begin{aligned} \frac{d\delta p}{dr} + \rho \frac{d\delta\phi}{dr} &= \rho\Omega^2 r \sin(\theta)^2 \\ \frac{d}{d\theta}(\delta p + \rho\delta\phi) &= \rho\Omega^2 r^2 \sin(\theta)\cos(\theta) \end{aligned} \tag{2.64}$$

which in terms of Legendre polynomials give:

$$\begin{aligned} (\frac{d\delta p^l}{dr} + \rho\frac{d\delta\phi^l}{dr})P_l(\theta) &= \frac{2}{3}\rho\Omega^2 r - \frac{2}{3}\rho\Omega^2 r P_2(\theta) \\ (\delta p^2 + \rho\delta\phi^2)\frac{dP_2}{d\theta} &= -\frac{1}{3}\rho\Omega^2 r^2 \frac{dP_2}{d\theta} \end{aligned} \tag{2.65}$$

As we have seen that the $l = 0$ component must vanish, let us concentrate on the $l = 2$ components, and omit the superscript 2. We must also consider the perturbed Poisson equation, which for $l = 2$ reads:

$$\frac{d^2\delta\phi}{dr^2} + \frac{2}{r}\frac{d\delta\phi}{dr} - \frac{6}{r^2}\delta\phi = 4\pi G\delta\rho \tag{2.66}$$

now, as the star is incompressible, $\delta\rho$ has support only between R and the new radius $R(1+\epsilon_s)$. As we are assuming that ϵ_s (the deformation at the surface) is a small perturbation, integrating between these two radii gives us:

$$\Delta\frac{d\delta\phi}{dr}\Big|_R^{R(1+\epsilon_s)} = \int_R^{R(1+\epsilon)} 4\pi G\rho \tag{2.67}$$

This allows us to calculate the discontinuity in $\frac{d\delta\phi}{dr}$ at the surface. The exterior solution has the form $\delta\phi = \frac{A}{r^3}$, so if we also impose the continuity of $\delta\phi$ at the surface we obtain a solution for $\delta\phi$ in the interior:

$$\delta\phi_{int} = \frac{4}{5}\pi G\rho\epsilon_s r^2. \tag{2.68}$$

We can now insert this result into the second of equations (2.65) and obtain

$$\delta p(r) = -\frac{1}{3}\Omega^2 r^2 - \frac{4}{5}\pi G\rho^2 \epsilon_2 r^2 \tag{2.69}$$

In order to solve for ϵ_s let us evaluate this expression at the surface and remember that

$$\delta p(r) = \delta p(x) + \epsilon_s r \frac{dP}{dr} \tag{2.70}$$

which at the new surface (given by $\delta p(x) = 0$) reduces to

$$\delta p(r) = \epsilon_s r \frac{dP}{dr}. \tag{2.71}$$

With the aid of equation (2.60) we can thus write

$$-\epsilon_s \frac{4}{3}\pi G\rho^2 R^2 = -\frac{4}{5}\pi G\rho^2 \epsilon_s R^2 - \frac{1}{3}\rho\Omega^2 R^2 \tag{2.72}$$

which with some manipulation gives us the same result as the Clairaut-Legendre expansion for the surface deformation

$$\epsilon_s = \frac{5}{6}\frac{\Omega^2 R^3}{GM} \tag{2.73}$$

We shall see in chapter 6 that this method can be used in exactly the same way to calculate a "magnetic" deformation of a star.

2.5.4 $n = 1$ polytrope

Let us now calculate the rotational deformation for an $n = 1$ polytrope. Our equation of state is thus of the form $p = K\rho^2$ and as we have seen this allows us to write the density as a function of radius in a closed form:

$$\rho(r) = \rho_0 \frac{\sin(\xi)}{\xi} = \frac{\pi M}{4R^3}\frac{\sin(\xi)}{\xi} \tag{2.74}$$

where $\xi = \pi r/R$ and $M(r) = M/\pi(\sin(\xi) - \xi\cos(\xi))$. We can now use the density in equation (2.74) in equation (2.53) and solve for ϵ. The deformation we obtain is:

$$\epsilon_2 = -\frac{1}{9}\frac{r\psi_2 R^2}{GM(r)}\Omega^2 \tag{2.75}$$

where

$$\psi_2(\xi) = 15\left(\frac{\pi}{2\xi}\right)^{1/2} J_{5/2}(\xi) = \frac{15}{\xi}\left[\left(\frac{3}{\xi^2} - 1\right)\sin(\xi) - \frac{3}{\xi}\cos(\xi)\right] \tag{2.76}$$

The surface deformation is:

$$\epsilon_{2s} = -5\frac{\Omega^2 R^3}{\pi^2 GM} \tag{2.77}$$

in agreement with that given by Chandrasekhar and Lebovitz [24].The same result can again be obtained by solving the perturbed Euler equations and Poisson equation. This time we must include density perturbations $\delta\rho$ in the Euler equations, that for $l = 2$ take the form:

$$\begin{aligned} \frac{d\delta p}{dr} + \rho\frac{d\delta\phi}{dr} + \delta\rho\frac{d\phi}{dr} &= 2\frac{2}{3}\rho\Omega^2 r \\ \delta p + \rho\delta\phi &= -\frac{1}{3}\rho\Omega^2 r^2 \end{aligned} \tag{2.78}$$

After some manipulation we can obtain

$$\delta\rho = -\frac{\pi^2}{4\pi GR^2}\delta\phi - \frac{\pi^2}{4\pi GR^2}\frac{\Omega^2 r^2}{3} \tag{2.79}$$

Substituting this into Poisson's equation gives

$$\frac{d\delta\phi^2}{dr^2} + \frac{2}{r}\frac{d\delta\phi}{dr} - \frac{6}{r^2}\delta\phi = -\frac{\pi^2}{R^2}\delta\phi - \frac{\pi^2}{R^2}\frac{\Omega^2 r^2}{3} \tag{2.80}$$

We can now solve this equation numerically, imposing regularity at the centre of the star and continuity in $\delta\phi$ and it's derivative at the surface, as we know that the external solution is of the form $\delta\phi = \frac{A}{r^3}$. We can thus calculate $\delta\rho$ from equation (2.79) and obtain the surface deformation from the relation

$$\epsilon_{2s} = \frac{\delta\rho(R)}{R\frac{d\rho}{dr}(R)} \tag{2.81}$$

The result is, as with the previous method,

$$\epsilon_{2s} = -5\frac{\Omega^2 R^3}{\pi^2 GM}. \tag{2.82}$$

the star is thus oblate.

2.6 Relativistic Models

Let us now turn our attention to the construction of a relativistic equilibrium model. We still want a static, spherically symmetric star, so we need to write a general static, spherically symmetric line element

$$d\tau^2 = e^{2\Phi(r)}dt^2 - e^{2\Lambda(r)}dr^2 - r^2\left(d\theta^2 + \sin\theta^2 d\phi^2\right) \tag{2.83}$$

with Φ and Λ going to 0 at infinity (asymptotic flatness). If we take matter to be a perfect fluid we have

$$T^{\alpha\beta} = (\rho + p)u^{\alpha}u^{\beta} - pg^{\alpha\beta} \tag{2.84}$$

where u^{α} is the four velocity and we are now taking $c = G = 1$. We can obtain the equations of motion for Λ and Φ by imposing that the metric we have written should be a solution to Einstein's equations and the hydrostatic equations

$$\begin{aligned} G^{\alpha\beta} &= 8\pi T^{\alpha\beta} \\ T^{\alpha\beta}_{;\beta} &= 0 \end{aligned} \tag{2.85}$$

this leads to

$$\begin{aligned} (\rho + p)\Phi_{,r} &= -p_{,r} \\ \Phi_{,r} &= \frac{m + 4\pi r^3 p}{r(r-2)} \\ m &= \frac{1}{2}r\left(1 - e^{-2\Lambda}\right) \end{aligned} \tag{2.86}$$

a derivation of which can be found for example in [94]. Recombining these equations lead to the **standard form of the TOV equations** (Tolman-Oppenheimer-Volkov equations)

$$\frac{dp}{dr} = -(\rho + p)\frac{m + 4\pi r^3 p}{r(r - 2m)} \tag{2.87}$$

$$\frac{dm}{dr} = 4\pi r^2 \rho \tag{2.88}$$

These equations must be integrated from the centre to the point where p vanishes. This is the radius R of the star and $M = m(R)$ is the mass. Note that this gives us the correct Schwarzshild metric outside the star as we have

$$\Phi_{,r} = \frac{M}{r(r-2M)} \longrightarrow e^{-2\Phi} = \frac{1}{1 - 2M/r} \tag{2.89}$$

so we have a good definition for mass (the mass that determines satellite orbits, NOT the baryonic mass obtained summing the mass of the single constituent particles, as this does not account for the gravitational binding energy). The initial values are the pressure p_c at the centre of the star and $m = 0$ at $r = 0$. However what we usually want is the Mass-Radius relation, which is not that simple to obtain from these equations,

as the radius is found by integrating the equation for the pressure until it vanishes. The procedure can be made much easier by using the Enthalpy h rather than the pressure [74]

$$h(p) = \int_0^p \frac{dp'}{\rho(p') + p'} \tag{2.90}$$

which simply vanishes at the surface. The TOV equations then become

$$\frac{dm}{dh} = -\frac{4\pi\rho(h)r^3(r-2m)}{m + 4\pi r^3 p(h)} \tag{2.91}$$

$$\frac{dr}{dh} = -\frac{r(r-2m)}{m + 4\pi r^3 p(h)} \tag{2.92}$$

and the domain of integration is now fixed from h_c at the centre of the star to 0 at the surface. The initial values for m and r near h_c are calculated as a power series in [74]

$$\begin{aligned} r(h) &= \left[\frac{3(h_c - h)}{2\pi(\rho_c + 3p_c)}\right]^{1/2} \\ &\quad \times \left[1 - \frac{1}{4}\left[\rho_c - 3p_c - \frac{3}{5}\left(\frac{d\rho}{dh}\right)_c\right]\frac{h_c - h}{\rho_c + 3p_c}\right] \end{aligned} \tag{2.93}$$

$$m(h) = \frac{4\pi}{3}\rho_c r^3(h)\left[1 - \frac{3}{5}\left(\frac{d\rho}{dh}\right)_c \frac{h_c - h}{\rho_c}\right] \tag{2.94}$$

In usual physical units these equations read:

$$\frac{dm}{dh} = -\frac{c^4}{G}\frac{4\pi\rho(h)r^3(r - 2Gm/c^2)}{mc^2 + 4\pi r^3 p(h)} \tag{2.95}$$

$$\frac{dr}{dh} = -\frac{c^4}{G}\frac{r(r - 2Gm/c^2)}{mc^2 + 4\pi r^3 p(h)} \tag{2.96}$$

and the initial values are:

$$\begin{aligned} r(h) &= \left[\frac{c^2}{G}\frac{3(h_c - h)}{2\pi(\rho_c c^2 + 3p_c)}\right]^{1/2} \\ &\quad \times \left[1 - \frac{1}{4}\left[\rho_c c^2 - 3p_c - \frac{3}{5}\left(\frac{d\rho c^2}{dh}\right)_c\right]\frac{h_c - h}{\rho_c c^2 + 3p_c}\right] \end{aligned} \tag{2.97}$$

$$m(h) = \frac{4\pi}{3}\rho_c r^3(h)\left[1 - \frac{3}{5}\left(\frac{d\rho c^2}{dh}\right)_c \frac{h_c - h}{\rho_c c^2}\right] \tag{2.98}$$

This formulation now allows us to read off the Mass-Radius relation directly by integrating equations (2.92) or (2.96) and is also much easier

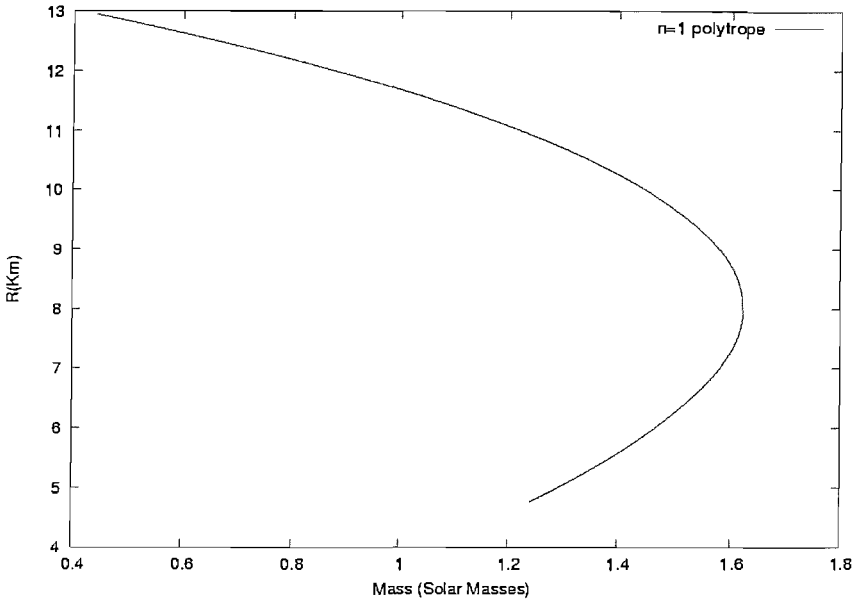

Figure 2.7: The Mass-Radius relation for a relativistic n=1 polytrope. The coefficient of the equation of state is taken to be $K = 10^4\ \mathrm{g}^{-1}\mathrm{cm}^5\mathrm{s}^{-2}$. The calculation has been done by integrating the equations given above, written in enthalpy.

to implement numerically because of the fixed domain of integration. Figure 2.7 shows the Mass-Radius relation for a $n = 1$ polytrope obtained with a code I have written using such a formulation. As can be seen the relativistic equations give a maximum mass for the Neutron star (in this case $\approx 1.6 M_\odot$), any mass greater than this must thus be unstable and collapse to a black hole.

Chapter 3

Accreting binaries

3.1 Introduction

Binary systems are some of the most interesting objects in the sky. This is mainly due to the fact that they allow us to learn, by their very nature, a lot more about them than other systems. By studying the orbits it is possible to obtain such parameters as the masses and the separation. In the case of an eclipsing binary we can also, by studying the light-curves, infer the dimensions of the stars. It is thus not surprising that binaries have proved to be some the best probes for studying a vast range of effects in astrophysics. For example the binary pulsar PSR 1913+16 provided the first indirect proof of the existence of gravitational waves. Binaries, especially the X-ray binaries, are also some of the systems in which accretion is best understood. In most of these systems the accreted material could not land on the accreting star without losing angular momentum. This leads to the material spreading out in a *accretion disc*, which is a good mechanism for transferring angular momentum and also for extracting gravitational potential energy and converting it into radiation [35]. There are two main reasons for mass transfer to occur in a binary:

1. During the evolution of the system the separation of the binary shrinks, or one of the stars expands, to the point where its outer layers begin to be feel the gravitational pull of its companion and are stripped off (Roche lobe overflow).

2. One of the stars may at some point eject much of its mass in the form of stellar wind; some of this material will be captured gravitationally by its companion (stellar wind accretion).

In the following we shall discuss the first case, as this is the one relevant for the Low Mass X-ray Binaries (LMXBs). The aim of this chapter is, in fact, to provide an introduction to accreting binaries in order to then focus, in the following chapter, on the specific case of the LMXBs, in which, as we shall see, gravitational waves are thought to play a role in the evolution. Moreover, it is by accretion that old, slow spinning pulsars, are recycled to fast rotation rates. Such rapidly rotating objects, with periods of the order of milliseconds, are quite aptly known as millisecond pulsars and are potentially interesting sources of gravitational waves. The mechanisms that could lead these stars to radiate will be investigated in the following chapters; let us now focus on the accretion process and the binary evolution.

3.2 Roche lobe overflow

To see when the outer layers of one star will be disrupted by the gravitational attraction of the other we can study the problem of a test particle in the gravitational potential due to two bodies orbiting each other. This problem was first studied by Edouard Roche in connection with planetary satellites, and is usually associated with his name. We will assume the two stars to be point masses on Keplerian orbits, which we will take to be circular. This is a good approximation because the orbits are circularised by tidal forces on a time scale which is small compared to that of mass transfer (at least in most cases). We thus have two masses, m_1 and m_2 ($M{=}m_1+m_2$) orbiting around their centre of mass at a distance a from each other with an orbital angular velocity

$$\omega = \sqrt{\frac{M}{a^3}} \tag{3.1}$$

in units where $G{=}c{=}1$. Any gas flow between the two stars will be governed by the Euler equation:

$$\rho\frac{\partial \mathbf{v}}{\partial t} + \rho\mathbf{v}\cdot\nabla\mathbf{v} = -\nabla P + \mathrm{f} \tag{3.2}$$

where P is the pressure and $\mathbf{f}$ is the force per unit volume. For our problem we will write the Euler equation in the frame co-rotating with the binary, with angular velocity ω defined above. This introduces extra terms into the Euler equation, due to the Coriolis force and the centrifugal force. The Euler equation thus takes the form:

$$\rho\frac{\partial \mathbf{v}}{\partial t} + \rho\mathbf{v}\cdot\nabla\mathrm{v} = -\nabla\Phi_R - 2\omega\wedge\mathbf{v} - \nabla P \tag{3.3}$$

Where the potential Φ_R now includes the effects centrifugal force and is known as the Roche potential:

$$\Phi_R(\mathbf{r}) = -\frac{m_1}{|\mathbf{r}-\mathbf{r}_1|} - \frac{m_2}{|\mathbf{r}-\mathbf{r}_2|} - \frac{1}{2}(\omega \wedge \mathbf{r})^2 \tag{3.4}$$

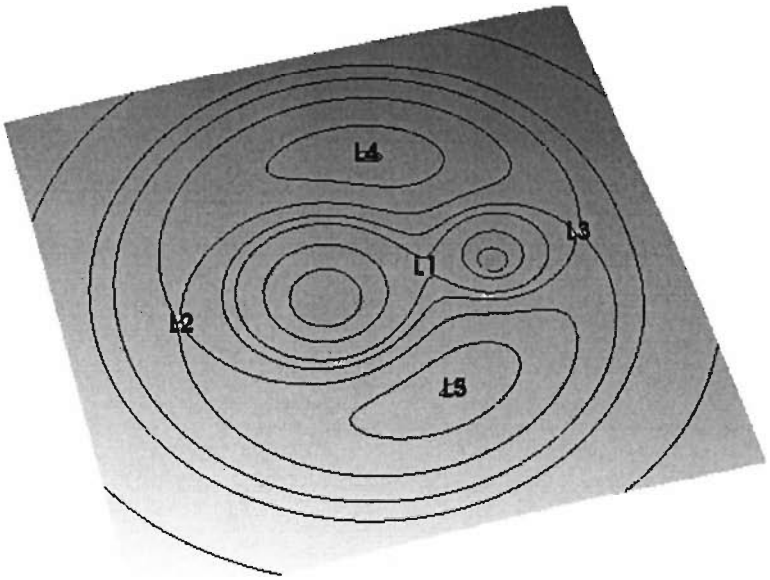

Figure 3.1: The Roche potential plotted on the equatorial plane, plotted for a mass ratio $q = m_1/m_2$ of 0.25. The points denoted L_i are the stationary points of the potential, the Lagrangian points described in the main text.

In fig. 3.1 we plot the equipotential lines for a mass ratio $q = m_1/m_2$ of 0.25. From the figure we can see that far out the equipotential lines are those of a mass M concentrated at the centre of mass. On the other hand close to the two stars the motion is dominated by the pull of the closest mass. We can see how the two regions of 'influence' of the stars are connected by looking at the critical surface that joins them, the figure of eight shape in the diagram. The two zones, or 'Roche lobes', join at the inner Lagrangian point L_1, which is one of the five stationary points of the potential. It is thus easier for matter orbiting near L_1 to enter the

lobe of the other star than to escape the critical surface altogether The other Lagrangian points are also maxima, although orbits near the outer Lagrangian points L_4 and L_5 may be stabilised by the Coriolis force. For example the Trojan asteroids lie at these points for the Sun-Jupiter system. So let us examine the case of two stars for which the rotation around their axis has been synchronised with the orbital rotation. This is a good approximation, as the timescale over which tidal forces will achieve this synchronisation is comparable with that over which they will circularise the orbits. For such a system the Roche lobe is the maximum area a star can fill and still be in hydrostatic equilibrium. So if at some point of its evolution one of the stars swells up to fill its Roche lobe, then mass transfer will begin, as any perturbation (provided for example by the pressure force) will push matter over the Lagrangian point and cause it to fall from the *secondary* (the lobe-filling star) to the *primary*. This mass transfer will be stable as long as the secondary continues to fill its Roche lobe. Such systems are called *semi-detached* binaries. In *detached* binaries both stars are much smaller than their Roche lobes, while in *contact* binaries both stars simultaneously fill their Roche lobes.

3.3 Stability of mass transfer

In order to study the stability of mass transfer let us first consider how angular momentum varies with mass transfer. As we have said we consider circular orbits and the two masses, m_1 and m_2 ($M{=}m_1 + m_2$) will orbit around their centre of mass at a distance a from each other on Keplerian orbits. Thus the total angular momentum will be

$$\begin{aligned} J &= (m_1 a_1^2 + m_2 a_2^2)\omega \\ &= m_1 m_2 \sqrt{\frac{a}{M}} \end{aligned} \tag{3.5}$$

where the last equality is obtained by using the expression for the distances of the two stars from the centre of mass

$$a_1 = \frac{m_2}{M} a \qquad a_2 = \frac{m_1}{M} a \tag{3.6}$$

Logarithmic differentiation with respect to time of (3.5) gives:

$$\frac{\dot{J}}{J} = \frac{\dot{m_1}}{m_1} + \frac{\dot{m_2}}{m_2} + \frac{1}{2}\frac{\dot{a}}{a} - \frac{1}{2}\frac{\dot{M}}{M} \tag{3.7}$$

We now have to consider the details of the mass transfer. We shall assume that the total mass M is conserved, and therefore that $\dot{m}_1 = -\dot{m}_2$. In this case equation (3.7) reduces to:

$$\frac{\dot{a}}{a} = \frac{2\dot{J}}{J} - \frac{2\dot{m}_2}{m_2}\left(1 - \frac{m_2}{m_1}\right) \tag{3.8}$$

The simplest case we can consider is that of **conservative** mass transfer, i.e. with $\dot{J} = 0$ (no viscous or gravitational wave torques). Let us assume that $m_2 \leq m_1$. We can see that if $\dot{m}_2 < 0$ then $\dot{a} > 0$, that is if mass is transfered from the less massive to the more massive star, then more matter is placed close to the centre of mass and so m_2 must move further out to conserve angular momentum. On the other hand mass transfer from the more massive to the less massive star would shrink the binary separation. However we also need to consider how the mass transfer occurs. We will assume that mass m_2 fills its Roche lobe and matter spills out from the inner Lagrangian point L_1. The distance b_1 of L_1 from the centre of the primary can be fitted with the formula of Plavec and Kratochvil [35]:

$$\frac{b_1}{a} = 0.500 - 0.227 \log m_2/m_1 \tag{3.9}$$

while for the mean radius of the Roche lobe (R_2 as it refers to the secondary star) we can use Paczynski's formula [35]:

$$R_2 = a\frac{2}{3^{4/3}}\left(\frac{q}{1+q}\right)^{1/3} \tag{3.10}$$

where $q = m_2/m_1$. If we logarithmically differentiate this we obtain:

$$\frac{\dot{R}_2}{R_2} = \frac{\dot{a}}{a} + \frac{\dot{m}_2}{3m_1} \tag{3.11}$$

therefore the Roche radius is also affected by the change in mass ratio and in the orbital separation. If we combine this with (3.8) we obtain:

$$\frac{\dot{R}_2}{R_2} = \frac{2\dot{J}}{J} - \frac{2\dot{m}_2}{m_1}\left(\frac{5}{6} - \frac{m_2}{m_1}\right) \tag{3.12}$$

It is clear from the above formula that (for conservative mass transfer) if $q < 5/6$ mass flowing from the less massive star ($\dot{m}_2 < 0$) will increase the Roche radius, thus ending the mass transfer. In the case $q > 5/6$ on the

other hand the Roche lobe will shrink onto the star, and unless this can contract quickly enough, the process will become very violent and stop when q becomes smaller than 5/6. However, this kind of violent mass transfer is not the kind we are interested in, as we shall later be studying binary systems in equilibrium. For mass transfer to be stable, as we shall see in the following, we need the system to **lose angular momentum**. The first mechanism we investigate is the emission of **gravitational waves**. In this case we would have, from the quadrupole formula:

$$\dot{J} = -\frac{32}{5}\sqrt{M}\frac{m_1^2 m_2^2}{a^{7/2}} \tag{3.13}$$

As an effect of emitting gravitational waves, the system would lose energy and angular momentum, and the two stars would spiral together, until the secondary fills its Roche lobe. At this point the mass transfer is self sustained if gravitational waves can remove enough angular momentum to stop the Roche lobe from growing faster than the stellar radius. It is therefore clear that we need an equation of state to know how the stellar radius will be affected by the mass loss. We will consider the case of a polytrope

$$r_2 = A m_2^{\gamma} \tag{3.14}$$

with various values for γ in order to describe different astrophysical objects. If we substitute (3.13) into (3.8) we obtain

$$\frac{\dot{a}}{a} = -\frac{64}{5}M\frac{m_1 m_2}{a^4} - \frac{2\dot{m}_2}{m_2}\left(1 - \frac{m_2}{m_1}\right) \tag{3.15}$$

If we now impose that the mass transfer be stable, i.e. that the star continues to fill its Roche lobe ($r_2 = R_2$) we have

$$a\frac{2}{3^{4/3}}\left(\frac{q}{1+q}\right)^{1/3} = A m_2^{\gamma} \tag{3.16}$$

which gives

$$a = \frac{A m_2^{\gamma - 1/3} M^{1/3} 3^{4/3}}{2} \tag{3.17}$$

By differentiating this equation we obtain

$$\dot{a} = \dot{m}_2(\gamma - 1/3)\frac{a}{m_2} \tag{3.18}$$

By using this equation and (3.8) we can write a set of first order differential equations for a, m_1 and m_2

$$\dot{a} = -(\gamma - 1/3)\frac{64}{5}\frac{Mm_1m_2}{a^3((\gamma - 1/3) + 2(1-q))} \tag{3.19}$$

$$\dot{m}_2 = -\frac{64}{5}\frac{Mm_1m_2^2}{a^4((\gamma - 1/3) + 2(1-q))} \tag{3.20}$$

$$\dot{m}_1 = -\dot{m}_2 \tag{3.21}$$

We can now consider the different **equations of state** we wish to use, in order to choose the parameter γ that enters the equations. One of the most interesting cases, which shall be discussed in the next chapter, is that of the Low Mass X-ray Binaries (LMXBs). In these systems the primary is a neutron star and the secondary is usually a white dwarf or a brown dwarf. We can approximate the equation of state of these stars with a $n = 3/2$ polytrope which gives $\gamma = -1/3$. Other interesting possibilities are listed below.

1. main sequence star
   $R \propto M$
2. white dwarf or brown dwarf as in [105]
   $\frac{R}{R_\odot} = 1.26 \times 10^{-2}(1+X)^{5/3}\left(\frac{M}{M_\odot}\right)^{-1/3}$
3. low density neutron star as in [57]
   $R = 15.12\left(\frac{M}{M_\odot}\right)^{-1/3}$
4. neutron star with $n = 1$ polytrope
   $R = const$
5. strange star as in [71] (ρ =constant)
   $R = AM^{1/3}$

3.4 Disc formation

Up to this point we have assumed that all the material that leaves the secondary is accreted directly onto the primary. Let us now consider more carefully the details of the mass transfer. As we have seen, material leaves the secondary star via the inner Lagrangian point L_1. From the point of view of the primary it is as if a nozzle were rotating around it

and squirting material. Unless the binary period is quite long the nozzle will rotate so rapidly that the material appears to be ejected almost orthogonally to the line of centres. In fact if we denote with $v_\perp$ the velocity orthogonal to the line of centres in a non-rotating frame, and with $v_{||}$ the velocity parallel to the line of centres, we have:

$$v_\perp \approx b_1 \omega \tag{3.22}$$

while

$$v_{||} \lesssim c_s \tag{3.23}$$

where c_s is the sound speed in the envelope of the secondary, as we can assume that the material will be pushed through the Lagrangian point by pressure forces. If matter is ejected orthogonally to the line of centres ($v_\perp \gg v_{||}$), it has a specific angular momentum

$$j = b_1^2 \omega \tag{3.24}$$

where ω is the angular velocity of the binary system. As the gas enters the Roche lobe of the primary the equipotential surfaces are essentially those due to the primary itself. The stream of gas will therefore orbit the primary at a distance determined by the angular momentum it carries. The gas will orbit at a frequency given by:

$$\Omega_g = \sqrt{\frac{m_1}{R_c^3}} \tag{3.25}$$

where the distance R_c is determined by conservation of angular momentum

$$R_c^2 \Omega_g = b_1^2 \omega \tag{3.26}$$

which inserting the Kepler frequency ω becomes

$$R_c = a(1+q)(b_1/a)^4 \tag{3.27}$$

and inserting the expression for b_1 (3.9)

$$R_c = a(1+q)[0.500 - 0.227 \log q]^4 \tag{3.28}$$

This is known as the *circularisation radius*, if it is smaller than the radius of the primary the gas will crash obliquely into the primary. Conversely, if it is located outside the star, then the gas stream will begin crossing itself as the stars orbit, and the viscous forces will dissipate energy and the gas will start falling towards the star. On the other hand viscous torques due

to the differential Keplerian rotation will transport angular momentum outwards. We thus have the formation of a disc of matter slowly spiralling towards the primary. The amount of angular momentum that can be stored in the disc will therefore affect the binary evolution. We can write the specific angular momentum carried by the ejected material as

$$\delta j = \dot{m}_2 a^{1/2} m_1^2 M_t^{-3/2} \tag{3.29}$$

(note that this term is removing angular momentum from the orbital motion because $\dot{m}_2$ is negative).
We can parametrise the amount of angular momentum lost to the disc by

$$\dot{J} = (1-f)\delta j \tag{3.30}$$

If viscous forces are efficient all the angular momentum is transfered back to the system and $f = 1$. In contrast $f = 0$ corresponds to the case in which all the angular momentum is stored in the disc. So if we now take

$$\dot{J} = -\frac{32}{5}\sqrt{M}\frac{m_1^2 m_2^2}{a^{7/2}} + (1-f)\dot{m}_2 \frac{m_1^2\sqrt{a}}{M_t^{3/2}} \tag{3.31}$$

and insert this in (3.7) we can, following the same procedure as before, obtain the set of equations:

$$\begin{aligned}
\dot{a} &= -(\gamma - 1/3)\frac{64}{5}\frac{M m_1 m_2}{a^3}\frac{1}{((\gamma-1/3)+2(1-q)-2m_1/M(1-f))} \\
\dot{m}_2 &= -\frac{64}{5}\frac{M m_1 m_2^2}{a^4}\frac{1}{((\gamma-1/3)+2(1-q)-2m_1/M(1-f))} \\
\dot{m}_1 &= -\dot{m}_2
\end{aligned} \tag{3.32}$$

As we have pointed out the parameter "f" will be 1 for conservative mass transfer (viscous torques in the disc transfer angular momentum back to the orbital motion). However for NS-NS binaries the donor star is disrupted within a few orbits, and there is not time for this viscous mechanism to take place, so a certain amount of angular momentum will be lost to the disc. For these cases we can approximate f with a numerical fit from [16]:

$$f = \frac{5}{3}q^{1/3} - \frac{3}{2}q^{2/3} \tag{3.33}$$

3.5 Stability revisited

We can now ask the question: how does the exchange of angular momentum with the disk affect the stability of mass transfer? Furthermore, is mass transfer stable for every choice of donor star mass, and how does the choice of the equation of state affect this? Following [16] we will plot the mass loss time scale $t_{ml} = -m_2/\dot{m}_2$ for a NS-NS binary, for various values of m_2. From the equations above we obtain

$$t_{ml} \approx \frac{1}{9}\left[\frac{d\ln R}{d\ln m_2} - \frac{1}{3} + 2\frac{(fm_1^2 - m_2^2)}{m_1 M}\right]\frac{M^{1/3}m_2^{2/3}}{m_1}\left(\frac{R}{m_2}\right)^{5/2} \tag{3.34}$$

Let us consider for example the case of an $n = 1$ polytrope, which gives a constant radius. Plotting t_{ml} we obtain figure (3.2): There is clearly

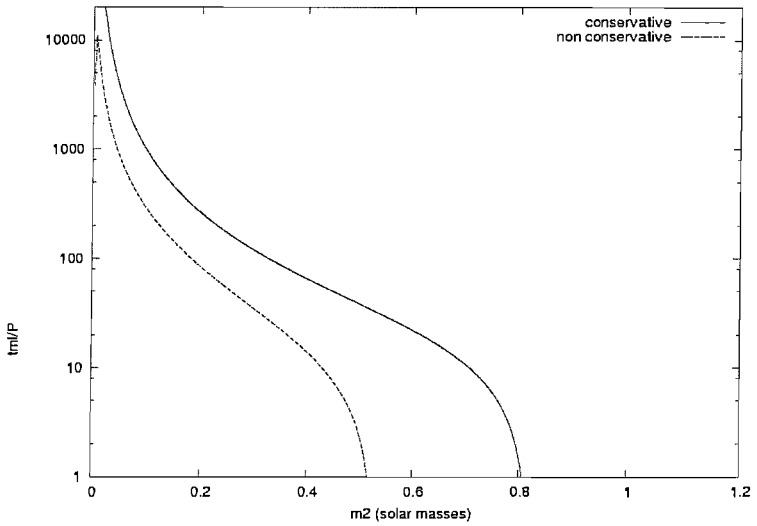

Figure 3.2: t_{ml} for an $n = 1$ polytrope, both in the conservative (c) and non-conservative (nc) case, the latter being when angular momentum is lost to the disk

a maximum mass for the donor star ($\approx 0.8M_\odot$) however there does not appear to be a minimum mass, and t_{ml} has an asymptote at $m_2 = 0$. This is the consequence of using a polytrope, as for this equation of state we can construct stars with arbitrarily small masses. Moreover, we can see that the maximum in the non-conservative case is also in the low mass region, where a n=1 polytrope is not a good approximation. Let us use a more reasonable equation of state, for example the Bethe-Johnson

V equation of state, to which we have fitted the analytical formula:

$$R = 0.004899 \left(\frac{m_2}{m_\odot}\right)^{-4.44661} + 11 \text{ km} \tag{3.35}$$

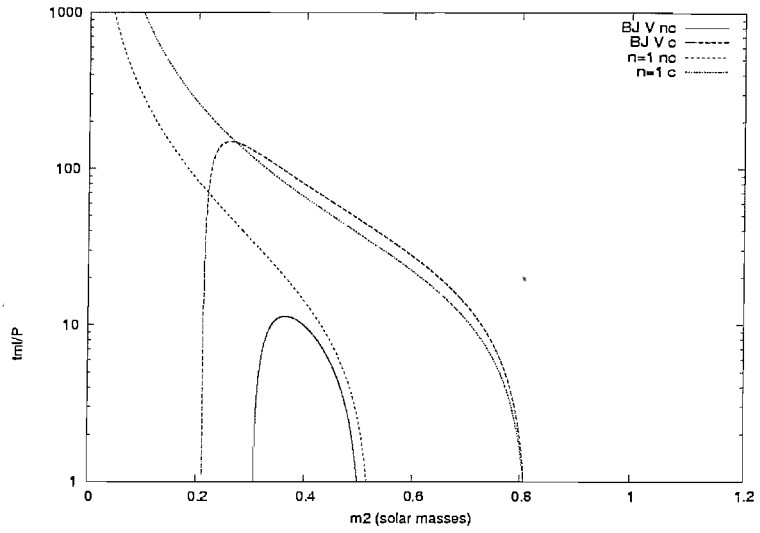

Figure 3.3: $t_m l$ for an n=1 polytrope, both in the conservative (c) and non-conservative (nc) case, the latter being when angular momentum is lost to the disk. We have both the results for the n=1 polytrope and for the Bethe-Johnson V (BJ V) equation of state

As is clear from figure 3.3 we can now have stable mass transfer for a donor mass between $0.2M_\odot$ and $0.8M_\odot$, with an even smaller parameter range for stable mass transfer in the non conservative case and, furthermore, in this case we would have very high values of $\dot{m}_2$, which would lead to the total disruption of the donor in a time scale of approximately 10 orbital periods.

3.6 Spin evolution

Another important consequence of the accretion is the fact that the central star will be spun up as it accretes angular momentum from the secondary, subtracting angular momentum from the orbital motion. This is a particularly interesting problem because we currently believe that the millisecond pulsars have been spun up by accretion in LMXBs. What

makes this problem particularly intriguing is the fact that the spins of the neutron stars appear to by clustered in a reasonably narrow range, well below 1 kHz, which is the break-up frequency for a typical neutron star. This would indicate that there is a mechanism at work providing a spin down torque that brings the system to equilibrium and gravitational waves have been suggested as a likely candidate. Luckily for this problem we do not need to consider the whole evolution of the system, but can treat $\dot{M}$ as a constant parameter, considering that for a typical LMXB it varies on long timescales (there are actually short term variations, but these will be discussed in the next chapter). The problem is complicated by the fact that we must consider the structure of the accretion disk, and take into consideration the effects due to the magnetic field of the neutron star. However the problem of the spin equilibrium of neutron stars in LMXBs will be considered in detail in the next chapter.

3.7 Conclusions

This chapter provides an introduction to the mechanisms that drive the evolution of binary systems. This problem is of particular interest for gravitational waves in two cases: that of white dwarf-white dwarf (WD-WD) binaries, and that of neutron star-white dwarf (NS-WD) binaries.

WD-WD binaries in our galaxies are some of the most important sources for the planned gravitational wave space antenna LISA and their number is so large that they are even expected to provide an unresolved background "noise" for the instrument. It is thus crucial to provide templates for the evolution of such systems, in order to detect the gravitational wave signal and extract information such as the distance and chirp mass of the system. Most studies to date have been carried out for detached WD-WD binaries, which are spiralling in as they lose angular momentum to gravitational radiation. Some of the interacting binaries, known from previous surveys, are, however, in the right frequency range and at the right distance to be a source for LISA [134]. The physics of these systems is not as "clean" as that of the detached binaries and, after the onset of accretion, mass transfer will play a part in the orbital evolution, causing the stars to spiral out and the orbital frequency to decrease. Tidal effects will also become important and the overall evolution of the system is likely to be driven by the competition of several processes [83]. If LISA is able to measure both the first and second derivative of the frequency it will be possible to test accurately whether a system is evolving purely due to radiation reaction or if accretion and tidal effects are

playing a role and, if this is the case, place constraints on models of WD binary evolution. If, however, only the first derivative of the frequency can be measured, then, unless one has an independent estimate of the distance, LISA will not be able to infer the chirp mass or distance of the system [134].

The main aim of this chapter is, however, to provide a background for the study of the LMXBs, in which a neutron star is accreting from a white dwarf companion. These systems are particularly interesting as they are thought to be the progenitors of the millisecond pulsars and, what is more, gravitational waves may be playing a role in their evolution. These arguments and the gravitational wave emission mechanisms will be studied in detail in the following chapters, so let us simply point out that the rapidly rotating neutron stars in these systems will be important sources for Advanced LIGO.

In order to model LMXBs the simple model presented in this chapter must clearly be refined. Recent work has been devoted to studying the importance that relativistic effects, due to the central neutron star, can have on the evolution of the system [2], [73]. These effects are, however, small compared to other uncertainties regarding the accretion process and the torque acting on the neutron star. In the next chapter we shall thus devote our attention to constructing a detailed model for such a torque and study the spin equilibrium of the LMXBs.

Chapter 4

Low Mass X-ray Binaries

In the last few years the evidence in favour of the notion that neutron stars are spun up to millisecond periods in accreting systems has strengthened significantly. The discovery of the millisecond X-ray pulsar SAX J1808.4-3658 in an accreting low-mass X-ray binary (LMXB) provided the long anticipated missing link between the general LMXB population and the millisecond radio pulsars. Since then four similar systems have been observed further strengthening the connection [155]. Furthermore, the link between the twin-peak separation of the kHz quasiperiodic oscillations seen in a number of systems and the spin of the neutron star has become somewhat clearer (although the underlying mechanism is still under debate) following the observation of QPOs in SAX J1808.4-3658. It now appears as if the QPO separation is either equal to or half the spin period [90].

When the first indications of rapidly spinning neutron stars in LMXBs were discussed more than five years ago, the results suggested that the systems were clustered in a surprisingly narrow range of spin frequencies 250-370 Hz. As such spin rates are far below the predicted break-up limit of about 1 kHz, the data pointed towards the presence of a mechanism that could counteract the accretion spin-up torque. The obvious candidate — the interaction between the accretion disk and the magnetosphere of the neutron star — was discussed in [153]. Their results seemed to indicate the need for a surprising link between the accretion rate and the magnetic field strength. Since there is no reason to expect such fine-tuning in these systems, Bildsten [18] argued that an additional spin-down mechanism may be in operation. He proposed that this torque could be provided by gravitational-wave emission, and that the required asymmetries would be induced in the neutron star crust by accretion. This idea echoed earlier suggestions by [108] and [146] that neutron stars

may reach a spin-equilibrium with gravitational waves balancing the accretion torque.

The possibility that accreting neutron stars may radiate gravitational waves is of great interest given the generation of groundbased interferometers (LIGO, GEO600, TAMA300 and VIRGO) that is now reaching design sensitivity. It has been recognized that there are three distinct mechanisms that may be able to generate gravitational waves at the required rate. First of all, a more detailed study by Ushomirsky suggests that the accretion induced crustal asymmetry proposed by Bildsten remains viable, as we shall see in the next chapter. The second possibility is that the stars spin fast enough that the gravitational-wave driven instability of the r-mode oscillations in the neutron star core is activated [7]. Finally, Cutler has suggested that an internal toroidal magnetic field could lead to unstable free precession resulting in the star "tipping over" and becoming an orthogonal rotator, an efficient gravitational-wave source [26].

Our present investigation is motivated by the following facts:

- The observational data has improved considerably since the original discussions in 1997-98. We now know that the LMXBs are not clustered in as narrow a range of spins as was originally thought, the current range being 250-620 Hz. It is relevant to ask to what extent the more recent data supports the need for an additional spin-down torque, eg. gravitational radiation, in these systems.

- A question that does not seem to have attracted much interest concerns whether a more refined model of the interaction between the accretion disk and the magnetosphere of the neutron star would be able provide a satisfactory description of the LMXBs. After all, many important physical mechanisms were not accounted for in the analysis of White and Zhang [153] and it may not be wise to refine the various gravitational-wave scenarios before their relevance is investigated.

- If we suppose that the LMXBs radiate gravitational waves at a relevant level, then we need to address many difficult issues associated with the detection of such signals. A key issue concerns the spin-evolution of the system. Can we assume that the spin-period remains stable on a time-scale of a few months? After all, the signal needs to be integrated for at least two weeks in order to be detectable in the noisy data-stream. If the system tends to wander,

as the data for slower spinning systems suggests [17], then we need to be able to model the accretion torque reliably.

We shall attempt to address the second of these points. We discuss the argument that an additional spin-down torque is needed in the LMXBs, and provide a more detailed accretion model that is able to describe these systems without particular fine-tuning of the magnetic field. From this exercise we conclude that it may not be appropriate to assume that the neutron stars in LMXBs radiate gravitational waves at a rate that exactly balances the accretion spin-up torque expected for a non-magnetic star. We do not think this should be taken as meaning that these systems are irrelevant for gravitational-wave physics. The proposed mechanisms for generating gravitational radiation should certainly still work. Yet, our discussion makes it clear that modelling these systems is significantly more difficult than has been assumed so far (at least in the gravitational-wave community). Of course, by constructing a more detailed accretion model, we are beginning to address this issue.

4.1 LMXBs and the "standard" accretion model

In the simplest models of accreting non-magnetic stars it is assumed that matter falling onto the surface of the star provides a torque proportional to the angular momentum associated with a Keplerian orbit at the stars equator;

$$N \approx \dot{M}\sqrt{GMR} \tag{4.1}$$

where M is the mass, R the radius and $\dot{M}$ the accretion rate. Despite it being well-known that this torque only provides an order-of-magnitude estimate, it has been used in most studies of gravitational waves from LMXBs so far (see [8] for a summary). The line of reasoning has been that, if the neutron star is at spin equilibrium, then the radiated gravitational waves provide an equal and opposite torque. The strength of the gravitational waves can be inferred from the X-ray luminosity, since (assuming that the gravitational potential released by the infalling matter is radiated as X-rays)

$$L_X \approx \frac{GM\dot{M}}{R} \tag{4.2}$$

provides a link between the observations and the mass accretion rate.

Accretion onto a magnetised star is different since the pressure of the infalling gas is counteracted by the magnetic pressure. By balancing these two pressures (for spherical infall) one obtains the so-called

magnetosphere radius

$$R_M \approx 7.8 \left(\frac{B_0}{10^8 \text{ G}}\right)^{4/7} \left(\frac{R}{10 \text{ km}}\right)^{12/7} \left(\frac{M}{1.4M_\odot}\right)^{-1/7} \left(\frac{\dot{M}}{\dot{M}_{\text{Edd}}}\right)^{-2/7} \text{ km} \tag{4.3}$$

inside which with the flow of matter is dominated by the magnetic field. For a strongly magnetised star the magnetic field is expected to channel the accreting matter onto the polar caps [35], while the situation may be more complex for a weakly magnetised object.

The maximum accretion rate we should expect follows from balancing the infalling gas pressure to that of the emerging radiation. This leads to the Eddington limit;

$$\dot{M}_{\text{Edd}} \approx 1.5 \times 10^{-8} \left(\frac{R}{10 \text{ km}}\right) \frac{M_\odot}{\text{yr}} \tag{4.4}$$

with associated X-ray luminosity

$$L_X \approx 1.8 \times 10^{38} \left(\frac{M}{1.4M_\odot}\right) \left(\frac{\dot{M}}{\dot{M}_{\text{Edd}}}\right) \text{ erg/s} \tag{4.5}$$

From this estimate we see that, for accretion at a fraction ϵ of the Eddington rate, eg. $\dot{M} = \epsilon \dot{M}_{\text{Edd}}$, the magnetic field must be accounted for (in the sense that $R_M > R$) as long as it is stronger than

$$B_0 \geq 1.6 \times 10^8 \epsilon^{1/2} \text{G} \tag{4.6}$$

Since observations indicate that rapidly rotating neutron stars have magnetic fields of the order of 10^8 G, and many transient LMXBs accrete with $\epsilon \sim 0.01$, we infer that the magnetic field is likely to play a role in these systems.

The interaction between a geometrically thin disk and the neutron star magnetosphere is a key ingredient in the standard model for accretion. The basic picture is that of a rotating magnetised neutron star surrounded by a magnetically threaded accretion disk. Accreting matter follows magnetic field lines and gives up angular momentum on reaching the surface, exerting a spin-up torque. The contribution of the magnetically threaded disk is, however, more complex. Interaction between the stellar field and the disk results in a positive torque for small radii, where the field lines rotate more slowly than the local Keplerian speed of the gas. The material torque at the inner edge of the disk is usually approximated by

$$N = \dot{M} \sqrt{GMR_M} \tag{4.7}$$

It is important to note that this torque can be significantly stronger than the rough estimate for non-magnetic stars.

Meanwhile, outside the co-rotation radius,

$$R_c \approx 17 \left(\frac{P}{1 \text{ ms}}\right)^{2/3} \left(\frac{M}{1.4 M_\odot}\right)^{1/3} \text{ km} \tag{4.8}$$

the field lines rotate faster than the local Keplerian speed, resulting in a negative torque. If $R_M > R_c$ the accretion flow will be centrifugally inhibited and matter may be ejected from the system. It is easy to see that this will happen if the spin period becomes very short, or the rate of flux of material onto the magnetosphere drops. This is known as the propeller regime. As accreting matter is flung away from the star in this phase, the star experiences a spin-down torque. To account for this effect we change the material torque according to

$$N = \dot{M} R_M^2 (\Omega_\text{K} - \Omega) = \dot{M} \sqrt{GMR_M} \left[1 - \left(\frac{R_M}{R_c}\right)^{3/2}\right] \tag{4.9}$$

where Ω is the spin frequency of the star and and Ω_K is the angular velocity of a particle in a Keplerian orbit;

$$\Omega_\text{K}(r) = \left(\frac{GM}{r^3}\right)^{1/2} \tag{4.10}$$

Even though this expression only accounts for the propeller regime in a phenomenological way, it accounts for the expectation that accretion will not spin the star up beyond the point where $R_M = R_c$. This leads to the equilibrium period

$$P_\text{eq} \approx 0.30 \left(\frac{B_0}{10^8 \text{ G}}\right)^{6/7} \left(\frac{R}{10 \text{ km}}\right)^{18/7} \left(\frac{M}{1.4 M_\odot}\right)^{-5/7} \left(\frac{\dot{M}}{\dot{M}_\text{Edd}}\right)^{-3/7} \text{ ms} \tag{4.11}$$

Conversely, given an observed spin period we can (assuming that the system is at equilibrium) deduce the neutron star's magnetic field. Comparing this estimate to observations, cf. Figure 4.1 and the data in Table 4.1, we see that the model leads to inferred magnetic fields that are in agreement with those of the millisecond radio pulsars for LMXBs accreting at the level of $10^{-2}\dot{M}_\text{Edd}$ and below. The model does not, however, perform well for systems accreting with $\dot{M} \approx \dot{M}_\text{Edd}$. The discrepancy is not large and there are of course many uncertainties in the data that could explain it Nevertheless, the conclusion drawn by Bildsten [18] is that there is a need for an additional spin-down torque in the systems that accrete at near-Eddington rates.

Source	Type	$\nu_{\rm psr}$ (Hz)	$\nu_{\rm burst}$ (Hz)	$\Delta\nu_{\rm QPO}$ (Hz)	$\dot{M}/\dot{M}_{Edd}$ (%)
SAX J1808.4-3658	P(T)	401 [158]	401 [22]	$\sim$ 200 [156]	4 [37]
XTE J1751-305	P(T)	435 [80]			11 [37]
XTE J0929-314	P(T)	185 [116]			3 [37]
XTE J1807-294	P(T)	191 [79]		$\sim$ 190 [82]	2 [37]
XTE J1814-338	P(T)	314 [78]	314 [136]		4 [37]
IGR J00291+5934	P(T)	599 [77]			5 [36]
4U 1608-522	A(T)		619 [49]	225–325 [87]	60 [39]
SAX J1750.8-2980	A(T)		601 [64]	$\approx$ 317 [101]	10 [39]
4U 1636-536	A		582 [42]	242–323 [60]	16 [39]
MXB 1658-298	U(T)		567 [157]		10 [39]
Aql X-1 (1908+005)	A(T)		549 [164]		50 [39]
KS 1731-260	A(T)		524 [130]	250–270 [160]	40 [39]
SAX J1748.9-2021	U(T)		410 [63]		25 [39]
4U 1728-34	A		363 [138]	274–350 [89]	7 [39]
4U 1702-429	A		330 [81]	328–338 [81]	6 [33]
4U 1916-053	A		270 [38]	290,348 [19]	7 [19, 128]
GX 340+0 (1642-455)	Z			280–410 [62]	$\sim$ 100 [33]
Cyg X-2 (2142+380)	Z			346 [159]	$\sim$ 100 [33]
4U 1735-44	A			296–341 [34]	15 [33]
4U 0614+09	A			240–360 [145]	1 [33]
GX 5-1 (1758-250)	Z			232–344 [61]	$\sim$ 100 [33]
4U 1820-30	A			230–350 [165]	30 [33]
Sco X-1 (1617-155)	Z			240–310 [86]	$\sim$ 100 [33]
GX 17+2 (1813-140)	Z			239–308 [52]	$\sim$ 100 [33]
XTE J2123-058	A(T)			255–275 [53, 143]	16 [53, 143]
GX 349+2 (1702-363)	Z			266 [166]	$\sim$ 100 [33]

Table 4.1: Data for rapidly rotating neutron stars (with spins above 100 Hz), with references given in square brackets. Source type classifications are P (pulsar), A (Atoll), Z (Z source) or U (Unknown) (Hasinger & van der Klis 1998, van der Klis 2005). (T) indicates that the source is transient. The frequencies given are pulsar spin frequency ($\nu_{\rm psr}$), burst oscillation frequency ($\nu_{\rm burst}$) and separation between the two kHz Quasi-Periodic Oscillations ($\Delta\nu_{\rm QPO}$). The accretion rates shown are estimates of maximum accretion rate, as discussed in the main text.

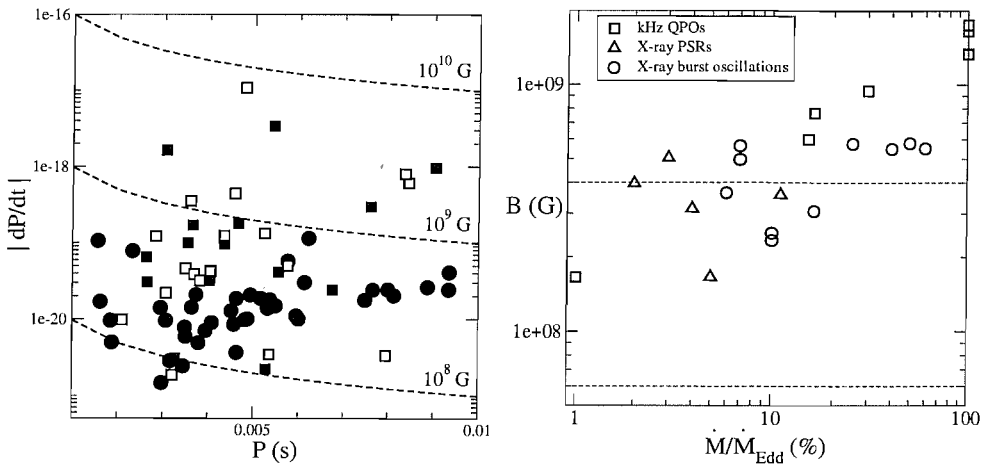

Figure 4.1: Comparing the neutron stars in LMXBs to the millisecond radio pulsar population. The left-hand panel shows the periods and spin-down rates of all millisecond radiopulsars (with periods below 10 ms). We distinguish between three sets: The millisecond pulsars in the galaxy, which are all seen to spin-down, are shown as black circles. Millisecond pulsar in globular clusters are shown as squares, the filled squares represent objects that are seen to spin down, while the open squares are objects which appear to spin up. The latter effect is likely due to motion relative to the core of the globular cluster [111]. The data in the figure suggests that the magnetic fields inferred for the globular cluster sample (from the standard dipole argument) is at best dubious. The right-hand panel relates the inferred magnetic fields for the accreting systems to the accretion rate compares the inferred magnetic fields (using the simplest estimate for the spin-equilibrium [Eq. (4.11)]) to the accretion rate (as a percentage of the Eddington rate). This figure indicates that the fields are most seriously overestimated for the fastest accreting systems. Systems showing burst oscillations are represented by open circles, data from systems where the spin period is estimated from the kHz peak separation are open squares and the accreting X-ray pulsars are shown as open triangles. We also indicate the (rough) range of magnetic fields for the galactic radio pulsars $6\times10^{7}-4\times10^{8}$ G. [Radio pulsar data from the radio pulsar catalogue http://www.atnf.csiro.au/research/pulsar/psrcat/ [76]. Accreting neutron star data determined from Table 4.1.]

4.2 A magnetically threaded disk

The interaction between an accretion disk and a spinning compact object involves much poorly known physics. The key issues were discussed in a number of seminal papers in the late 1970s (see Frank,King and Raine [35] for an excellent introduction). Although much effort has been invested in this area of research since then — after all, accretion is a cornerstone of astrophysics — these early papers remain the "standard" description of the problem.

In this Section we will focus on the contribution to the accretion torque from a magnetically threaded, thin disk. Our description is based on the work by [147, 149] and [162, 163, 161].

We begin by pointing out that our previous description of the accretion problem was somewhat inconsistent since our various estimates, eg., of the size of the magnetosphere, were based on spherical infall of matter. The model can be improved, albeit at the cost of introducing several largely unknown parameters. First of all, we need a description of the viscosity on the disk. Viscosity is the main agent that dissipates energy and angular momentum, and thus enables matter to flow towards the central object. Since the microphysical viscosity is unknown it is common to use the so-called α-viscosity introduced by [126], i.e. let the kinematic viscosity be parametrised as

$$\nu = \alpha c_s H = \alpha \frac{c_s^2}{\Omega_{\rm K}} \tag{4.12}$$

Here c_s is the sound speed in the disk, $H \sim c_s/\Omega_{\rm K}$ is the vertical scale height. In this description, ν is a function of r since both c_s and $\Omega_{\rm K}$ vary with position, but α is taken to be constant. In effect, this leads to a model where the viscosity ensures that the disk remains Keplerian as matter is transferred through the disk.

In the case of a magnetically threaded disk, we need to provide a description of the interaction between the disk flow and the magnetic field. Figure 4.2 provides a schematic illustration of the problem. To provide a detailed model of this complicated physics problem is, however, not a simple task. Nevertheless, one may hope that a somewhat simplistic description will be able to capture the main features of the complete problem.

Let us consider the φ-component of the Euler equations for the disk flow

$$\frac{\partial}{\partial r}(r\rho v_r \Omega r^2) + \frac{\partial}{\partial z}(r\rho v_z \Omega r^2) = \frac{\partial}{\partial r}\left(\rho\nu r^3 \frac{\partial \Omega}{\partial r}\right) + \frac{r^2}{4\pi}\frac{\partial}{\partial z}(B_z B_\varphi) \tag{4.13}$$

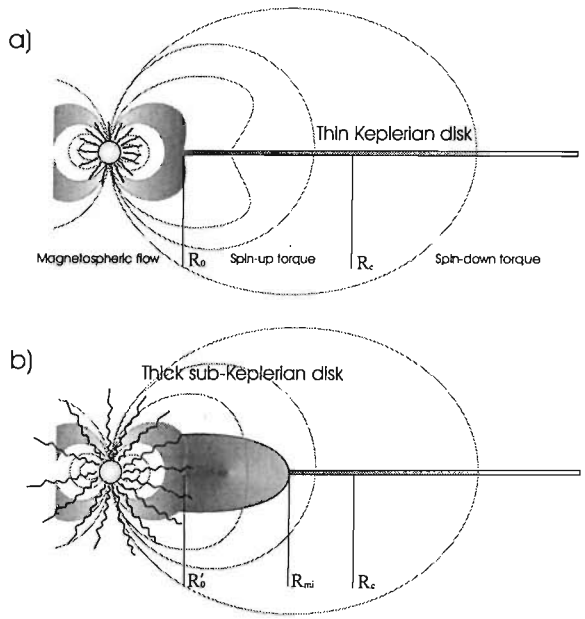

Figure 4.2: A schematic illustration of the accretion problem for a magnetically threaded disk. a) The standard thin disk picture, see [35]. b) The proposed model for rapidly accreting systems. Radiation pressure leads to a thick, sub-Keplerian disk in the inner region.

integrating this in the vertical direction yields

$$-\dot{M}\frac{d}{dr}(\Omega_K r^2) = r^2 B_z B_\varphi + \frac{d}{dr}\left(2\pi r^3 \nu\Sigma\frac{d\Omega}{dr}\right) \tag{4.14}$$

where we have defined

$$\Sigma(r) = \int_{z^-}^{z^+} \rho dz = 2\int_0^{z^+} \rho dz \tag{4.15}$$

and

$$\dot{M} = -4\pi \int_0^{z^+} r\rho v_r dz \tag{4.16}$$

In a steady state, where there is no net transfer of angular momentum to and from the star, (4.16) can be integrated to give:

$$-\dot{M}(\Omega_K r^2) - 2\pi r^3 \nu\Sigma\frac{d\Omega}{dr} - \int_{R_0}^{r} r^2 B_z B_\varphi dr = 0 \tag{4.17}$$

where R_0 represents the inner edge. If we now assume that the velocity profile is maintained Keplerian mainly by the viscosity (cfr. 10.2.4 of [88]) we can neglect the magnetic term and obtain the estimate

$$\nu\Sigma = \dot{M}/3\pi \tag{4.18}$$

We can now use this estimate in (4.16) to find the radius at which magnetic stresses balance the magnetic and material stresses. We thus find

$$\dot{M}\frac{d}{dr}\left[\Omega_{\mathrm{K}}(r) r^2\right] = -r^2 B_\varphi B_z \tag{4.19}$$

The mass transfer rate $\dot{M}$, which will be assumed constant throughout the disk. This relation illustrates the difficulty involved in constructing a consistent model. If we consider a thin accretion disk, then the z-component of the magnetic field can be taken to be that associated with a rotating dipole

$$B_z = -\frac{\mu}{r^3} = -B_0\left(\frac{R}{r}\right)^3 \tag{4.20}$$

where B_0 is the surface field of the star. Even though the field may be much more complicated close to the stellar surface the dipole contribution will dominate far away. The problem is associated with B_φ. This component, which vanishes in the absence of a disk, represents the degree to which the magnetic field is dragged along with the matter flow. It is

this interaction which leads to the torque on the star that we are aiming to model.

From the MHD induction equation we find that

$$\partial_t B_\varphi \approx \frac{B_\varphi}{\tau_\varphi} \approx \nabla \times (\vec{v} \times \vec{B}) = \gamma(\Omega - \Omega_{\rm K}) B_z \tag{4.21}$$

where the star (and the magnetic field) is rotating at the constant rate Ω. In this equation, it is assumed that the disk flow changes from quasi-rigid to Keplerian over a lengthscale R/γ. Wang [149] has considered several different mechanisms for the timescale τ_φ (and by implication the toroidal component of the magnetic field). He concludes that the various models lead to quite similar predictions for the accretion torque. This is fortunate, since it means that the model is not very sensitive to the unknown physics. Here we will assume that the main mechanism that prevents the field from being dragged along with the flowing matter is turbulent diffusion. This leads to [149],

$$\tau_\varphi \approx \frac{H}{\alpha c_s} \approx \frac{1}{\alpha \Omega_{\rm K}} \tag{4.22}$$

and consequently

$$B_\varphi \approx \frac{\gamma}{\alpha} \frac{\Omega - \Omega_{\rm K}}{\Omega_{\rm K}} B_z \tag{4.23}$$

We can now return to Eq. (4.19) and determine the "inner" edge of the accretion disk R_0, at which the matter flow departs significantly from a Keplerian profile;

$$\left(\frac{R_0}{R_c}\right)^{7/2} = \frac{2N_c}{\dot{M}\sqrt{GMR_c}} \left[1 - \left(\frac{R_0}{R_c}\right)^{3/2}\right] \tag{4.24}$$

where R_c is the co-rotation radius and we have defined

$$N_c = \frac{\gamma}{\alpha} \frac{\mu^2}{R_c^3} = \frac{\gamma}{\alpha} B_z^2 R_c^3 \tag{4.25}$$

Comparing the radius R_0 to the previously determined magnetosphere radius R_M we find that, in the case $R_0 << R_c$, we have

$$R_0 \approx \left(\frac{4\gamma}{\alpha}\right)^{2/7} R_M \approx 1.5 R_M \tag{4.26}$$

where we have taken $\alpha \approx \gamma \approx 1$ in the last step. We will use these as our canonical values throughout the chapter. It should, of course, be noted

that both α and γ are largely unknown. In a sense, they can be viewed as free parameters that can be fixed by comparing to observed data. In addition, there are many uncertainties (at the level of factors of order unity) in this model.

We can also account for the torque due to the magnetically threaded disk outside R_0. The corresponding torque follows (essentially) from integrating Eq. (4.19) and we get

$$N_{\rm disk} = -\int_{R_0}^{\infty} B_\varphi B_z r^2 dr = -\frac{N_c}{3}\left[2\left(\frac{R_c}{R_0}\right)^{3/2} - \left(\frac{R_c}{R_0}\right)^3\right] \qquad (4.27)$$

As discussed previously, the region $R_0 < r < R_c$ contributes a (positive) spin-up torque, while the region $R_c < r < \infty$ provides a (negative) spin-down torque, cf. Figure 4.2.

Finally, assuming that the matter gives up all its angular momentum (relative to the frame of the star) upon reaching R_0, i.e. that the matter flows along the field lines like "beads on a wire" in the region where the magnetic field dominates the flow, we find that the total accretion torque is

$$\begin{aligned} N &= \dot{M}\sqrt{GMR_0}\left[1 - \left(\frac{R_c}{R_0}\right)^{3/2}\right] + N_{\rm disk} \\ &= \frac{1}{3}\dot{M}\sqrt{GMR_0}\left[\frac{7/2 - 7(R_0/R_c)^{3/2} + 3(R_0/R_c)^3}{1-(R_0/R_c)^{3/2}}\right] \end{aligned} \qquad (4.28)$$

This result shows that the system reaches spin-equilibrium ($N = 0$) when

$$\left(\frac{R_0}{R_c}\right)^{3/2} = \frac{7-\sqrt{7}}{6} \longrightarrow R_0 \approx 0.8 R_c \qquad (4.29)$$

This should be compared to the result of [149]. The difference arises from the fact that Wang uses Eq. (4.7) rather than Eq. (4.9) for the material torque at the inner edge of the disk (now at R_0 instead of R_M).

Having added the spin-down torque exerted on the star by the outer parts of the disk we find that the system reaches equilibrium slightly before R_0 reaches R_c. Nevertheless, the predicted spin-period at equilibrium

$$P_{\rm eq} \approx 0.44\left(\frac{\alpha}{\gamma}\right)^{-3/7}\left(\frac{B_0}{10^8\ {\rm G}}\right)^{6/7}\left(\frac{R}{10\ {\rm km}}\right)^{18/7}\left(\frac{M}{1.4M_\odot}\right)^{-5/7}\left(\frac{\dot{M}}{\dot{M}_{\rm Edd}}\right)^{-3/7} {\rm ms} \qquad (4.30)$$

does not differ much from the more naive prediction provided by Eq. (4.11).

In order to proceed we note that the viscosity parameter α is usually assumed to lie in the range $0.01 - 0.3$ [35], while γ has been assumed to be of order unity [147]. If we consider values in this range, what does the model imply for the magnetic fields of the accreting LMXB neutron stars? From Eq. (4.30) we find that a canonical neutron star will have equilibrium of 3 ms if

$$B_0 \approx 9.4 \times 10^8 \left(\frac{\alpha}{\gamma}\right)^{1/2} \left(\frac{\dot{M}}{\dot{M}_{\rm Edd}}\right)^{1/2} \ {\rm G} \tag{4.31}$$

We see that for $\alpha/\gamma \approx 0.1$ a star accreting at the Eddington rate is predicted to have a magnetic field within the range deduced for the millisecond radiopulsars. On the other hand, a star accreting at 1% of this rate will require a larger value of order $\alpha/\gamma \approx 1$ in order to lie in the range indicated in Figure 4.1. This means that the inclusion of the torques from a magnetically threaded thin disk is, in principle, sufficient to remove the direct need for an addition spin-down mechanism like gravitational radiation in these systems. Of course, this is achieved at the cost of introducing the poorly constrained parameters α and γ. If we want to adjust these parameters in such a way that the inferred magnetic fields agree with those for the radio pulsars in Figure 4.1 we essentially need to introduce a suitable $B_\varphi = B_\varphi(\dot{M})$. Despite this possibility, we do not think that the thin-disk model is entirely satisfactory. As we will argue in the next section, additional physics should be included in order to describe the fastest accreting systems. In essence, this means that we will only rely on the thin disk model for systems accreting below a few percent of the Eddington rate. From the above estimates we see that these systems are adequately described if we take $\alpha/\gamma \approx 1$. Hence, this will be our canonical value from now on.

4.3 Thick disks near Eddington accretion

The thin disk model we have discussed so far is able to explain many features of accreting neutron star systems. Yet, as indicated above, it seems to fail for rapidly spinning stars accreting near the Eddington limit. Given this, it is meaningful to ask what the crucial missing piece of physics is in our model. At this point, the most naive assumption in our discussion concerns the accretion torque arising from the inner edge of the disk, at R_0. While it seems reasonable to assume that the matter

moves along the magnetic field lines in the inner region for low rates of accretion, it is not so clear that this model will work for faster accretors. Several mechanisms may alter this picture. Obvious possibilities are: radiation pressure from the emerging X-rays, the near balance between centrifugal and gravitational forces for rapidly spinning stars, heating of the disk in the inner region etcetera.

As a first stab at including these effects we will consider the radiation pressure. Let us consider the equations we need to solve to find an equilibrium disk solution [35]

$$\begin{cases} 1. & \rho = \Sigma/H; \\ 2. & H = c_s R^{3/2}/(GM)^{1/2}; \\ 3. & c_s^2 = P/\rho; \\ 4. & P = \frac{\rho k T_c}{\mu m_p} + \frac{4\sigma}{3c} T_c^4; \\ 5. & \frac{4\sigma T_c^4}{3\tau} = \frac{3GM\dot{M}}{8\pi R^3}\left[1 - \left(\frac{R_\odot}{R}\right)^{1/2}\right]; \\ 6. & \tau = \Sigma k_R(\rho, T_c) = \tau(\Sigma, \rho, T_c); \\ 7. & \nu\Sigma = \frac{\dot{M}}{3\pi}\left[1 - \left(\frac{R_\odot}{R}\right)^{1/2}\right]; \\ 8. & \nu = \nu(\rho, T_c, \Sigma, \alpha, ..). \end{cases} \tag{4.32}$$

Here c_s is the sound speed, ρ the density, k is Boltzmann's constant, σ is Stefan-Boltzmann's constant, m_p is the mass of the proton, μ is the mean molecular weight and k_R is the opacity. In order to solve the set of equations we have to give a prescription for ν for example the "alpha" prescription:

$$\nu = \alpha c_s H \tag{4.33}$$

We must also give a prescription for the opacity. In the outer regions we expect Kramers opacity (mainly caused by free-free processes) to be the dominant mechanism [35], while in the inner regions Thomson scattering becomes dominant. In fact we can take the Thomson opacity

$$K_R(\text{Thomson}) = \sigma_{Th}/m_p = 0.4\text{cm}^2\text{g}^{-1} \tag{4.34}$$

and the Kramers opacity

$$K_R(\text{Kramers}) = 6.6 \times 10^{22} \rho T_c^{-7/2} \text{cm}^2\text{g}^{-1} \tag{4.35}$$

We can now solve the equations assuming that the disc is gas pressure dominated and that Kramers opacity is the dominant mechanism. One can then use the solution to show that Thomson opacity becomes dominant at a radius $R \lesssim 2500 \left(\frac{\dot{M}}{10^{16} g s^{-1}}\right)^{2/3} \left(\frac{M}{M_\odot}\right)^{1/3} f^{8/3}\text{km}$, in a region

where the disc is still gas pressure dominated. We can then show that, in the region where Thomson opacity is dominant, radiation pressure balances the gas pressure at a radius

$$R_{mi} \approx 880\alpha^{2/21}\left(\frac{\dot{M}}{\dot{M}_{\rm Edd}}\right)^{16/21}\left(\frac{M}{1.4M_\odot}\right)^{1/3} f^{64/21}\ {\rm km} \tag{4.36}$$

where

$$f = \left[1-\left(\frac{R_\odot}{R}\right)^{1/2}\right]^{1/4} \tag{4.37}$$

Inside this radius radiation pressure will be dominant. However, it is easy to show that the factor involving f will be near unity apart from in the absolute vicinity of the stellar surface. In fact if we try to solve the expression above by expanding in the small factor $\frac{R}{R_M}$ we obtain, defining

$$Z \approx 880\alpha^{2/21}\left(\frac{\dot{M}}{\dot{M}_{\rm Edd}}\right)^{16/21}\left(\frac{M}{1.4M_\odot}\right)^{1/3}\ {\rm km} \tag{4.38}$$

for R_{mi}

$$R_{mi} \approx Z - R_\odot \tag{4.39}$$

We can use this solution to test the validity of the approximation, i.e. check where $R_\odot/R_{mi} \ll 1$. This is easily satisfied for accretion rates greater than $\approx 0.2\dot{M}_{Edd}$, for which $R_\odot$ is also negligible compared to Z. For the high accretion rates we will be interested in we can then safely take $f = 1$, and use:

$$R_{mi} \approx 880\alpha^{2/21}\left(\frac{\dot{M}}{\dot{M}_{\rm Edd}}\right)^{16/21}\left(\frac{M}{1.4M_\odot}\right)^{1/3}\ {\rm km} \tag{4.40}$$

as a good approximation. Let us contrast this to the standard radius of the magnetosphere, R_M. We find that $R_{mi} = R_M$ when

$$\left(\frac{\dot{M}}{\dot{M}_{\rm Edd}}\right) \approx 2\times 10^{-2}\alpha^{-1/11}\left(\frac{B_0}{10^8{\rm G}}\right)^{6/11} \tag{4.41}$$

The key lengthscales in the problem are illustrated in Fig. 4.3. This figure shows that, for a neutron star with a weak magnetic field (a typical millisecond pulsar) radiation pressure will be important for accretion rates above a few percent of the Eddington rate.

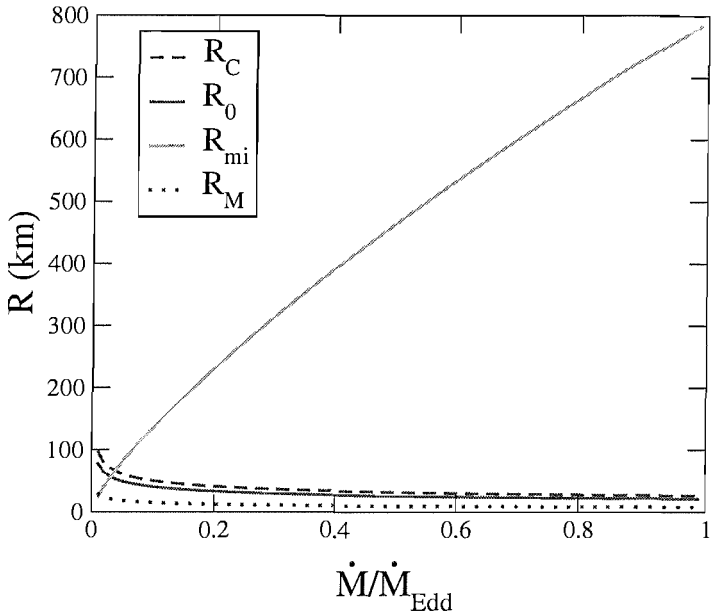

Figure 4.3: The main lengthscales in the accretion problem. The relevant parameters are taken to be $\alpha = 1$, $P = 3$ ms and $B_0 = 10^8$ G. The standard magnetosphere radius (for spherical accretion) R_M is shown as a thin dashed line, and the corresponding radius for a thin magnetically threaded disk R_0 is a thin solid line. The co-rotation radius R_c, at which a Keplerian disk co-rotates with the star, is a thick dashed line. Finally, the distance at which radiation pressure balances gas pressure R_{mi} is shown as a thick solid line. The figure shows clearly that $R_{mi} >> R_c > R_0 > R_M$ above a few percent of the Eddington accretion rate. This suggests that radiation pressure must be accounted for, likely leading to a thickening of the disk and a sub-Keplerian flow in the inner region.

We thus have to ask how the radiation pressure affects the model outlined in the previous section. Phenomenologically, the disk is likely to expand leading to the flow becoming sub-Keplerian. In fact, that the thin disk model is unstable in a region where the radiation pressure dominates the gas pressure was demonstrated a long time ago in [72] (see also [127]). In order to account for this quantitatively, let us consider the following model. The thin disk description is relevant outside R_{mi}, and hence describes systems accreting below the critical rate. For faster accretors, there will exist an inner region inside R_{mi} where the disk is no longer thin. To model this region we follow Yi et al.[162], and assume that the flow is such that $\Omega = A\Omega_{\rm K}$ with $A \leq 1$. It should be noted that the study in [162] pertains to advection dominated accretion below a critical accretion rate, while our model concerns radiation pressure dominated disks above a critical accretion rate. This may seem a cause for concern, especially since advection dominated flows are almost exclusively used in discussions of slowly accreting systems. However, as pointed out in [98] the corresponding solution the equations describing the accretion problem is likely to be relevant also for rapid accretion. Furthermore, the model is sufficiently simple to serve our present purposes.

Repeating the arguments from the thin disk analysis, we find a new co-rotation radius $A^{2/3}R_c$ and the inner edge of the thick disk region R_0' is determined from

$$\left(\frac{R_0'}{A^{2/3}R_c}\right)^{7/2} = \frac{2N_c'}{A^{4/3}\dot{M}\sqrt{GMR_c}}\left[1 - \frac{1}{A}\left(\frac{R_0'}{R_c}\right)^{3/2}\right] \tag{4.42}$$

where we have defined

$$N_c' = \frac{\gamma}{\alpha}\frac{\mu^2}{A^2R_c^3} = \frac{\gamma}{\alpha}B_z^2A^2R_c^3 \tag{4.43}$$

The torque from the inner disk region is now determined from

$$N_{\rm thick} = -\int_{R_0'}^{R_{mi}} B_\varphi B_z r^2 dr = \frac{\mu^2\gamma}{\alpha}\int_{R_0'}^{R_{mi}} \frac{1}{r^4}\left[1 - \frac{1}{A}\left(\frac{r}{R_c}\right)^{3/2}\right] dr \tag{4.44}$$

while the outer (thin) disk contributes a torque

$$N_{\rm thin} = -\int_{R_{mi}}^{\infty} B_\varphi B_z r^2 dr = \frac{\mu^2\gamma}{\alpha}\int_{R_{mi}}^{\infty} \frac{1}{r^4}\left[1 - \left(\frac{r}{R_c}\right)^{3/2}\right] dr \tag{4.45}$$

Working out the algebra, we find that the total torque can be written

$$N = \dot{M}\sqrt{GMR_0'}\frac{A}{1-\bar{\omega}}\left\{\frac{7}{6} - \frac{7\bar{\omega}}{3} + \bar{\omega}^2 + \frac{A(1-A)}{3}\left(\frac{R_c}{R_{mi}}\right)^{3/2}\bar{\omega}^2\right\} \tag{4.46}$$

where

$$\bar{\omega} = \frac{1}{A}\left(\frac{R_0'}{R_c}\right)^{3/2} \tag{4.47}$$

In this slightly more complicated model, the system will reach spin-equilibrium when

$$\frac{7}{6} - \frac{7\bar{\omega}}{3} + \bar{\omega}^2 + \frac{A(1-A)}{3}\left(\frac{R_c}{R_{mi}}\right)^{3/2}\bar{\omega}^2 = 0 \tag{4.48}$$

Since we must have $R_0' < R_{mi}$ we are always interested in the smallest of the two roots to this quadratic. The problem simplifies considerably if we note that

$$\frac{R_c}{R_{mi}} \approx 2 \times 10^{-2}\alpha^{-2/21}\left(\frac{\dot{M}}{\dot{M}_{\rm Edd}}\right)^{-16/21}\left(\frac{P}{1\ {\rm ms}}\right)^{2/3} \tag{4.49}$$

for a canonical neutron star, cf. Fig. 4.3. This means that, for a sizeable fraction of the Eddington accretion rate and millisecond spin periods, we have equilibrium when

$$\bar{\omega} \approx \frac{7-\sqrt{7}}{6} \longrightarrow R_0' \approx 0.8A^{2/3}R_c \tag{4.50}$$

From this we can infer the spin period at equilibrium;

$$P_{\rm eq} \approx 0.44A^{-10/7}\left(\frac{\alpha}{\gamma}\right)^{-3/7}\left(\frac{\dot{M}}{\dot{M}_{\rm Edd}}\right)^{-3/7}\left(\frac{B_0}{10^8\ {\rm G}}\right)^{6/7}\left(\frac{M}{1.4M_\odot}\right)^{-5/7}\left(\frac{R}{10\ {\rm km}}\right)^{18/7}\ {\rm ms} \tag{4.51}$$

This result differs from the thick-disk model only by the factor of A. However, it is easy to see that the predicted equilibrium spin periods may be significantly different for small values of A.

At this point it is worth mentioning the work of Yi et al. ([161] and [163]) where similar results are obtained for more slowly accreting and spinning X-ray pulsars assumed to accrete through an advection dominated flow.

To complete the thick disk model, we need to estimate the coefficient A which describes the nature of the sub-Keplerian flow. To do this, we consider the radial Euler equation which can be written

$$v_r\frac{\partial v_r}{\partial r}+v_z\frac{\partial v_r}{\partial z}-\frac{v_\varphi^2}{r}=-\frac{1}{\rho}\frac{\partial}{\partial r}\left(p+\frac{B^2}{8\pi}\right)-\frac{GM}{r^2}+\frac{1}{4\pi\rho}\left[(\vec{B}\cdot\nabla)B_r-\frac{B_\varphi^2}{r}\right] \tag{4.52}$$

For a thin disk this simplifies to

$$v_r\frac{\partial v_r}{\partial r}-\frac{v_\varphi^2}{r}\approx-\frac{1}{\rho}\frac{\partial}{\partial r}\left(p+\frac{B^2}{8\pi}\right)-\frac{GM}{r^2}+\frac{B_\varphi^2}{4\pi\rho r} \tag{4.53}$$

This equation will remain approximately relevant in the case of a thick disk provided that it is interpreted as a height average [99, 100]. Apart from very near the Eddington accretion rate the dominant velocity component is v_φ. The situation near $\dot{M}_{\rm Edd}$ is complicated by the fact that the matter in the disk becomes highly virialised. In our thick disk model, we expect the radiation pressure to dominate in the region $R_0'<r<R_{mi}$. (It is worth noting the difference between the radial and azimuthal Euler equations here. In the latter the axisymmetric radiation pressure will not play a role and the magnetic stress terms dominate.)

We express the radiation pressure gradient in terms of the co-moving radiation flux L_{co} [91, 95]

$$\frac{dp_{\rm rad}}{dr}=-\frac{k\rho}{c}\frac{L_{co}}{4\pi r^2} \tag{4.54}$$

where k is the opacity of the matter. Since the Eddington luminosity follows from

$$L_{\rm Edd}=\frac{4\pi GMc}{k} \tag{4.55}$$

we have

$$\frac{dp_{\rm rad}}{dr}=-\rho\frac{GM}{r^2}\frac{L_{co}}{L_{\rm Edd}} \tag{4.56}$$

Using this relation in Eq. (4.53) we see that the velocity profile becomes sub-Keplerian with

$$v_\varphi\approx A\sqrt{\frac{GM}{r}}\qquad\text{where}\qquad A=\sqrt{1-\frac{L_{co}}{L_{\rm Edd}}} \tag{4.57}$$

As a rough approximation we can assume that the co-moving flux is equal to the stationary flux observed at infinity $L_X=GM\dot{M}/d$ where d is the distance to the source. Then

$$\frac{L_{co}}{L_{\rm Edd}}\approx\frac{\dot{M}}{\dot{M}_{\rm Edd}} \tag{4.58}$$

and we see that

$$v_\varphi \approx Ar\Omega_K \quad \text{with} \quad A = \sqrt{1 - \frac{\dot{M}}{\dot{M}_{\rm Edd}}} \tag{4.59}$$

The results we obtain by combining this approximation with the predicted equilibrium period for the thick disk model are illustrated in Figure 4.4. This figure shows that the thick disk model leads to significantly longer equilibrium spins for rapidly accreting systems. Conversely, we can use Eq. (4.51) to deduce that a system will have an equilibrium period of 3 ms if

$$B_0 \approx 9.4 \times 10^8 \left(\frac{\alpha}{\gamma}\right)^{1/2} \left(\frac{\dot{M}}{\dot{M}_{\rm Edd}}\right)^{1/2} \left(1 - \frac{\dot{M}}{\dot{M}_{\rm Edd}}\right)^{5/6} \ {\rm G} \tag{4.60}$$

This tells us that a system accreting at 90% of the Eddington rate should have a magnetic field of $B \approx 1.4 \times 10^8$ G. A field of this strength would put this system well within the range of fields inferred for the millisecond radio pulsars, cf. Figure 4.4. The figure shows that our thick disk model leads to predicted magnetic fields for the LMXBs which accord well with those of the galactic millisecond radio pulsars. (In order to infer the magnetic fields shown in Figure 4.4 we have assumed that the fastest accreting systems have $\dot{M} = 0.95\dot{M}_{\rm Edd}$. This is somewhat ad hoc, but it should be noted that the model breaks down, in the sense that $A \to 0$ which leads to $P_{\rm eq}$ diverging, as $\dot{M} \to \dot{M}_{\rm Edd}$. There is also significant uncertainty in the accretion rates given in Table 4.1.)

The fact that radiation pressure will affect accretion disk structure, and hence the spin period of neutron stars in LMXBs, has previously been discussed by several authors ([152, 40, 41], see also [92, 114]). These models, like ours, give lower inferred magnetic fields for high accretion rate sources when radiation pressure is taken into account. One issue associated with the previous models is that if one assumes spin equilibrium, the models predict a strong correlation between magnetic field and accretion rate (see for example Eq. (25) of [92]). No direct measurements of LMXB magnetic fields have yet been made, so this correlation cannot be tested, but the physical basis for such a strong relation is at best unclear. In fact, this has been one of the arguments against magnetic spin equilibrium models [18, 144]. The model outlined in this paper also predicts a correlation between magnetic field and accretion rate. The "dependence" of B on $\dot{M}$ is however weaker, due to the dependence on accretion rate of the factor A. This illustrates that small modifications to the accretion

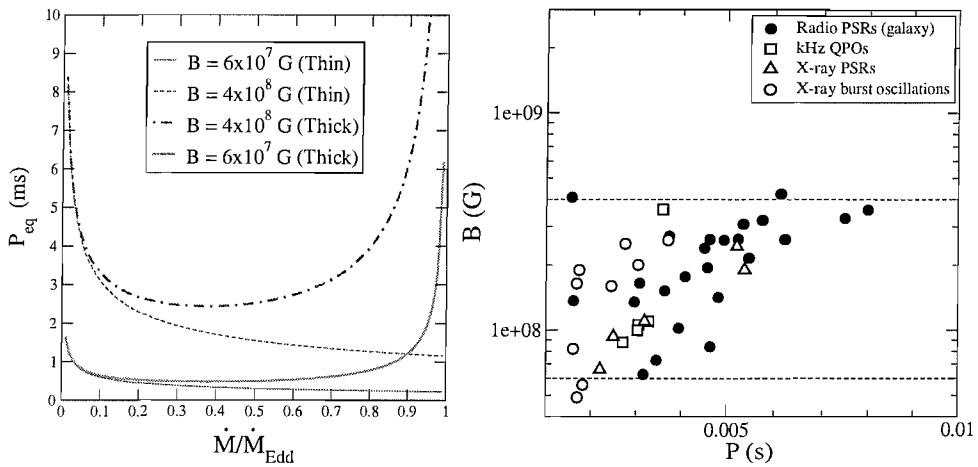

Figure 4.4: The predicted spin periods at equilibrium for the thick disk model, for $\alpha = \gamma = 1$. In the left panel we show $P_{\rm eq}$ as function of the accretion rate for magnetic field which bracket the range for the millisecond radio pulsars: $B = 6 \times 10^7$ G (thick dashed curve) and $B = 4 \times 10^8$ G (thick solid curve). For comparison we also show the prediction of the naive model where spinup ceases at $R_c = R_M$ (thin solid curve). The right panel compares the inferred magnetic fields for LMXBs to those of the radio pulsars.

model may be able to remove some of the perceived difficulties associated with magnetic equilibrium models.

We conclude this section with a brief discussion of the observational consequences of this model with regard to the detection of X-ray pulsars. Naively one expects the X-ray pulsars to have higher inferred magnetic fields than the other, non-pulsing, LMXBs [25]. As is clear from Figure 4.4, the thick disk model does not lead to the pulsars clustering at higher magnetic fields than the other sources. One possibility, suggested by [142], is that we are prevented from seeing pulsations in many systems due to atmospheric scattering. A preliminary study by [66] suggests that the scattering hypothesis may not be borne out by the data, but this is an area of ongoing research.

4.4 Spin evolution

The most important next step in modelling the LMXBs concerns the variability in the spin with varying accretion rate. The spin of accreting X-ray pulsars is known to vary considerably [17] on a timescale which is roughly similar to the variations in the accretion rate. But the data also suggests that there may not be a direct link between increased accretion and an increase in the spin-up torque. It is important to understand this variability in general. This is also a very important issue for attempts to search for gravitational waves from the LMXBs. Any variability on timescales shorter than the observation time that remains unaccounted for will likely lead to a significant loss in signal-to-noise ratio.This problem was first discussed, albeit not in the context of gravitational waves data analysis, by Lamb and Pines in two seminal papers [67, 68] in which the authors examined period variations in X ray binaries and adopted a statistical description of torque fluctuations in terms of noise processes. Such fluctuations can result both from variations of the external torque on the stellar crust (associated with variations in the accretion flow) or from internal torque variations (associated with oscillations of the fluid core or the unpinning of vortexes in the inner crust). More recently a simple model of the disc-magnetosphere interaction was suggested by Perna et al. [110] to explain the spin up/spin down transitions in some accreting X-ray binaries.

In the following we shall present a simple model for the spin evolution of an accreting neutron star, based on the torque model presented in this chapter. We shall consider the torque to act only on the crust, which is coupled to the core on a timescale τ. This timescale is usually assumed

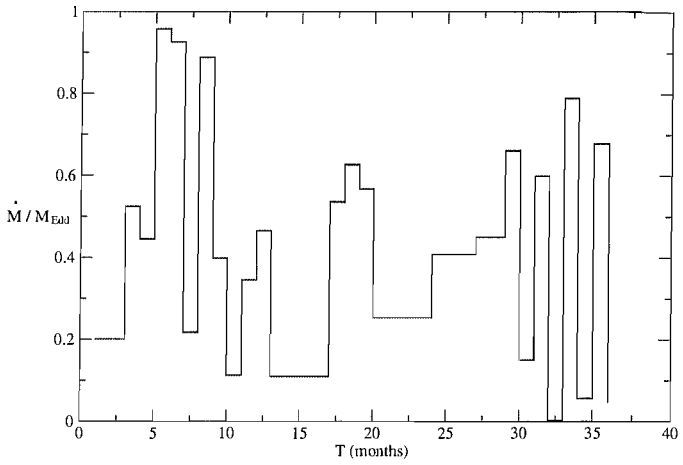

Figure 4.5: Random fluctuations in the accretion rate over a period of 40 months. The period remains constant on a timescale of $\approx$ 1 month.

to be of the order of seconds [4, 3], although there have been suggestions that it may actually be much longer, of the order of days or even months [124], or much shorter, of the order of tenths of seconds [10]. We shall thus investigate the whole range of timescales.

The equations we integrate for the evolution of the angular velocity are:

$$\begin{aligned} I_{cr}\dot{\Omega}_{cr} &= N(t) - \alpha(\Omega_{cr} - \Omega_B) \\ I_B\dot{\Omega}_B &= \alpha(\Omega_{cr} - \Omega_B) \end{aligned} \tag{4.61}$$

where $N(t)$ is the torque acting on the crust and $\alpha = I_{cr}/\tau$. Quantities with the subscript cr refer to the crust, those with the subscript B refer to the core. The equations then reduce to:

$$\begin{aligned} \dot{\Omega}_{cr} &= \frac{N(t)}{I_{cr}} - \frac{(\Omega_{cr} - \Omega_B)}{\tau} \\ \dot{\Omega}_B &= \frac{I_{cr}}{I_B}\frac{(\Omega_{cr} - \Omega_B)}{\tau} \end{aligned} \tag{4.62}$$

We can now take for $N(t)$ the torqe appropriate for the thick disc model from equation (4.46). We will also insert a random fluctuation in the accretion rate $\dot{m}$, which varies on a timescale t_a. We shall take variations over a timescale of $\approx$ 1 month, an example can be seen in figure 4.5. The question we would like to answer is whether the spin variability can be important for gravitational wave detection and data analysis. This problem was first considered by Jones [58]. His suggestion is that a template

where we consider the spin rate to vary smoothly (either to be constant, or increasing/decreasing as a power law) will not allow us to detect the emission from a rotating neutron star if it drifts out of phase more than one radian over a three year detection period. In order to implement this in the following we shall make the assumption that the GW emission is tied to the crust and that gravitational waves are thus emitted at twice the spin frequency. This is not necessarily the case, however we shall see in chapter 5 that if there is a deformation, a "mountain", on the neutron star, most of the contribution to the quadrupole comes from the elastic crust. It is thus reasonable to assume that GW emission is linked to the spin frequency. The amount by which the crustal spin period deviates from a template obviously depends on the coupling timescale τ between the crust and the core; if this is of the same order, or larger than, the timescale over which the accretion rate changes (t_a), then only the crust will react to the changes and the spin variation will be much larger, as the moment of inertia is much smaller. If on the other hand the τ is much smaller than t_a then the star will react as a whole, and the spin variation will be less substantial.

To investigate this problem let us consider a neutron star accreting at a random rate $\dot{M}$, with an average accretion rate $\dot{M}_a = 0.47\dot{M}_{Edd}$. Let us consider a star spinning at the spin equilibrium period given by $\dot{M}_a$ in equation (4.51). For a $1.4M_\odot$ star with a 10^8 G surface magnetic field and a radius of 10 km, the equilibrium frequency is $\nu_e = 1044.8935$ Hz. We can then record the phase difference between our model and a neutron star rotating with this constant frequency dictated by the spin equilibrium. The results are plotted in figures 4.6, 4.7 and 4.8. As was expected if we take a large coupling timescale (e.g. 1 day), the spin frequency of the crust will experience large variations and a constant spin template will become inaccurate in less than a day. On the other hand the phase difference is less than a radian for ≈ 1 year already for τ =1 minute, and for τ =10 seconds or less the template remains in phase for the whole three year period. It is also important to note that here we are taking a random variation of the accretion rate, which can vary between $\dot{M} = 0$ and $\dot{M}_a = \dot{M}_{Edd}$. In reality the excursion is unlikely to be this large, but rather to be a smaller oscillation around a mean value. In this case the oscillations of the torque (and consequently of the spin of the star) would be smaller than the ones in our model. If the coupling timescale is thus of the order of seconds, as is the general consensus, we do not expect the fluctuations of the spin to be a problem for gravitational wave detection.

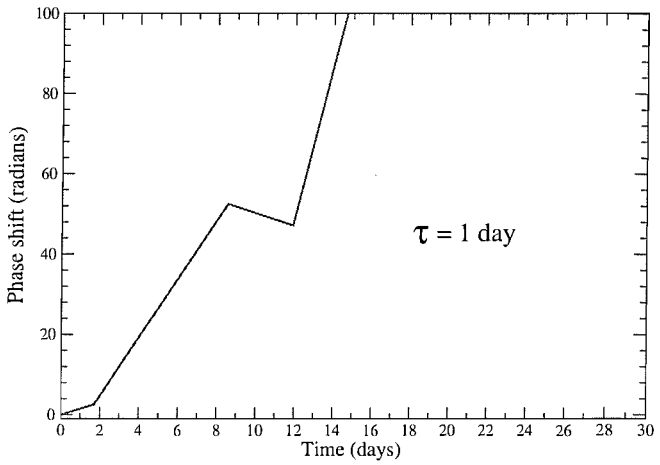

Figure 4.6: Phase difference between the crust and a template with a constant spin for a coupling timescale of τ =1 day. The constant spin template drifts out of phase of more than 1 radian in $\approx$ 1 day.

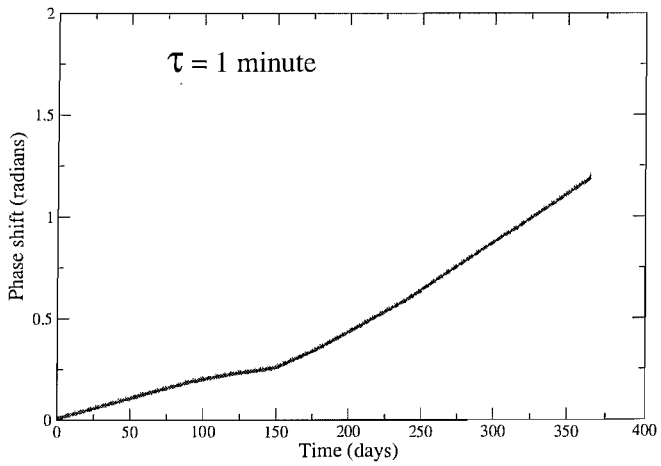

Figure 4.7: Phase difference between the crust and a template with a constant spin for a coupling timescale of τ =1 minute. As we can see the constant spin template drifts out of phase in less than a year.

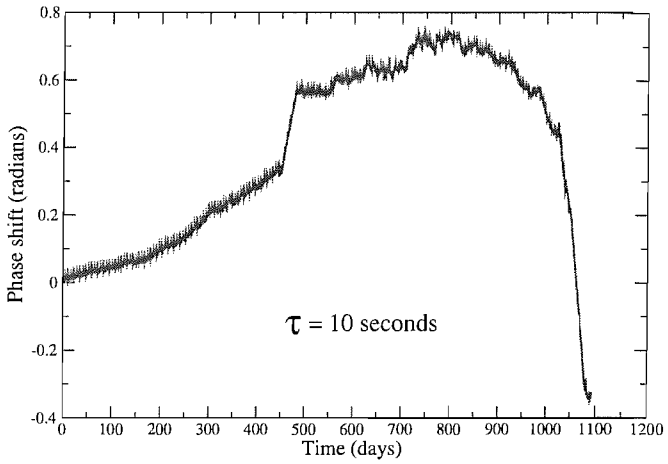

Figure 4.8: Phase difference between the crust and a template with a constant spin for a coupling timescale of τ =10 seconds. The phase shift from a constant spin template remains less than 1 radian for the whole three year period.

We can also include a gravitational wave torque of the form:

$$N_{gw} = \frac{256}{75}\frac{G\Omega c r^5}{c^5}Q_{22}^2 \tag{4.63}$$

where Q_{22} is the crustal quadrupole. This however only changes the spin equilibrium period, it does not qualitatively alter the results.

4.5 Conclusions

We have discussed the accretion spin-equilibrium for neutron stars in LMXBs. The outcome of this study is a more detailed model of the accretion torques and an appreciation that it is possible to construct a reasonably simple and consistent model for these systems without invoking additional spin-down torques due to, for example, gravitational radiation. This result is not particularly surprising. After all, the accretion problem is extremely complex [35], and the torques considered in the studies that argued for the need for an additional spin-down mechanism (see [153] and [18]) were somewhat simplistic.

Of course, our results should not be taken as proof that the LMXBs do not radiate gravitational waves. The various proposed mechanisms for generating asymmetries in rapidly spinning, accreting neutron stars remain (essentially) as viable as before. The key difference is that we have

eliminated the rationale for locking the gravitational radiation luminosity to the non-magnetic torque $\dot{M}\sqrt{GMR}$, which has been used as an order of magnitude estimate in most studies to date. In our picture, one would not be able to infer how the spin down due to gravitational radiation combines with the accretion torque from the observed spin periods. In fact, this alleviates some "problems" with the gravitational-wave models. In the case of accretion induced asymmetries in the crust [18], one can show that the quadrupole deformation required to balance accretion is

$$\epsilon \approx 10^{-7} \left(\frac{\dot{M}}{\dot{M}_{\rm Edd}} \right)^{1/2} \left(\frac{P}{3 \text{ ms}} \right)^{5/2} \tag{4.64}$$

This should be compared to the maximum deformation that the crust can sustain, which according to [144] (and as we shall see in the following chapters) can be approximated as

$$\epsilon_{\rm max} < 5 \times 10^{-7} \left(\frac{u_{\rm break}}{10^{-2}} \right) \tag{4.65}$$

where the breaking strain $u_{\rm break}$ is usually (based on results for terrestrial materials) assumed to be in the range $10^{-4} - 10^{-2}$. These estimates show that the breaking strain must be near the upper limit of the expected range in order for these asymmetries to balance near Eddington accretion in a star spinning at a period of a few milliseconds. By weakening the accretion torque, while at the same time not altering the mechanism generating the asymmetry (eg. the accretion rate), this issue is made less critical.

Our results also impacts the suggestion that the gravitational waves are emitted by unstable r-mode oscillations in the stellar fluid. In this case, the r-modes are expected to become unstable below a critical rotation period $P_{\rm crit}$. The point at which the instability becomes relevant depends on many complicated issues concerning viscosity, superfluidity etcetera (see [8] for a discussion) but it is plausible that $P_{\rm crit} \approx 1 - 3$ ms. In the context of the present model, we obviously need $P_{\rm crit} > P_{\rm eq}$ in order for the r-mode instability to be relevant. Considering the results illustrated in the left panel of Figure 4.4, the instability may still come into operation in weak magnetic field systems which are neither very slow nor very fast accretors.

We have also considered the impact that the spin variability may have on gravitational wave detection. Our results suggest that if the crust is coupled to the core of the neutron star on a timescale of the order of seconds, then timing noise should not be a problem, and a template with

a smooth spin evolution should be sufficient. However, if the coupling timscale is of the order of days, timing noise can become a problem and using long stretches of data would not be possible. One would have to use much shorter segments of data during which the templates do not drift out of phase, thus losing signal to noise, unless more detailed models of the spin evolution become available.

Chapter 5

Mountains on Neutron Stars

As discussed at the end of Chapter 1, a deformation or "mountain" on a rotating neutron star could lead to it having a time varying quadrupole moment and thus to the emission of gravitational waves. This is one of the mechanisms that was suggested for the LMXBs, in order to remove angular momentum from the system and lead to the observed spin period (Chapter 4). Clearly the amount of gravitational waves emitted, and thus the amount of angular momentum lost by the star, depends on the size of the "mountain". In order to understand if gravitational waves could lead to the observed spin equilibrium period it is thus crucial to understand how large a mountain the crust of the neutron star can sustain before cracking.

Although there has been some exploratory work in this field, there are in fact many questions that can still be asked, the main one being if there is a difference between the "mountain" that one can build on the non-accreted crust of a rotating neutron star and the one that can be built on the accreted crust of a neutron star in a binary system (such as the LMXBs). We shall see that these two different scenarios can lead to significantly different compositions for the crust. The case of isolated neutron stars is particularly interesting as current gravitational wave detectors are beginning to put astrophysically relevant limits on the ellipticities of known pulsars ([1]). In this chapter we will discuss this issue, and present a new scheme for calculating the maximum quadrupole which allows us to have better control of the boundary conditions at the base of the crust.

This calculation was first attempted in detail by Ushomirsky, Cutler and Bildsten in [144], using the perturbation formalism presented in [84]. In the following I shall give a brief overview of their maximization argument, then move on to present a formalism in terms of perturbations of a

spherically symmetric crust, without making the Cowling approximation that was made in [144].

5.1 Maximum Quadrupole

Let us assume that the crust responds elastically to pressure and density perturbations. We can thus treat it as a solid with a shear modulus $\mu(r)$ and write the stress energy tensor as:

$$\tau_{ab} = -pg_{ab} + T_{ab} \tag{5.1}$$

Where g_{ab} is simply the flat 3-metric and T_{ab} is the shear stress tensor of the crust, which vanishes in the fluid interior. We will consider the equilibrium shape of the star to be spherical, and treat T_{ab} as a first order quantity, denoting it as t_{ab}, so that we have:

$$\delta\tau_{ab} = -\delta p g_{ab} + t_{ab} \tag{5.2}$$

The equations we need to solve for equilibrium are thus:

$$\nabla^a \delta\tau_{ab} = \rho\nabla^a\Phi \tag{5.3}$$

which reduce to

$$\nabla^a \delta\tau_{ab} = \delta\rho g(r) r^a + \rho\nabla^a\delta\Phi \tag{5.4}$$

where now ρ indicates the background quantity and $g(r) = -\frac{d\Phi}{dr} = GM/r^2$. If we expand the perturbation in tensor spherical harmonics we have:

$$t_{ab} = t_{rr}Y_{lm}(r_a r_b - \frac{1}{2}e_{ab}) + t_{r\perp}(r)f_{ab} + t_\Lambda(r)(\Lambda_{ab} + \frac{1}{2}Y_{lm}e_{ab}) \tag{5.5}$$

where

$$\begin{aligned} \beta &= \sqrt{l(l+1)} \\ e_{ab} &= g_{ab} - r_a r_b \\ f_{ab} &= \beta^{-1} r(r_a \nabla_b Y_{lm} + r_b \nabla_a Y_{lm}) \\ \Lambda_{ab} &= \beta^{-2} r^2 \nabla_a \nabla_b Y_{lm} + f_{ab}\beta^{-1} \end{aligned} \tag{5.6}$$

This allows us to consider directly the components of the stress tensor but gives us no information on the perturbations that give rise to the stress. In order to do this we will need to write the vectors that describe

the displacements of the crust in terms of vector spherical harmonics and then calculate the stress tensor (it is in fact quite obvious that the tensor spherical harmonics we are using are built from the vector spherical harmonics). The two expansions should give the same results and the choice is just a matter of convenience. Projecting eq.(5.4) along the unit vector r^b we obtain

$$\delta\rho = \frac{1}{g(r)}\left[-\frac{d\delta p}{dr} + \frac{dt_{rr}}{dr} + t_{rr}\frac{3}{r} - \frac{\beta}{r}t_{r\perp}\right] - \frac{\rho}{g(r)}\frac{d\delta\Phi}{dr} \tag{5.7}$$

If we now project eq.(5.4) along $\nabla^b Y_{lm}$ we obtain

$$\delta p(r) = -\frac{1}{2}t_{rr} + \frac{3}{\beta}t_{r\perp} - \frac{1}{3}t_\Lambda + \frac{r}{\beta}\frac{dt_{r\perp}}{dr} - \rho\delta\Phi \tag{5.8}$$

Substituting into eq.(5.7) we obtain

$$\begin{aligned}\delta\rho &= \frac{1}{g(r)}\left[\frac{3}{2}\frac{dt_{rr}}{dr} - \frac{4}{\beta}\frac{dt_{r\perp}}{dr} - \frac{r}{\beta}\frac{d^2t_{r\perp}}{dr^2} + \frac{1}{3}\frac{dt_\Lambda}{dr}\right.\\ &\left. + t_{rr}\frac{3}{r} - \frac{\beta}{r}t_{r\perp}\right] + \frac{\delta\Phi}{g(r)}\frac{d\rho}{dr}\end{aligned} \tag{5.9}$$

We can now calculate the quadrupole moment $Q_{22} = \int \delta\rho r^4 dr$. By integrating by parts we obtain

$$\begin{aligned}Q_{22} &= -\int \frac{r^3}{g}\left[\frac{3}{1}(4-U)t_{rr} + \sqrt{\frac{3}{2}}\left(8 - 3U + \frac{U^2}{3} - \frac{1}{3}r\frac{dU}{dr}\right)t_{r\perp}\right.\\ &\left. + \frac{1}{3}(6-U)t_\Lambda\right] + \frac{r^4}{g}\frac{d\rho}{dr}\delta\Phi dr\end{aligned} \tag{5.10}$$

where $U = \frac{d\ln g}{d\ln r} + 2$. It is important to note that we have assumed that the surface terms in the integral vanish because we have assumed (as in [144]) that the shear stress vanishes above and below the crust. In these equations we have retained the perturbations of the gravitational potential $\delta\Phi$. In [144] the authors go on to solve the problem in the "Cowling approximation", i.e. neglecting $\delta\Phi$.

5.1.1 Maximum strain and the Von Mises criterion

Up to now we have considered a purely elastic response of the crust. However, real solids behave elastically only up to a maximum strain $\sigma_{\max}$ after which they either crack or deform plastically. In order to

estimate the maximum size of the mountain that can be built we shall assume that the crust cracks upon reaching a certain yield strain. Let us investigate this in detail. We will consider the strain tensor rather than the stress tensor, as this allows us to use a simple criterion to establish when the crust breaks. The strain tensor is defined as:

$$\sigma_{ab} = t_{ab}/\mu \tag{5.11}$$

where the solid is assumed to be isotropic and thus μ is the "average" shear modulus defined in (2.23). If we define $\bar{\sigma}$ as $\bar{\sigma}^2 = \frac{1}{2}\sigma_{ab}\sigma^{ab}$, the Von Mises criterion ([144] and references therein) then states that the crust will yield when

$$\bar{\sigma} > \bar{\sigma}_{\max} \tag{5.12}$$

Other criteria exist, such as the Tresca criterion which depends on the difference between the maximum and minimum eigenvalue of the strain tensor. Let us return to our expansion of the stress tensor in tensor spherical harmonics. If we assume the physical variables to be the real part of our complex variables we can write

$$\begin{aligned} \sigma_{ab}\sigma^{ab} &= \frac{3}{2}\sigma_{rr}^2[\Re(Y_{lm})]^2 + \sigma_{r\perp}^2[\Re(f_{ab})]^2 \\ &\quad +\sigma_{\Lambda}^2[\Re(\Lambda_{ab} + \frac{1}{2}Y_{lm}e_{ab})]^2 \end{aligned} \tag{5.13}$$

we can also obtain the following identity in the $l = m = 2$ case

$$\frac{3}{4}[\Re Y_{lm}]^2 + \frac{3}{4}[\Re f_{ab}]^2 + \frac{9}{2}[\Re(\Lambda_{ab} + \frac{1}{2}Y_{lm}e_{ab})]^2 = \frac{15}{32\pi} \tag{5.14}$$

If we assume that the quadrupole is maximised when the equality is satisfied (which is trivial in the Cowling approximation), the only point that satisfies relation (5.14) subject to (5.13) is then:

$$\begin{aligned} \sigma_{rr} &= \sqrt{\frac{32\pi}{15}}\bar{\sigma}_{\max} \\ \sigma_{r\perp} &= \sqrt{\frac{16\pi}{5}}\bar{\sigma}_{\max} \\ \sigma_{\Lambda} &= \sqrt{\frac{96\pi}{5}}\bar{\sigma}_{\max} \end{aligned} \tag{5.15}$$

The constraint surface is thus this one point, which will then give the maximum quadrupole moment. One can now compute the maximum quadrupole in the Cowling approximation by using $Q_{22} = \int \delta\rho r^4 dr$ and

assuming that the shear stress vanishes above and below the crust. This gives us:

$$Q_{22} = -\int_{rb}^{R} \frac{r^3}{g}\left[\frac{3}{2}(4-U)t_{rr} + \frac{1}{3}(6-U)t_{\Lambda} + \sqrt{\frac{3}{2}}\left(8 - 3U - \frac{1}{3}U^2 - \frac{r}{3}\frac{dU}{dr}\right)t_{r\perp}\right] dr \tag{5.16}$$

where $U = \frac{d\ln g}{d\ln r} + 2$. This led Ushomirsky, Cutler and Bildsten to conclude that the maximum quadrupole is

$$Q_{22}^{max} \approx 10^{38}\text{g cm}^2(\sigma_{\max}/10^{-2}) \tag{5.17}$$

no matter how the strain arises and in the assumption that all the strain is in the Y_{22} spherical harmonic; strain in other harmonics would push the crust closer to the yield point without contributing to the quadrupole. This estimate is thus an upper limit for the quadrupole the crust could sustain, and on the energy the star would emit in Gravitational Waves, which is related to the quadrupole by:

$$\dot{E}_{gw} = \frac{256\pi}{75}\frac{G\Omega^6}{C^5}Q_{22}^2 \tag{5.18}$$

where Ω is the rotation rate of the star. The value $\sigma_{\max} = 10^{-2}$ was chosen because it puts Q_{22} in the right range to balance the accretion torque in the LMXBs, the quadrupole required to do this is in fact

$$Q_{gw} = 1.6 \times 10^{38} gcm^2(300Hz/\nu_{spin})^{5/2} \tag{5.19}$$

if we assume the most basic accretion model presented in chapter 4.

5.2 Accreted v. Non-accreted crust

Having reviewed the formalism of [144], let us apply it to the problem of determining the maximum quadrupole that an accreted and a non-accreted crust can sustain, and present some of the issues involved. The maximum quadrupole defined in equation (5.16) depends on an integral over the crust involving the quantities g and μ (which is contained in the components of the stress tensor $t_{ab} = \sigma_{ab}/\mu$). As we have seen in chapter 2 these quantities depend on the equation of state and composition of the crust, which are quite different in the accreted and non-accreted case.

The equation of state, for example, determines the thickness of the crust, while the composition of the crust determines the shear modulus ([104]) through

$$\mu = 0.1194 \left(\frac{3}{4\pi}\right)^{1/3} \left(\frac{1-Xn}{A} n_b\right)^{4/3} (Ze)^2 \text{g cm}^{-1} \text{ s}^{-2} \qquad (5.20)$$

where Xn is the fraction of neutrons outside nuclei, n_b is the baryon density, Z is the proton number and A is the atomic number, as we have seen in chapter 2. One could then ask which kind of crust could support a larger deformation, which is the same as asking which kind of neutron star is a better source of gravitational waves. In fact it has been suggested that an accreted crust would sustain a smaller "mountain" as Z is much lower throughout than in a non-accreted crust [121]. To answer the question we can evaluate the expression in equation (5.10) in the two cases, using the results of [28] and [46] for the composition and EOS of the crust. The main obstacle is that the composition of the accreted crust is only given up to neutron drip density, because at higher densities the equation of state is basically that of a neutron gas, and thus can be matched to that of a non-accreted crust. However, even if the EOS is the same, the composition (specifically Z and A) is not ([46]). In order to obtain an estimate we have extrapolated the results available up to neutron drip density to higher densities by noting that the ratio Z/A is roughly constant in the two kinds of crust and assuming that it will remain so even in the denser regions at the base of the crust. Having done this we can calculate the maximum quadrupole for the two cases. To do this we need to integrate the equations of hydrostatic equilibrium for the star (as the core is unperturbed) and we can use Newtonian equations or the TOV equations. We shall examine both cases in order to obtain an estimate of how important relativistic effects can be. The question is relevant, because even though relativistic effects are not very important in the crust, they do contribute significantly to the structure of the star, and thus affect parameters such as the crust thickness which are relevant for our calculation. It would then not seem appropriate to use realistic equations of state if we are still describing the core with Newtonian equations of equilibrium, as the relativistic effects we are neglecting may be as large as the corrections we expect from the equation of state. We will always use Newtonian equations in the crust.

As we can see from Table 5.1 the non-accreted crust allows for a slightly larger quadrupole, but the results are essentially the same for the two models. This is mainly due to the fact that the slight decrease

	Accreted	Non Accreted	Accreted
TOV			
Mass ($M_\odot$)	1.4	1.4	1.6
Radius (km)	12.56	12.3	12.3
Crust Thickness (km)	1.76	1.5	1.5
Qmax($(\frac{\sigma}{10^{-2}})$ g cm^2)	1.6×10^{38}	2.0×10^{38}	1.1×10^{38}
ϵ	1.1×10^{-7}	1.5×10^{-7}	7.3×10^{-8}
NEWTONIAN			
Mass($M_\odot$)	1.4	1.4	1.7
Radius (km)	14.1	14	14.3
Crust Thickness (km)	2.2	1.9	1.9
Qmax($(\frac{\sigma}{10^{-2}})$ g cm^2)	2.8×10^{38}	4.2×10^{38}	2.5×10^{38}
ϵ	1.6×10^{-7}	2.4×10^{-7}	1.1×10^{-7}

Table 5.1: The first two columns show the maximum quadrupole for two stars of equal mass, one with an accreted crust and one with a non-accreted crust. The last column is a star with an accreted crust of the same thickness as that of the star with a non-accreted crust, but a different mass. Both Newtonian equations and the TOV equations are used for the core, in order to illustrate General Relativistic effects. The equation of state is taken from [28] for the core and for the non-accreted crust, while the equation of state for the accreted crust is taken from [46]. ϵ is the ellipticity $\frac{I_x - I_y}{I_0}$.

in μ (as seen in figure 5.1) for the accreted crust is compensated for by it being thicker.We can try to compare the case of two stars with a crust of the same thickness and, as is obvious from Table 5.1, in this case there is approximately a factor 2 difference. This is close to what would be expected, as Saio [121] has predicted that the shear modulus of an accreted crust would be approximately half that of a non accreted crust, even if in reality this effect is counterbalanced by the accreted crust being thicker. However it is important to note that the result depends on how we extrapolate the composition at the base of the accreted crust. In order to confirm this result it would therefore be necessary to have a detailed calculation of the composition of the crust in this region. From Table 5.1, it is also clear that relativistic effects can play a role in this calculation, as they appear to make a difference of factors of up to a few in the final result (mainly because the crust is thicker in the Newtonian case, and the radius of the star is larger).

5.3 Validity of the Cowling approximation

Following [144], in the previous calculation we adopted the Cowling approximation. This simplifies the calculation considerably, because it means that the liquid core of the star cannot support any kind of perturbation (with no shear and no $\delta\Phi$ there would be no restoring force for a pressure perturbation δp). This allows us to consider only the crust. In [144] the authors consider the effect of the approximation and conclude that retaining the perturbations of the gravitational potential could lead to changes in the quadrupole from 20% to 200%. A calculation of the strain that arises in the crust, dropping the Cowling approximation, is carried out in [27], but for the case of a perturbation with a Y_{20} angular dependance, given by rotation. In order to investigate the effects of such an approximation for our problem we will present a series of model calculations where the $\delta\Phi$ terms have been retained. These simple examples can be solved analytically and allow us to estimate how much the Cowling approximation can affect the final solution.

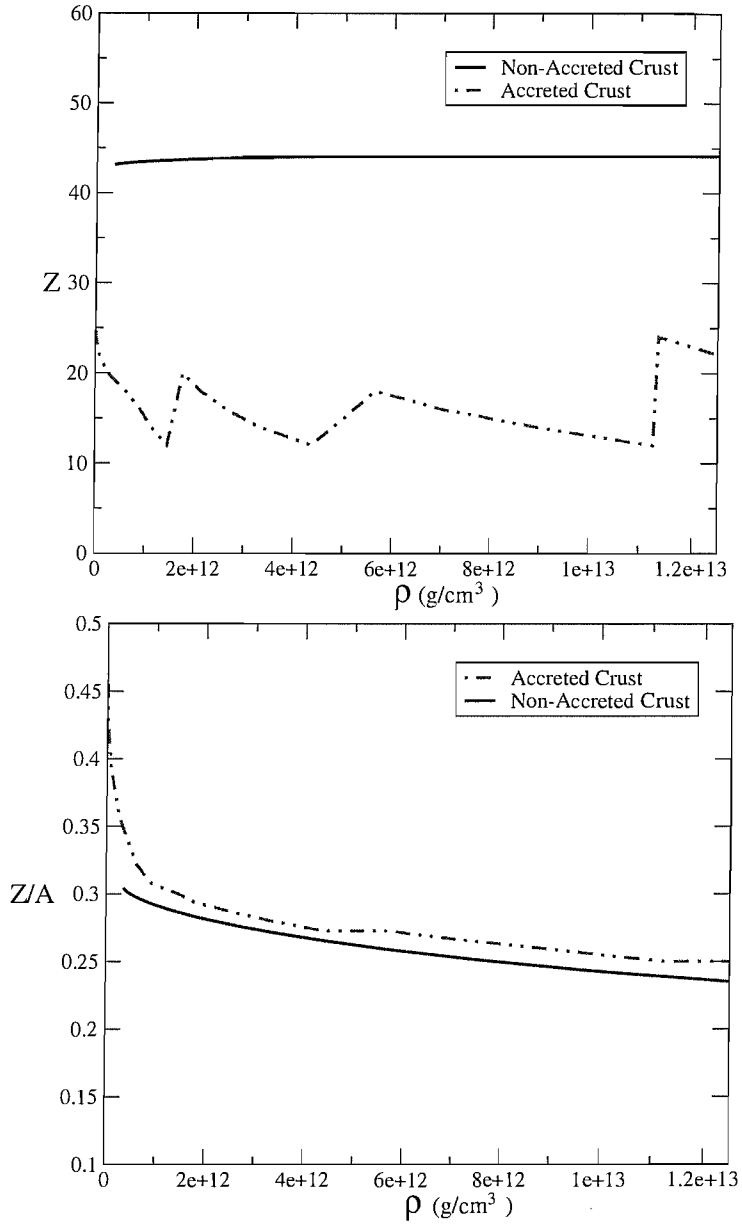

Figure 5.1: Comparison of the proton number Z and of the ratio Z/A for an accreted and a non-accreted crust. EOS from [28] for the non-accreted case and from [46] for the accreted case.

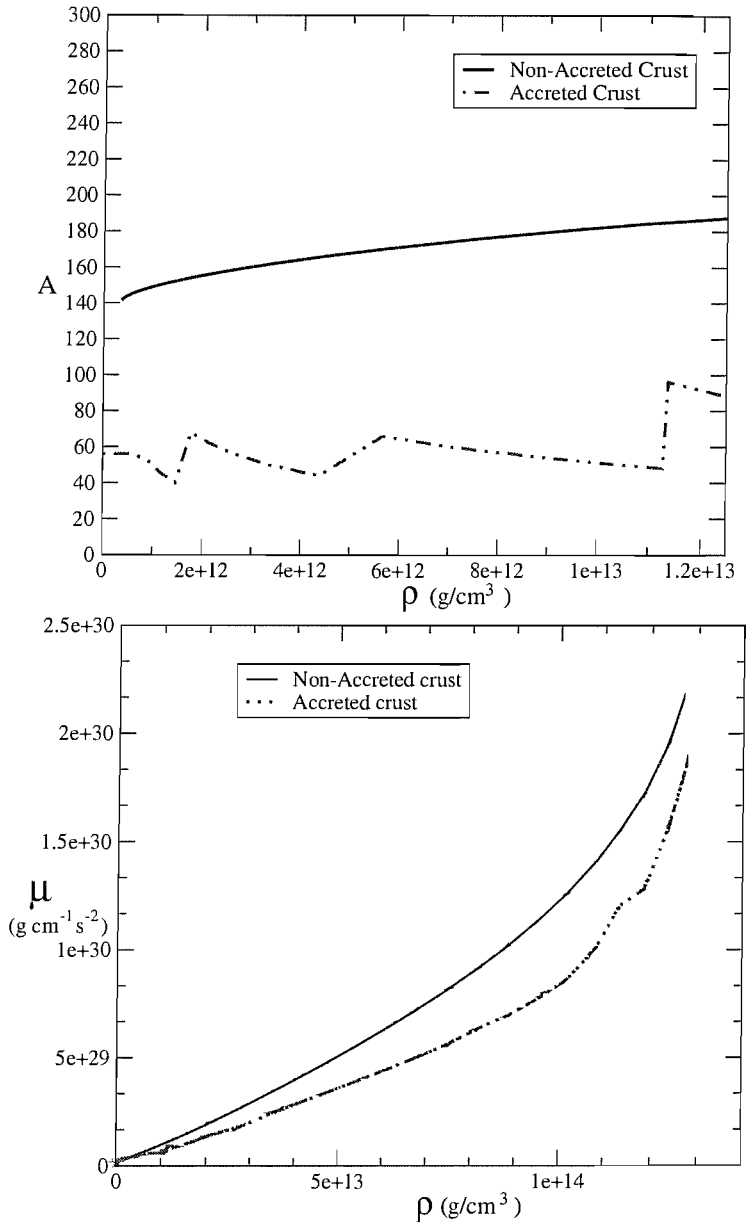

Figure 5.2: Comparison of the atomic number A and the shear modulus μ for an accreted and a non-accreted crust. The EOS is taken from [28] for the non-accreted case and from [46] for the accreted case, and then extrapolated as described in the text.

5.3.1 Constant Density and Shear

Let us first of all consider a constant density, elastic sphere. In this case we will have

$$\rho(r) = \rho\Theta(R-r) \quad \text{and} \quad \mu(r) = \mu\Theta(R-r)$$
$$\frac{\mu}{\rho} = \text{Const} \tag{5.21}$$

where we have taken the shear modulus constant over the whole star rather than just the crust, in order to make the algebra simpler. R is the stellar radius. We now need to solve the perturbed Poisson equation

$$\nabla^2\delta\Phi = 4\pi G\delta\rho \tag{5.22}$$

Let us then examine the source term containing $\delta\rho$. Take for the components of the strain tensor the maximum values obtained in the previous section. This means that the stress tensor is simply $t_{ab} = \mu\sigma_{ab}$ and depends on r only through μ. If we assume that the crust is everywhere strained to the maximum and insert our definitions for μ and ρ into eq. (5.9) we obtain

$$\begin{aligned}\delta\rho &= -\frac{\delta(R-r)\mu}{g(r)}\left[\frac{3}{2}\sqrt{\frac{32\pi}{15}}\bar{\sigma}_{\max} - \frac{4}{\beta}\sqrt{\frac{16\pi}{5}}\bar{\sigma}_{\max} + \frac{1}{3}\sqrt{\frac{96\pi}{5}}\bar{\sigma}_{\max}\right] + \\ &+\frac{\Theta(R-r)\mu}{g(r)}\left[\frac{3}{r}\sqrt{\frac{32\pi}{15}}\bar{\sigma}_{\max} - \frac{\beta}{r}\sqrt{\frac{16\pi}{5}}\bar{\sigma}_{\max}\right] \\ &-\frac{\delta'(R-r)\mu}{g(r)}\frac{r}{\beta}\sqrt{\frac{16\pi}{5}}\bar{\sigma}_{\max} - \frac{\delta(R-r)}{g(r)}\rho\delta\Phi\end{aligned} \tag{5.23}$$

which gives the quadrupole:

$$\begin{aligned}Q &= -\frac{\mu}{R^4 g(R)}\left[\frac{3}{2}\sqrt{\frac{32\pi}{15}}\bar{\sigma}_{\max} - \frac{4}{\beta}\sqrt{\frac{16\pi}{5}}\bar{\sigma}_{\max} + \frac{1}{3}\sqrt{\frac{96\pi}{5}}\bar{\sigma}_{\max}\right] + \\ &+\int_0^R \frac{r^4\mu}{g(r)}\left[\frac{3}{r}\sqrt{\frac{32\pi}{15}}\bar{\sigma}_{\max} - \frac{\beta}{r}\sqrt{\frac{16\pi}{5}}\bar{\sigma}_{\max}\right] \\ &+\frac{4rR^3g(R) - g'(R)R^4}{g(R)^2}\frac{1}{\beta}\sqrt{\frac{16\pi}{5}}\bar{\sigma}_{\max} - \frac{1}{g(R)}\rho\delta\Phi(R)\end{aligned} \tag{5.24}$$

The shear term of the quadrupole in this case is

$$Q_{sh} = \frac{8}{15}\frac{R^4\sqrt{30\pi}}{g(R)} - \frac{2}{15}\frac{R^5\sqrt{30\pi}}{g(R)^2}\frac{dg(r)}{dr}(R) \tag{5.25}$$

Returning to Poisson's equation, in the $l = m = 2$ case we have to solve:

$$\delta\Phi'' + \frac{2}{r}\delta\Phi' - \frac{6}{r}\delta\Phi = -\delta(R-r)\left[\frac{3\mu\bar{\sigma}_{max}}{r\rho}\sqrt{\frac{8\pi}{15}} + \frac{3}{r}\delta\Phi\right], \tag{5.26}$$

subject to the conditions that the solution should be regular at the centre of the star, fall off at infinity and be continuous at the surface of the star. The step in the first derivative can be computed by integrating between $R-\epsilon$ and $R+\epsilon$ and then taking the limit $\epsilon \longrightarrow 0$; this gives

$$\delta\Phi(R+\epsilon) - \delta\Phi(R-\epsilon) = -\left[\frac{3\mu\bar{\sigma}_{max}}{R\rho}\sqrt{\frac{8\pi}{15}} + \frac{3}{R}\delta\Phi(R)\right] \tag{5.27}$$

The solutions of the homogeneous equation are of the form

$$Ar^2 + \frac{B}{r^3} \tag{5.28}$$

We then clearly have Ar^2 for the interior and B/r^3 for the exterior. Matching at the surface gives us $B = AR^5$ which can be used to compute the step in the first derivative

$$\begin{aligned} -3\frac{B}{R^4} - 2AR &= -\frac{3\mu\bar{\sigma}_{max}}{R\rho}\sqrt{\frac{8\pi}{15}} - \frac{3}{R}AR^2 \\ 2AR &= \frac{3\mu\bar{\sigma}_{max}}{R\rho}\sqrt{\frac{8\pi}{15}} \\ A &= \frac{3}{2}\frac{\mu\bar{\sigma}_{max}}{R^2\rho}\sqrt{\frac{8\pi}{15}} \end{aligned} \tag{5.29}$$

which gives us the interior solution

$$\delta\Phi = \frac{3}{2}\frac{\mu\bar{\sigma}_{max}}{R^2\rho}\sqrt{\frac{8\pi}{15}}r^2 \tag{5.30}$$

We can now substitute this back into the expression for $\delta\rho$ and calculate:

$$\begin{aligned} Q_{22} &= \left[\frac{9\mu\bar{\sigma}_{max}R^3}{4\pi G\rho}\sqrt{\frac{8\pi}{15}} - \frac{3}{4\pi G}\frac{3}{2}\frac{\mu\bar{\sigma}_{max}R^3}{\rho}\sqrt{\frac{8\pi}{15}}\right] \\ &= Q_{sh} + Q_\Phi \end{aligned} \tag{5.31}$$

which gives us the ratio

$$\frac{Q_\Phi}{Q_{sh}} = -\frac{1}{2} \tag{5.32}$$

Let us see what this means in terms of the ellipticity $\epsilon = \frac{I_x - I_y}{I_0}$. We can write the torque acting on a constant density ellipsoid as

$$\dot{J} = \frac{32G}{5c^5}\epsilon^2(2/5MR^2)^2\Omega^5 \tag{5.33}$$

However we can also write this as

$$\dot{J} = \frac{256\pi}{75}G\Omega^5 Q_{22}^5 c^5 \tag{5.34}$$

If we compare these two expressions we see that, in the constant density case

$$\epsilon = \sqrt{30\pi}\frac{Q_{22}}{3R^2M} \tag{5.35}$$

$$= \frac{9\mu\bar{\sigma}_{max}}{4G\pi\rho^2R^2}\left(1 + \frac{Q_\Phi}{Q_{sh}}\right) \tag{5.36}$$

Let us take as canonical values $\mu = 10^{30}\ dyne/cm^2$, $\rho = 10^{15}\ g/cm^3$, $R = 10\ km$. Substituting these into the above expression gives

$$\epsilon = 5.3 \times 10^{-8}\left(\frac{\bar{\sigma}_{max}}{10^{-2}}\right) \tag{5.37}$$

5.3.2 Constant Shear in the Crust

A slight improvement one can make is to impose that the shear modulus vanishes outside the crust. We can then take an expression of the kind

$$\mu(r) = \mu\left[\Theta(R - r) - \Theta(r_b - r)\right] \tag{5.38}$$

where r_b is the location of the base of the crust and the Heaviside function is defined to include the boundary points. This gives us a source term:

$$\delta\rho_s = -\frac{3\bar{\sigma}_{max}\mu}{4\pi Gr\rho}\sqrt{\frac{8\pi}{15}}\left[\delta(R - r) - \delta(r_b - r)\right] - \frac{3}{4\pi Gr}\delta(R - r)\delta\Phi \tag{5.39}$$

while the shear part of the quadrupole is

$$Q_{sh} = \frac{8}{15}\frac{R^4\sqrt{30\pi}}{g(R)} - \frac{2}{15}\frac{R^5\sqrt{30\pi}}{g(R)^2}\frac{dg(r)}{dr}(R)$$
$$-\frac{8}{15}\frac{r_b^4\sqrt{30\pi}}{g(r_b)} + \frac{2}{15}\frac{r_b^5\sqrt{30\pi}}{g(r_b)^2}\frac{dg(r)}{dr}(r_b) \tag{5.40}$$

We now have to match the solutions at R and r_b and impose the step in the derivative at these two points. The interior solution is still of the form Ar^2, the exterior solution is of the form D/r^3 and in the crust we have $Br^2 + C/r^3$. The steps in the derivative are

$$\begin{aligned} \Delta\delta\Phi'(r_b) &= \frac{2\bar{\sigma}_{max}\mu}{5\rho r_b}\sqrt{30\pi} \\ \Delta\delta\Phi'(R) &= -\frac{2\bar{\sigma}_{max}\mu}{5\rho R}\sqrt{30\pi} \end{aligned} \tag{5.41}$$

Solving the equations gives

$$\begin{aligned} A &= -\frac{\bar{\sigma}_{max}\mu\sqrt{30\pi}(3r_b^5 - 5r_b^2R^3 + 2R^5)}{25R^5r_b^2\rho} \\ B &= -\frac{\bar{\sigma}_{max}\mu\sqrt{30\pi}(-3r_b^3 + 5R^3)}{25R^5\rho} \\ C &= -\frac{2\bar{\sigma}_{max}\mu\sqrt{30\pi}r_b^3}{25\rho} \\ D &= -\frac{\bar{\sigma}_{max}\mu\sqrt{30\pi}(-r_b^3 + R^3)}{5\rho} \end{aligned} \tag{5.42}$$

We can then calculate

$$Q_{22} = \int_0^R r^4\delta\rho dr = Q_{sh} + Q_\Phi \tag{5.43}$$

which gives us

$$\begin{aligned} Q_{sh} &= \frac{3\bar{\sigma}_{max}\mu(R^3 - r_b^3)}{10G\rho}\sqrt{\frac{30}{\pi}} \\ Q_\Phi &= -\frac{3\bar{\sigma}_{max}\mu(R^3 - r_b^3)}{20G\rho}\sqrt{\frac{30}{\pi}} \end{aligned} \tag{5.44}$$

The ratio between the two is

$$\frac{Q_\Phi}{Q_{sh}} = -\frac{1}{2} \tag{5.45}$$

and

$$Q_{sh} = 1.9 \times 10^{37} \tag{5.46}$$

In terms of ϵ we have

$$\begin{aligned} \epsilon &= \frac{\sqrt{30}Q}{4\pi^{3/2}R^5\rho} \\ &= \frac{\sqrt{30}Q_{sh}}{4\pi^{3/2}R^5\rho}\left(1 + \frac{Q_\Phi}{Q_{sh}}\right) \end{aligned} \tag{5.47}$$

which gives us, for our canonical values

$$\epsilon = 7.2 \times 10^{-9} \left(\frac{\bar{\sigma}_{max}}{10^{-2}} \right) \tag{5.48}$$

which is now nearly an order of magnitude smaller than the previous result for the elastic sphere. So the shell is, as is intuitive, "weaker" than the sphere.

5.3.3 n=1 Polytrope

A slightly more realistic density profile is that given by an $n = 1$ polytrope

$$p = K\rho^2 \tag{5.49}$$

As we have seen in chapter 2 this gives us a density profile:

$$\rho(r) = \rho_c \frac{\sin(\pi r/R)}{r\pi} \tag{5.50}$$

Let us still take $\mu(r) = \mu\left[\Theta(R-r) - \Theta(r_b - r)\right]$ with μ constant. The source term that we need to calculate is then

$$\delta\rho = -\frac{r}{\beta g^2}\frac{dg}{dr}\left[\delta(R-r) - \delta(r_b - r)\right]\sqrt{\frac{16\pi}{5}}\bar{\sigma}_{max}\mu + \frac{d\rho}{dr}\frac{\delta\Phi}{g} \tag{5.51}$$

The shear part of the quadrupole has the same form as in equation (5.40). First of all we need to evaluate $g = GM_r/r^2$

$$\begin{aligned} M_r &= 4\pi \int_0^r r^2\rho(r)dr = 4\pi \int_0^r \rho_c r R \frac{\sin(\pi r/R)}{\pi} dr \\ &= 4\pi\rho_c \frac{R^2}{\pi^2}\left[\frac{R}{\pi}\sin(\pi r R) - r\cos(\pi r/R)\right] \end{aligned} \tag{5.52}$$

we also need

$$\frac{d\rho}{dr} = \left[\rho_c \frac{\cos(\pi r/R)}{r} - \rho_c \frac{\sin(\pi r/R)R}{r^2\pi}\right]\Theta(R-r) - \rho(r)\delta(R-r) \tag{5.53}$$

this allows us to evaluate

$$\frac{1}{g}\frac{d\rho}{dr} = -\frac{\pi^2}{4\pi G R^2} - \frac{\rho(r)}{g}\delta(R-r) \tag{5.54}$$

from now on we shall omit the last term, as the function $\rho(r) = 0$ at the surface $r = R$. The last quantity we need is

$$\begin{aligned} g(r) &= \frac{4G\rho R^2}{\pi^2 r^2}\left[\sin(\pi r/R)R - \pi r\cos(\pi r/R)\right] \\ \frac{dg}{dr} &= \frac{4G\rho R\sin(\pi r/R)}{r} - \frac{2g(r)}{r} \end{aligned} \tag{5.55}$$

The homogeneous Poisson equation thus becomes, in the interior:

$$\delta\Phi'' + \frac{2}{r}\delta\Phi' - \frac{6}{r^2}\delta\Phi + \frac{\pi^2}{R^2}\delta\Phi = 0 \tag{5.56}$$

which admits solutions of the form

$$\begin{aligned} \delta\Phi &= \frac{A}{r^3}\left[(3R^2 - \pi^2 r^2)\cos(\pi r/R) + 3\pi Rr\sin(\pi r/R)\right] + \\ &+ \frac{B}{r^3}\left[(3R^2 - \pi^2 r^2)\sin(\pi r/R) - 3\pi Rr\cos(\pi r/R)\right] \end{aligned} \tag{5.57}$$

By expanding this solution in a power series around the origin we can see that the regular part is that involving the constant B (thus $A = 0$). This must be matched with the whole solution at r_b, and we must then match with the exterior solution C/r^3 at the stellar surface R. Finally we must impose the steps in the derivative at r_b and R. The resulting solution is quite complicated, but allows us to calculate

$$Q_{22} = \int_0^R r^4 \delta\rho dr = Q_{sh} + Q_\Phi \tag{5.58}$$

The expressions are again quite involved, but for a radius R=10 km and a crust thickness of 1 km, we have

$$\frac{Q_\Phi}{Q_{sh}} \approx 0.1 \tag{5.59}$$

If we now calculate an ϵ confronting with the constant density ellipsoid model we obtain:

$$\begin{aligned} \epsilon &= \frac{\sqrt{30}Q}{4\pi^{3/2}R^5\rho} \\ &= = \frac{\sqrt{30}Q_{sh}}{4\pi^{3/2}R^5\rho}\left(1 + \frac{Q_\Phi}{Q_{sh}}\right) \end{aligned} \tag{5.60}$$

which gives us, with typical parameters for the crust and $r_b = 1\ km$,

$$\epsilon = 3.1 \times 10^{-7}\left(\frac{\bar{\sigma}_{max}}{10^{-2}}\right) \tag{5.61}$$

which is an order of magnitude larger than in the constant density cases.

5.3.4 Density dependent Shear

Let us now take a slightly more realistic model with a density dependent shear. We will take μ/ρ to be constant, so this gives us

$$\mu = C\rho\Theta(r - r_b) \tag{5.62}$$

where the step function ensures that the shear modulus vanishes in the core (r_b is the radius at the base of the crust). There is no need for a step at the surface, as the density goes to zero there anyway. We will take $C = 10^{16}$ cm^2/s^2, as can be infered from figure 5.3. As in the previous section we will take the equation of state to be a $n = 1$ polytrope, thus obtaining a density profile:

$$\rho(r) = \rho_c \frac{\sin(\pi r/R)}{r\pi} \tag{5.63}$$

which leads to

$$\mu = C\rho_c \frac{\sin(\pi r/R)}{r\pi}\Theta(r - r_b) \tag{5.64}$$

The components of the stress tensor will now also depend on r through the shear modulus.

$$\begin{aligned} t_{rr} &= \frac{4}{15}\Theta(r - r_b)\sigma \frac{C\rho_c \sin(\pi r/R)\sqrt{30}R}{r\sqrt{\pi}} \\ t_{r\perp} &= \frac{4}{5}\Theta(r - r_b)\sigma \frac{C\rho_c \sin(\pi r/R)\sqrt{5}R}{r\sqrt{\pi}} \\ t_{\lambda} &= \frac{4}{5}\Theta(r - r_b)\sigma \frac{C\rho_c \sin(\pi r/R)\sqrt{30}R}{r\sqrt{\pi}} \end{aligned} \tag{5.65}$$

The procedure we have to follow is identical to that of the previous sections, we have to solve Poisson's equation in the core, in the crust and outside the star. We must then impose the boundary conditions at the edge of these regions. These are the same as in the preceding sections, i.e. we need to impose the continuity of $\delta\Phi$ and the step in the derivative at the base of the crust.

This allows us to compute the part of the quadrupole that comes from the perturbations of the gravitational potential Q_Φ. For $\mu = 10^{30}$ cm^2/s^2, $\rho = 10^{15}$ g/cm^3, $R = 10$ km, $r_b = 1$ km we have

$$Q_\Phi = -2.277 \times 10^{38} \text{ g cm}^2 \tag{5.66}$$

We must also calculate the quadrupole that comes from the shear terms alone. As this contribution involves derivatives of the stress tensor, it also

involves delta functions and their derivatives. This means that we have two contributions: a surface term that comes from such delta functions and a term that comes from the interior integration.

For the stellar parameters given above we find that the integral term is:

$$Q_{int} = -3.3 \times 10^{38} \text{ g cm}^2 \tag{5.67}$$

while the surface term has opposite sign and gives

$$Q_{\Sigma} = 4 \times 10^{38} \text{ g cm}^2 \tag{5.68}$$

The two thus add up to

$$Q_{sh} = 7.4 \times 10^{37} \text{ g cm}^2 \tag{5.69}$$

the large cancellations due to the surface term lead to a total quadrupole where the dominant contribution is that given by the perturbations of the gravitational potential

$$\frac{Q_{\Phi}}{Q_{sh}} = -3 \tag{5.70}$$

$$Q_{tot} = -1.5 \times 10^{38} \text{ g cm}^2 \tag{5.71}$$

corresponding to an ϵ of

$$\epsilon = \frac{\sqrt{30\pi}Q}{3R^2M} = 6.3 \times 10^{-8} \tag{5.72}$$

Which is smaller than the previous result and is a direct consequence of the cancellations that occur at the base of the crust. It is thus quite clear that the correct treatment of the boundary can have an important effect on this calculation. In particular it would appear that one cannot take $\mu \longrightarrow 0$ at the base of the crust, as the step is actually quite sharp (as shown in Figure 5.2) and we have seen that this can lead to large surface terms. We can, however, conclude, similarly to [144], that including the perturbations of the gravitational potential $\delta\Phi$ will affect the results by a factor 0.5-3. Thus the Cowling approximation is not consistent, as the corrections given by $\delta\Phi$ are not negligible. It must, however, be noted that when we drop the Cowling approximation we are no longer guaranteed that the components of the strain tensor calculated in (5.4) will give us the maximum quadrupole.

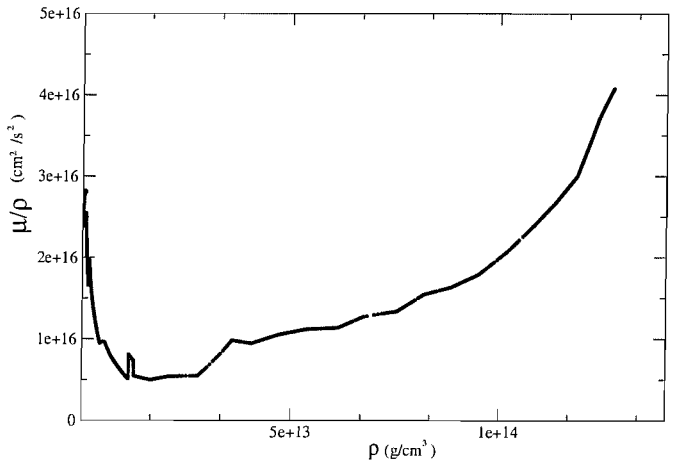

Figure 5.3: The ratio μ/ρ, which is taken to be constant in our approximation, is plotted for the case of an accreted crust (the case of an accreted crust is qualitatively similar). As we can see it is approximately constant to within factors of two.

5.4 Perturbation formalism

Up to now we have followed the method of [144] and simply taken the crust to be strained to the maximum throughout. However, as we have seen previously, the boundaries can have a strong impact on the result, so in order to carefully impose the boundary conditions at the surface of the star and at the base of the crust let us reformulate the problem in terms of perturbations in the crust. We shall impose (in a similar way as was done to calculate rotational deformations in the slow-rotation approximation, as presented for example in [141]) that the star has a small quadrupolar deformation, such that we can define a new variable a which is a function of the radial variable of the spherical background model

$$a(r) = r\left[1 + \psi(r)Y_{22}(\theta,\phi)\right]. \tag{5.73}$$

We shall assume that $a(r)$ labels the equipotential surfaces of the gravitational potential (which will thus have the same deformed shape). It is important to note that in the core these surfaces also describe the "isobaric" and "isopycnic" surfaces. This is a consequence of the hydrostatic equations. In the crust, where we also have elastic terms, this is no longer true. In the crust, surfaces of constant Φ are NOT surfaces of constant density, so while ψ is a good variable to use for the integration, it does not represent the "shape" of the star, which can be obtained by calculating the perturbations of the density ($\delta\rho$) or of the pressure (as we

will assume the equation of state to be barotropic). We expand the displacement vector along the orthonormal basis formed by the radial unit vector $\hat{r}$, $\frac{r}{\beta}\nabla Y_{lm}$ and $\frac{r}{\beta}\hat{r}\times\nabla Y_{lm}$. This allows us to use a flat background 3-metric g_{ab}. We shall ignore the axial part, proportional to $\bar{r}\times\nabla Y_{lm}$ as this does not couple to the scalar perturbations such as $\delta\rho$ which are proportional to Y_{lm}. The displacement vector thus takes the form:

$$\xi^a = \xi_r(r)Y_{lm}r^a + \xi_\perp \nabla^a Y_{lm} \tag{5.74}$$

If we assume that the crust responds elastically it is useful to define the stress-energy tensor of the solid τ_{ik} by

$$\tau_{ik} = -pg_{ab} + t_{ab} \tag{5.75}$$

where we have defined the trace-free tensor

$$t_{ab} = \mu\left(\nabla_a\xi_b + \nabla_b\xi_a - \frac{2}{3}g_{ab}\nabla^c\xi_c\right) \tag{5.76}$$

which describes the shear stress in the solid. This allows us to write the equations of static balance as

$$\nabla^a t_{ab} = \rho\nabla_b\Phi + \nabla_b p \tag{5.77}$$

which we can also write in the form

$$\nabla^a t_{ab} = \rho\nabla_b(\Phi + H) \tag{5.78}$$

where we have introduced the enthalpy

$$H = \int \frac{dp}{\rho(p)}. \tag{5.79}$$

We also have to supply a barotropic equation of state

$$p = p(\rho) \tag{5.80}$$

The remaining equations we need are the continuity equation and Poisson's equation

$$\delta\rho = -\partial_r\rho\xi_r - \rho\partial_r\xi_r + \rho\frac{\beta}{r}\xi_\perp - 2\frac{\rho}{r}\xi_r \tag{5.81}$$

$$\nabla^2\Phi = 4\pi G\rho \tag{5.82}$$

and the condition that the unit vector a^b given by the new radial variable is orthogonal to the equipotential surfaces of Φ, or parallel to the gradient of Φ, i.e.

$$\nabla a \times \nabla \Phi = 0 \tag{5.83}$$

The unit vector will thus be

$$a^b = \frac{\nabla^b a}{|\nabla^b a|} \tag{5.84}$$

It is important to note again that a is not related to the "shape" of the star (as the deformations of the density are) because we now have elastic terms in our equations of force balance. However the introduction of the variable ψ makes the equations for $\delta\Phi$ more tractable numerically. We will now carry out first order perturbations, treating ξ_a as a first order quantity. This corresponds to assuming that the background spherical configuration is at zero strain. We could imagine this to be plausible for a star which has been spun down by dipole radiation and been in an essentially non rotating configuration long enough for plastic flow to relax the crust. If this star then starts accreting it would be spun up and correspond to the situation we are describing. It is of course not relevant for the case of a spinning down star with a crust that formed while it was rapidly rotating and for which the reference zero-strain configuration would not be spherical. This problem is, however, a much more complicated one, as it would require us to know the reference shape of the star, which will in general depend on the history of the crust. We shall assume that every perturbation has a Y_{22} angular dependance, i.e. is of the form $\delta\rho(r,\theta,\phi) = \delta\rho(r)Y_{22}(\theta,\phi)$. This is because we are interested in the quadrupolar part of $\delta\rho$ which will give the dominant contribution for gravitational waves. However it is worthwhile noting that, even though they do not contribute to the gravitational wave emission, perturbations with a different angular dependance (e.g. a Y_{20} deformation due to rotation) still build up stress in the crust, and bring it closer to the breaking point, thus allowing a smaller quadrupolar deformation. For example, there could be a strong Y_{20} deformation, as the star is rotating, and this could build up high levels of strain in the crust. It is not however easy to evaluate this quantitatively, as the exact level of strain depends on the reference shape of the crust (the unstrained configuration), which in turn depends on the history of the star. Let us then write the perturbation equations we need ($\beta = \sqrt{l(l+1)} = \sqrt{6}$):

$$\nabla_b t^{ab} = \rho\nabla^a\left[(\delta H+\delta\Phi)Y_{22}\right] \quad \text{Hydrostatic equilibrium} \tag{5.85}$$

$$\delta\rho = -\partial_r\rho\xi_r - \rho\partial_r\xi_r + \rho\frac{\beta}{r}\xi_\perp - 2\frac{\rho}{r}\xi_r \quad \text{Continuity} \tag{5.86}$$

$$\delta p = \frac{dp(\rho)}{d\rho}\delta\rho = c_s^2\delta\rho \quad \text{Equation of state} \tag{5.87}$$

$$\delta H = \frac{\delta p}{\rho} \quad \text{Enthalpy} \tag{5.88}$$

$$\delta\Phi = -\psi r\partial_r\Phi \quad \text{Level surfaces (from eq.(5.83))} \tag{5.89}$$

$$4\pi G\delta\rho = \partial_r^2\delta\Phi + (2/r)\partial_r\delta\Phi - (\beta^2/r^2)\delta\Phi \quad \text{Poisson} \tag{5.90}$$

This gives us 7 equations for our 7 variables $\xi_r, \xi_\perp, \psi, \delta\rho, \delta p, \delta H, \delta\Phi$. Some of these equations are simply algebraic relations defining some quantities (such as the enthalpy). We can thus re-write the equations as three second order equations containing the variables $\xi_r, \xi_\perp$ and ψ. Once we have solved for these variables we can compute $\delta\rho$, for example from the continuity equation. Let us write the stress tensor t_{ab} in terms of our displacements:

$$\begin{aligned} t_{ab} = \mu\Bigg[& g_{ab}\left(-2/3\frac{d\xi_r}{dr} + 2/3\frac{\xi_\perp\beta}{r} + 2/3\frac{\xi_r}{r}\right)Y_{lm} + \\ & + \hat{r}_a\hat{r}_b\left(2\frac{d\xi_r}{dr} - 2\frac{\xi_r}{r}\right)Y_{lm}\left(\nabla_a\nabla_b Y_{lm}\right)\frac{r}{\beta}2\xi_\perp + \\ & \left(\hat{r}_a\nabla_b Y_{lm} + \hat{r}_b\nabla_a Y_{lm}\right)\left(\xi_r + \frac{d\xi_\perp}{dr}\frac{r}{\beta} + \frac{\xi_\perp}{\beta}\right)\Bigg] \end{aligned} \tag{5.91}$$

Working out some of the algebra we obtain for $\nabla_b t^{ab}$, breaking it down in its two components along $\hat{r}^a$ and $\nabla^a Y_{22}$:

$$\begin{aligned} \hat{r}_a\nabla_b t^{ab} = \frac{Y_{lm}}{3r^2}\Bigg[& 4\frac{d\mu}{dr}\left(\frac{d\xi_r}{dr}r^2 + r\beta\xi_\perp/2 - r\xi_r\right) + \\ & \mu\left(\frac{d^2\xi_r}{dr^2}r^2 - \frac{d\xi_\perp}{dr}\beta r + 7\xi_\perp\beta + 8\frac{d\xi_r}{dr}r - 8\xi_r - \xi_r\beta^2\right)\Bigg] \end{aligned} \tag{5.92}$$

and

$$\begin{aligned} \nabla_a Y_{22}\nabla_b t^{ab} = \frac{1}{\beta r}\Bigg[& \frac{d\mu}{dr}\left(r\beta\xi_r + r^2\frac{d\xi_\perp}{dr} + r\xi_\perp\right) + \\ & \mu\left(\frac{d\xi_r}{dr}r\beta/3 - 4/3\beta^2\xi_\perp + 8/3\xi_r\beta + 2\frac{d\xi_\perp}{dr}r + \frac{d^2\xi_\perp}{dr^2}r^2\right)\Bigg] \end{aligned} \tag{5.93}$$

The hydrostatic equilibrium equations then give

$$\hat{r}_a \nabla_b t^{ab} = \rho \partial_r (\delta H + \delta\Phi) \tag{5.94}$$

$$\nabla_a Y_{22} \nabla_b t^{ab} = \rho (\delta H + \delta\Phi) \tag{5.95}$$

Note that the term involving $\delta\rho\partial_r(H+\Phi)$ is not present because the background quantity $\partial_r(H+\Phi)$ vanishes in equilibrium (as the background spherical configuration is a zero-strain one). At this point we can write the equations as a set of four algebraic equations and three coupled second order equations for the displacements:

$$\begin{aligned}
&\frac{d^2\xi_r}{dr^2}\left(3c_s^2\rho + 4\mu\right)\rho r^2 = \\
&-\left(2\rho\frac{d\mu}{dr}r\beta + 7\rho\mu\beta + 3c_s^2\beta\rho^2 - 3\frac{d}{dr}c_s^2\right)\xi_\perp - \\
&-\left(-4\rho\frac{d\mu}{dr}r - 8\rho\mu - 3\rho\mu\beta^2 + 3c_s^2\rho\frac{d^2\rho}{dr^2}r^2\right. \\
&\left.-3c_s^2\left(\frac{d\rho}{dr}\right)^2 r^2 + 6\frac{d}{dr}c_s^2 r\rho^2 - 6c_s^2\rho^2\right)\xi_r - \\
&-\left(8\rho\mu r + 3c_s^2\rho\frac{d\rho}{dr}r^2 + 4\rho\frac{d\mu}{dr}r^2 + 3\frac{d}{dr}c_s^2 r^2\rho^2\right)\frac{d\xi_r}{dr} + \\
&+\left(\rho\mu\beta r + 3c_s^2\beta\rho^2 r\right)\frac{d\xi_\perp}{dr} + \left(3r^3\frac{dp}{dr}\frac{d\rho}{dr}\rho\right)\frac{d\psi}{dr} \\
&-\left(3r^3c_s^2\frac{d\rho}{dr}\rho + 12r^3\rho^3\pi G\right)\psi
\end{aligned} \tag{5.96}$$

$$\begin{aligned}
&\frac{d^2\xi_\perp}{dr^2}3\left(\mu r^2\right) = -\left(-4\mu\beta^2 + 3\frac{d\mu}{dr} - 3c_s^2\beta^2\rho\right)\xi_\perp \\
&-\left(3\frac{d\mu}{dr}r\beta + 8\mu\beta + 3\beta c_s^2\frac{d\rho}{dr}r + 6c_s^2\beta\rho\right)\xi_r - \\
&-\left(\mu\beta r + 3\beta c_s^2\rho r\right)\frac{d\xi_r}{dr} - \left(3\frac{d\mu}{dr}r^2 + 6\mu r\right)\frac{d\xi_\perp}{dr} \\
&+\left(3\beta c_s^2\frac{d\rho}{dr}r^2\right)\psi
\end{aligned} \tag{5.97}$$

$$\frac{d^2\psi}{dr^2}r^2\left(c_s^2\frac{d\rho}{dr}\right) = \left(4\pi G\beta\rho^2\right)\xi_\perp$$
$$-\left(4\pi Gr\frac{d\rho}{dr}\rho - 8\pi G\rho^2\right)\xi_r$$
$$+\left(4r^2G\frac{d\rho}{dr}\rho - \beta^2c_s^2 + 8\pi G\rho^2 r\right)\psi - \tag{5.98}$$
$$+\left(8\pi G\rho^2 r\right)\frac{d\psi}{dr} - \left(4\pi G\rho^2 r\right)\frac{d\xi_r}{dr}$$

If we make the Cowling approximation these equations reduce to those used by [84].

5.4.1 Boundary conditions

Let us now move on to the key issue that was ignored in our previous analysis. We need to prescribe boundary conditions at the surface and at the base of the crust. To do this in a consistent manner we should solve the perturbation problem in the core and then impose the continuity of the gravitational potential and the continuity of the perpendicular and radial components of the traction vector. We assume that the perpendicular tractions vanish outside the star and also in the liquid core, as it cannot support shearing. The core could in principle sustain pressure and density perturbations, and these will appear in the radial component of the traction. The definition of the traction vector is

$$t^a = T^{ab}\hat{a}_b \tag{5.99}$$

where T^{ab} is now the complete stress tensor, i.e.

$$T^{ab} = -\delta p g^{ab} + t^{ab} \tag{5.100}$$

This gives us

$$t^a = \hat{r}^a\left[\mu\left(\frac{4}{3}\frac{d\xi_r}{dr} - \frac{4}{3}\frac{\xi_r}{r} + \frac{2}{3}\frac{\xi_\perp}{r}\beta\right) + c_s^2\left(\frac{d\rho}{dr}\xi_r + \rho\frac{d\xi_r}{dr} - \rho\beta\frac{\xi_\perp}{r}\right)\right]$$
$$+\nabla^a Y_{lm}\mu\left(\xi_r + \frac{d\xi_\perp}{dr}\frac{r}{\beta} + \frac{\xi_\perp}{\beta}\right) \tag{5.101}$$

Imposing that the component of this along $\nabla^a Y_{22}$ must vanish gives us the condition (at the base of the crust):

$$\frac{d\xi_\perp}{dr}(r_b) = -\frac{\xi_r(r_b)\beta}{r_b} - \frac{\xi_\perp(r_b)}{r_b} \tag{5.102}$$

We then assume that the radial component of the traction is continous, thus equal to $t^a_{\rm core}$. This leads to

$$t^a_{\rm core} = \mu(r_b)\left(\frac{4}{3}\frac{d\xi_r}{dr}(r_b) - \frac{4}{3}\frac{\xi_r(r_b)}{r_b} + \frac{2}{3}\frac{\xi_\perp(r_b)}{r_b}\beta\right)$$
$$+c_s^2(r_b)\left(\frac{d\rho}{dr}(r_b)\xi_r(r_b) + \rho\frac{d\xi_r}{dr}(r_b) - \rho\beta\frac{\xi_\perp(r_b)}{r_b}\right) \qquad (5.103)$$

We shall consider the full perturbation problem in the following sections, but first, for simplicity, let us consider some simple boundary conditions: we shall assume that the fluid core is **unperturbed** and remains spherical. Such a condition is not physical, but will allow us to consider a full GR fluid core (as we only need the background model) and quantify how important relativistic effects can be. However, it is not a natural condition since it needs a force acting at the surface as well as some forces to be acting at the base of the crust to keep it spherical. This is why we cannot impose the traction conditions but will rather impose that the radial component of the displacement (ξ_r) vanishes (i.e. the core remains spherical and does not 'move' into the crust) and that the shape of the inner edge of the crust remains spherical, which implies that $\delta\rho$ must vanish (remember that the background is already spherical, so there must be no Y_{22} perturbations if it is to remain spherical). We also impose continuity of the gravitational potential, and thus impose $\psi(r_b) = 0$ (which corresponds to $\delta\Phi$ vanishing at the base of the crust). Our boundary conditions are thus

$$\xi_r = 0 \qquad (5.104)$$
$$\frac{d\xi_r}{dr} = \beta\frac{\xi_\perp}{r_b} - \xi_r\frac{d\ln\rho}{dr} - 2\frac{\xi_r}{r_b} \qquad (5.105)$$
$$\psi = 0 \qquad (5.106)$$

The shape can in fact be described by a variable defined to label the equipotential surface of the density or pressure (very much like ψ). We can thus define

$$\varepsilon_s = -\frac{\delta p}{r\partial_r p} \qquad (5.107)$$

At the surface we may impose that the shape is given by a certain $\bar{\varepsilon}_s = \varepsilon_s(R)$. We will then search for the value of $\bar{\varepsilon}_s$ that causes the crust to crack (at some interior point, not only at the surface), following the Von Mises criterion. The final thing we need, before considering the surface of the star, are the background quantities for our model, the density and the derivatives of the gravitational potential.

These calculations are all Newtonian, and thus not very accurate in the core where we expect relativistic effects to be important. As we are imposing that the core is not perturbed we can integrate the TOV equations in the core, and then match them to the Newtonian quantities we use in the crust (at the low densities of the crust the Newtonian approximation is reasonably accurate). This is important as it will allow us to use a realistic equation of state for the core, which would be pointless if we were considering a fully Newtonian star. It is in fact well known that stellar models with the same EOS and central density can give very different results in the Newtonian and relativistic cases.

As is obvious from the above equations, both the background quantities ρ and μ vanish at the surface of the star, thus causing the tractions to trivially vanish. We shall then need to impose regularity conditions. Starting from our background model we can expand our equations around $r = R$ (the surface) and thus obtain

$$\frac{d^2\xi_r}{dr^2} = \frac{1}{(r-R)}\left[\frac{\xi_r}{R} - \frac{\beta}{2}\frac{\xi_\perp}{R} - \frac{d\xi_r}{dr}\right] + O(1) + O(r-R) \quad (5.108)$$

$$\frac{d^2\xi_\perp}{dr^2} = -\frac{1}{(r-R)}\left[\frac{\xi_\perp}{R} + \beta\frac{\xi_r}{R} + \frac{d\xi_\perp}{dr}\right] + O(1) + O(r-R) \quad (5.109)$$

We now have two second order equations for ξ_r and $\xi_\perp$ which have decoupled from the equation for ψ (which we are not interested in, as we already know what boundary condition to use for ψ). The solution involves a combination of Bessel functions, this allows us to discard the ones that diverge at $r = R$ (the Bessel functions of the second kind).Thus by using the regular solution we can impose a relation between the functions and their derivatives:

$$\frac{d\xi_r}{dr} = -\frac{\xi_\perp\beta - 2\xi_r}{2R} - \xi_r\frac{\beta^2+2}{2R^2}(r-R) + O\left((r-R)^2\right) \quad (5.110)$$

$$\frac{d\xi_\perp}{dr} = -\frac{\xi_\perp + \xi_r\beta}{R} - \xi_\perp\frac{\beta^2+2}{2R^2}(r-R) + O\left((r-R)^2\right) \quad (5.111)$$

which is the boundary condition we impose close to the surface, together with the magnitude of the perturbation, i.e. the value $\bar{\varepsilon_s}$. We thus have a total of three conditions at the surface and three at the base of the crust.

5.4.2 Perturbations of the core

So far we have derived boundary conditions for the problem of an unperturbed core with a perturbed crust. We shall now turn our attention to

the more realistic problem of a perturbed crust with a perturbed core. Let us solve the whole set of equations in the core and the crust. In the core we need to solve the same set of equations as in the crust, but now we have no shear modulus, and so they reduce to simple hydrostatic equations

$$\nabla p = -\rho \nabla \Phi \tag{5.112}$$

which we can expand along our basis vectors

$$\hat{r}^a Y_{lm} \left(\partial_r \delta p + \rho \partial_r \delta \Phi + \delta \rho \partial_r \Phi \right) = 0 \tag{5.113}$$

$$\nabla^a Y_{lm} \left(\delta p + \rho \delta \Phi \right) = 0 \tag{5.114}$$

The equations simplify to

$$\delta p = -\rho \delta \Phi \tag{5.115}$$

$$\delta \rho = \frac{\partial_r \rho}{\partial_r \Phi} \delta \Phi \tag{5.116}$$

We can substitute these into Poisson's equation

$$\nabla^2 \delta \Phi = 4\pi G \delta \rho \tag{5.117}$$

and obtain an ODE for $\delta \Phi$

$$\frac{d^2 \delta \Phi}{dr^2} + \frac{2}{r} \frac{d \delta \Phi}{dr} - \frac{6}{r^2} \delta \Phi = 4\pi G \frac{\partial_r \rho}{\partial_r \Phi} \delta \Phi \tag{5.118}$$

which we can solve together with equations (5.116). The only boundary conditions we need to impose are those of regularity at the centre, i.e. that the solution close to $r = 0$ is of the form Ar^2 where A is a constant. This leads to

$$\frac{d \delta \Phi}{dr} = 2 \frac{\delta \Phi}{r} \qquad \text{close to the centre} \tag{5.119}$$

We then impose continuity of the tractions at the base of the crust.

5.5 Results for an n=1 polytrope

Let us consider a specific stellar model for which we take an $n = 1$ polytropic equation of state $p = K\rho^2$, which leads to

$$\delta p = 2K\rho \delta \rho \tag{5.120}$$

As in previous examples the shear modulus is taken to be such that $\mu/\rho = 10^{16}\ cm^2/s^2$. We solve the equations numerically by using a shooting

method with a Runge-Kutta 5th order variable step size routine (Cash-Karp). We calculate the quadrupole moment and gradually increase the value of ψ until the crust breaks (following the Von Mises criterion). The equations are integrated in three different cases:

1. Newtonian equations throughout the star, only perturbations of the crust
2. TOV equations in the core, Newtonian in the crust, only perturbations of the crust
3. Newtonian equations throughout the star, perturbations of the core and crust

In the first two cases the core is unperturbed, so we impose the boundary conditions derived in section 5.1, the last case includes a perturbed core, so the boundary conditions are the ones described in section 5.2. We choose these cases as an unperturbed core has the advantage that it can be obtained by integrating either the Newtonian equations of hydrostatic equilibrium, or the TOV equations. This allows us to estimate how important overall relativistic effects may be. The results are presented in Figure 5.4 taking different densities for the base of the crust. This allows us both to compare with Ushomirsky et al. [144], who take the density at the base of the crust to be $2.1 \times 10^{14}\mathrm{g/cm^3}$, and to use the value $1.6 \times 10^{14}\mathrm{g/cm^3}$, suggested by Haensel [48]. The results for these two particular cases are shown in Table 5.2. The Newtonian calculation with the unperturbed core can be fitted to the formula

$$Q_{\max} = 1.1 \times 10^{37} \left(\frac{\rho_b}{1.6_{14}\frac{g}{cm^3}}\right)^2 \left(\frac{R}{10km}\right)^{6.9} \left(\frac{M}{1.4M_\odot}\right)^{-1.1} \left(\frac{\bar{\sigma}\max}{10^{-2}}\right) \mathrm{g\ cm^2} \tag{5.121}$$

The dependence on ρ_b of the calculation with the relativistic core is not well fitted by a simple power law, as we can see from figure 5.4, where it is evident that for thicker crusts the maximum quadrupole is growing at a slower rate. However, if we take $\rho_b = 1.6 \times 10^{14}$ g/cm^3 and $R = 10$ km, the dependence on the stellar mass is well fitted by

$$Q_{\max} = 1.6 \times 10^{37} \left(\frac{M}{1.4M_\odot}\right)^{-0.3} \mathrm{g\ cm^2} \tag{5.122}$$

The Newtonian calculation including the perturbations of the core is also very interesting. As we can see from Figure 5.4 the quadrupole built up

in the core is predominant if we take the base of the crust at low densities, which is equivalent to having a thin crust. The crust quadrupole, on the other hand, becomes predominant for thick crusts, and is well approximated by the Newtonian calculation with the unperturbed crust, as we can see in Figures 5.4 and 5.5. It is also very instructive to observe, in the case of the perturbed core, how the maximum quadrupole depends on the mass of the star (Figure 5.5). Unlike the other two cases the quadrupole gets larger as the star gets heavier. This is because the quadrupole from the perturbations of the core is growing as the star is made more massive, while the crustal quadrupole is in fact decreasing. The dependence on the stellar radius is shown in Figure 5.6 for the case of a perturbed Newtonian core and that of an unperturbed relativistic core; the two cases are similar and not altogether surprising. All calculations are linear in the breaking strain.

	$\|Q_{max}\|$ (g cm^2) ($\rho_b = 1.6 \times 10^{14}$g/cm^3)	$\|Q_{max}\|$ (g cm^2) ($\rho_b = 2.1 \times 10^{14}$g/cm^3)
Core&Crust-Newtonian	2.5×10^{37} ($\epsilon = 5.1 \times 10^{-8}$)	3.1×10^{37} ($\epsilon = 6.3 \times 10^{-8}$)
Crust-Newtonian	1.1×10^{37} ($\epsilon = 2.2 \times 10^{-8}$)	1.9×10^{37} ($\epsilon = 3.9 \times 10^{-8}$)
Crust-TOV+Newtonian	1.6×10^{37} ($\epsilon = 3.3 \times 10^{-8}$)	2.2×10^{37} ($\epsilon = 4.6 \times 10^{-8}$)
UCB(Newt)	6.8×10^{37} ($\epsilon = 1.4 \times 10^{-7}$)	1.2×10^{38} ($\epsilon = 2.5 \times 10^{-7}$)

Table 5.2: Maximum quadrupole, in the case of $\sigma_{max} = 10^{-2}$ for an $n = 1$ polytrope, and the base of the crust at $\rho_b = 1.6 \times 10^{14}$ g/cm^3 and $\rho_b = 2.1 \times 10^{14}$ g/cm^3. The parameters of the stellar models are given in table 5.3.(UCB indicates the result of [144]).

	M_{core} ($M_\odot$)	Δ_T (km)	K (g^{-1}cm^{5}s^{-2})	ρ_c (g/cm^3)	ρ_b (g/cm^3)
TOV+Newt	1.358	1.115	7.24×10^4	2.45×10^{15}	1.6×10^{15}
Newt	1.37	0.68	4.25×10^4	2.2×10^{15}	1.6×10^{15}
TOV+Newt	1.33	1.39	7.07×10^4	2.54×10^{15}	2.1×10^{15}
Newt	1.35	0.88	4.25×10^4	2.2×10^{15}	2.1×10^{15}

Table 5.3: Parameters of the two stellar models, the fully Newtonian model and the relativistic model with a Newtonian crust, for a density at the base of the crust of $\rho = 1.6\times10^{14}$ g/cm^3 and $\rho = 2.1 \times 10^{14}$ g/cm^3. Δ_T is the crust thickness.

It would appear from the results of our calculations that considering the perturbations of the core can make a difference in the result, mainly for thin crusts. On the other hand it appears that if the crust is thick, then the crustal quadrupole plays the predominant role, and is well approximated by taking a perturbed crust on top of an unperturbed core. In this case relativistic effects can become important, and it would then not seem appropriate to use realistic equations of state, but still describe the core with Newtonian equations of equilibrium. On the other hand it would seem to be the case that one can consider an unperturbed relativistic core (with a realistic EOS), then use a realistic EOS and μ in the Newtonian crust and still have a reasonable approximation to the full problem. We are of course still solving the problem in Newtonian elasticity, so not solving the problem in "full" GR, but at the densities of the crust the Newtonian approximation is a reasonable one, and makes the problem considerably simpler than it would be in relativistic elasticity.

5.6 Application to the Accreted vs. Non-Accreted problem

We can now consider the stellar models presented in Table 5.1 for two stars, one with a non-accreted crust and one with an accreted crust. We shall first take the two stars to have the same mass, then we shall also consider two stars with the same crust thickness. As the crust is now thick, as shown in Table 5.1, we expect the crustal quadrupole to dominate and can thus consider the approximation of an unperturbed core to be reasonable. This then allows us to use the equation of state given in [28] and solve the TOV equations in the core and the Newtonian equations of hydrostatic equilibrium in the crust, thus taking relativistic effects into account. The results are shown in Table 5.4. As expected the values for the quadrupole do not differ significantly. We also confirm that a neutron star with an non accreted crust could provide a slightly better source of gravitational waves, as was expected from the literature ([121]), if both kinds of crust have the same breaking strain. It should be noted that this may not be the case. In fact it is likely not to be so, as the two kinds of crust will have had a very different history. There is not, however, any physical model for such an effect an we shall, thus, take both breaking strains to be the same and equal to the maximum permissible value, in order to obtain an upper limit. The values of the quadrupole (or equivalently the ellipticity) are now larger than in the

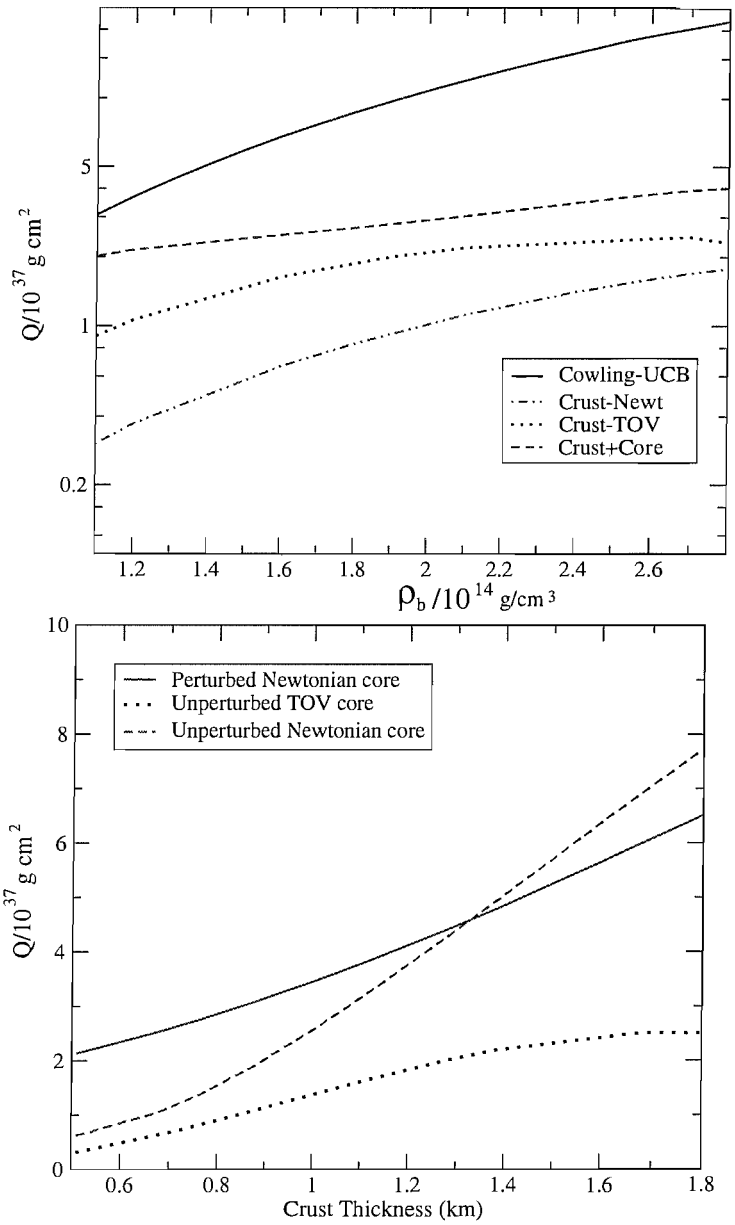

Figure 5.4: On the left hand side we have the maximum quadrupole plotted first with respect to the density of the base of the crust. We present the three cases described in the text and also the result in [144], marked as UCB. On the right hand side we have the maximum quadrupole, for the three cases considered in the main text, plotted with respect to the crust thickness.

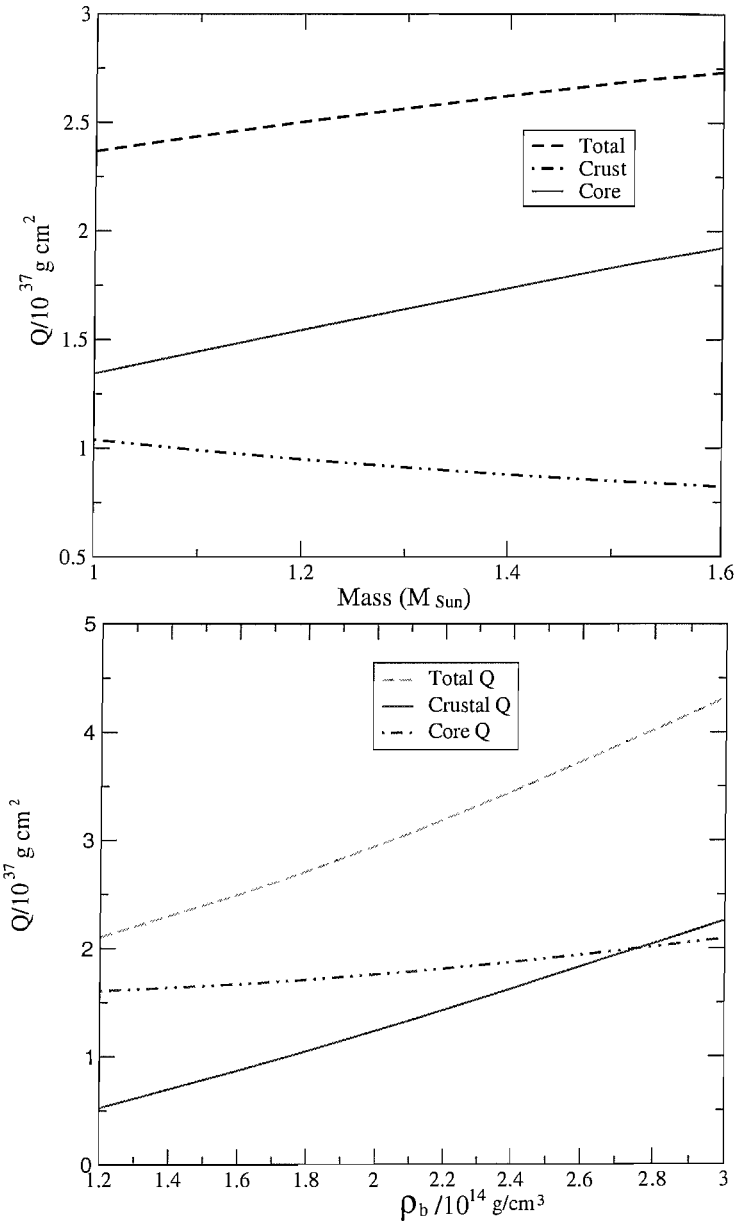

Figure 5.5: The dependence of the maximum quadrupole on ρ_b and on the mass of the star, in the case of a perturbed core. For this case we plot also the single contributions of the crust and the core.

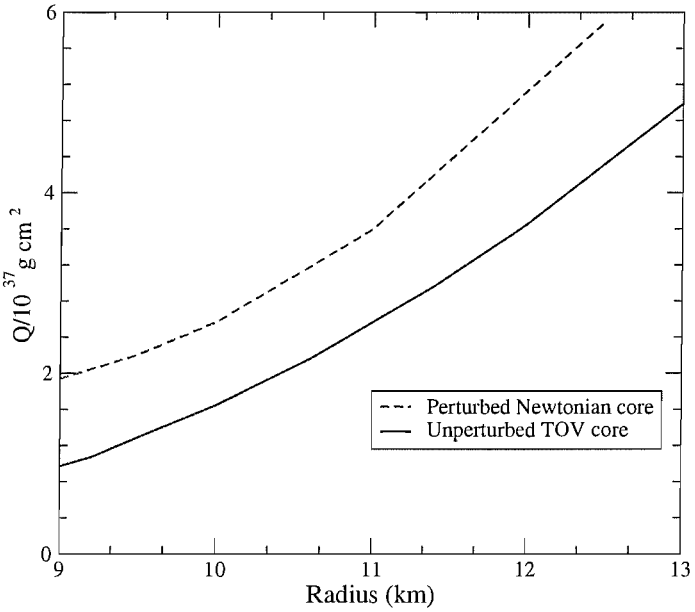

Figure 5.6: Dependence of the maximum quadrupole on the stellar radius, in the case of a perturbed Newtonian core and of an unperturbed TOV core.

previous case as we are taking a realistic model for the shear modulus (as shown in figure 5.2). This leads to values of μ which are significantly larger than in the constant ratio μ/ρ approximation, especially in the higher density regions close to the base of the crust, which give rise to most of the quadrupole.

The values we find for ϵ are now comparable with the upper limits of $\epsilon \approx 10^{-5}$ set by LIGO for some of the closer pulsars ([1]). The best limits, however, are still set by pulsar spindown, and can be seen in Figure 5.7, compared to the limits set by this work.

5.7 Rotational deformations

We can use the formalism we have developed to estimate how much strain is produced by rotational deformations. This is quite important as the stars we are considering will be rotating, so we would like to have an estimate of how much strain would build up due to these deformations. To do this we will calculate the deformation from equation (2.49) of chapter 2, which allows us to obtain, as a function of the rotation rate,

	Accreted	Non Accreted	Accreted
Mass ($M_\odot$)	1.4	1.4	1.6
Radius (km)	12.56	12.3	12.3
Crust Thickness (km)	1.76	1.5	1.5
Qmax $(\frac{\sigma}{10^{-2}})$g cm^2	1.8×10^{39}	3.1×10^{39}	1.6×10^{39}
ϵ	1.3×10^{-6}	2.4×10^{-6}	1.1×10^{-6}

Table 5.4: Maximum quadrupole for two stars of equal mass, one with an accreted crust and one with a non-accreted crust. The last column shows a star with an accreted crust of the same thickness as that of the non accreted crust, but a different mass. The perturbative formalism of section 5 is used and the base of the crust is taken to be at 1.3×10^{14}g/cm^3 as in [28].

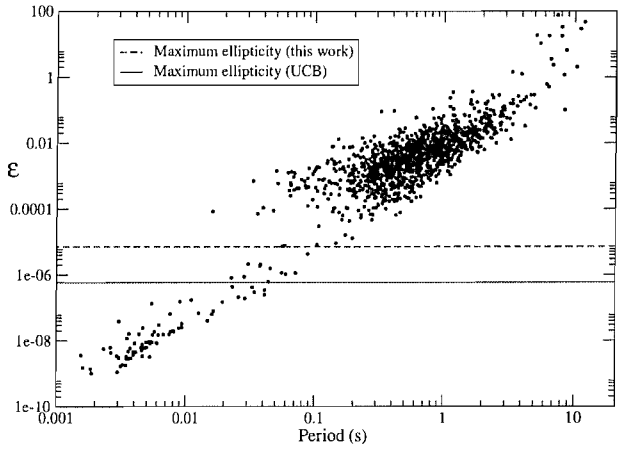

Figure 5.7: The upper limits on the ellipticity ϵ set by pulsar spin down and the theoretical upper limits set by the perturbative method this work (top line) and with the method of [144] (bottom line). Data taken from the ATNF pulsar database, www.atnf.csiro.au/research/pulsar/psrcat/, [76].

the variable

$$a(r) = r\left(1 + \epsilon(r) P_2(\cos\theta)\right) \tag{5.123}$$

As we want to use the same formalism as in the preceding section we want to project on Y_{20} rather than on P_2 and thus need to include the normalization in the variable $\epsilon(r)$ and thus take for the "shape"

$$\epsilon_s = \sqrt{\frac{5}{4\pi}}\epsilon. \tag{5.124}$$

We can then solve the differential equation (2.49) for ϵ_s and obtain the shape the star would have at a given roation rate if it were purely fluid. This of course is an approximation, however the main effect is that of rotation, and the contribution of the elastic crust to the magnitude of the deformation is minimal. We can thus use the value of ϵ_s to impose boundary conditions for the perturbation problem in the crust, which allows us to calculate the strain. We shall in fact impose that the shape of the star at the base of the crust is $\epsilon_s(r_b)$ (obtained from equation 2.49), and also that the shape at the surface is $\epsilon_s(R)$.

With these boundary conditions we integrate the Y_{20} part of the perturbation equations, which differs from the Y_{22} part presented in the preceeding sections because of the introduction of the centrifugal potential, which has a Y_{20} part

$$\Phi_{\text{tot}} = \Phi - \frac{1}{2} r^2 \Omega^2 \sin\theta^2 \tag{5.125}$$

$$\Phi_{\text{tot}} = \Phi - \frac{\sqrt{4\pi}}{3}\Omega^2 r^2 Y_{00} + \frac{1}{3}\sqrt{\frac{4\pi}{5}}\Omega^2 r^2 Y_{20} \tag{5.126}$$

The relation between the basis vectors now reads:

$$\frac{1}{4}\left[ReY_{20}\right]^2 + \frac{1}{4}\left[Re(f_{ab})\right]^2 + \frac{3}{2}\left[Re(\Lambda_{ab} + \frac{1}{2}Y_{20}e_{ab})\right]^2 = \frac{5}{16\pi} \tag{5.127}$$

And the strain $\bar{\sigma}$ can be calculated by

$$2\bar{\sigma}^2 = \frac{3}{2}\sigma_{rr}^2 Y_{20}^2 + \sigma_{r\perp}^2 \frac{15}{16\pi}\sin 2\theta^2 + \sigma_{\Lambda}^2 \frac{5}{32\pi}\sin\theta^4 \tag{5.128}$$

as can be found also in [27]. To obtain the full strain we should also consider the Y_{00} part of the deformation, as there is also a constant part in the centrifugal potential, but we shall neglect that part here, as we only want an order of magnitude estimate of how much strain there can be in other harmonics apart from Y_{22}. We find that the rotation rate

at which the crust breaks, if it spins up from an unstrained spherical configuration, corresponds to periods:

$$P \approx 0.1s \tag{5.129}$$

This means that, as argued in [27], in its life a Neutron Star will undergo a series of star quakes that relax the strains that build up as it spins down (or up) and bring them to be sub-critical everywhere. How much strain is built up obviously depends on the original shape the star had when the crust solidified and its spin down history. Solving this complex problem is beyond the scope of this simple investigation. From the calculation above it is, however, evident that there can be a large contribution to the strain in the Y_{20} harmonic, which can greatly reduce the size of a Y_{22} "mountain" that the crust can sustain. Our estimates of the quadrupole are thus obviously and upper limit, and could be greatly decreased if the crust is already close to its yield point.

5.8 Conclusions

We have reviewed the method of Ushomirsky et al. [144] to determine the maximum deformation that a neutron star crust can sustain. This procedure has then been applied to the case of an accreted and a non-accreted crust, in order to estimate whether one of the two would produce a better source of gravitational waves. It appears that the two kinds of crust are essentially equivalent, with the non-accreted crust being able to support a slightly larger quadrupole, as has been suggested in the literature (e.g. [121]). It is important to note, however, that to obtain this result is has been necessary to extrapolate the composition of the crust in the high density regions at the base of the accreted crust. In order to confirm this result it would therefore be necessary to have a precise model for the composition in this region.

We have then examined a series of toy models, to determine what effect the Cowling approximation can have on the problem and, more crucially, if it is safe to assume that the shear modulus $\mu \longrightarrow 0$ at the base of the crust. We conclude that this is not the case, as the shear modulus is expected to vanish over a thin transition region close to the base of the crust, which can lead to large boundary terms. The Cowling approximation can also make a difference of factors of a few in the final result.

In order to drop the Cowling approximation, and have better control over the boundary conditions, we have developed a perturbation formal-

ism and applied it to the case of an $n = 1$ polytrope with a constant ratio μ/ρ. The results of these tests have confirmed that the Cowling approximation used in [144] can have a large impact. Our results, however, also suggest that it is not a bad approximation to consider an unperturbed core and perturb the crust, if the crust is sufficiently thick. This allows us to solve relativistic equations in the core, which can give corrections that are significant if we intend to use a realistic equation of state for the star. Having developed the formalism we apply it to the original problem of accreted and non-accreted crusts, with a realistic model for μ, thus confirming that the two crusts can sustain very similar quadrupoles, the non accreted crust being able to sustain a slightly larger "mountain", if we assume the two breaking strains to be the same. This may not necessarily be the case, as the two kinds of crust will have had a different history, but, as we have no model for the breaking strain, we shall assume that it is simply the maximum permissible value in both cases. What is surprising is the fact that the quadrupole found with this formalism is approximately an order of magnitude greater than the results obtained with the formalism in [144]. Such a significant quadrupole, if it were confirmed, may allow us to put an upper limit on the breaking strain of the crust from observations. The problem, however, is not quite so simple. The calculations we have presented give a "maximum" quadrupole in as much as we have assumed all the strain to be in the Y_{22} harmonic. But the stars we consider are rotating and must therefore be rotationally deformed, thus putting strain also in the Y_{20} harmonic, as spin-up or spin-down moves the star away from its reference shape. This could bring the crust much closer to the yield point and significantly decrease the size of any additional "mountain" that it could sustain. Unfortunately, estimating exactly how much strain is built up by rotation is a complicated problem, as the unstrained configuration of the crust depends on the history of the crust, and there may have been many starquakes during the spin-down and subsequent spin-up phases. However, if a neutron star can sustain a quadrupole this large for a breaking strain of $\sigma_{\max} = 10^{-2}$, it would appear that even if the breaking strain is smaller there is still a possibility that the quadrupole may be large enough for gravitational waves to have a role in the spin evolution of the star.

Finally we should note that our approach was chosen in order to obtain a "maximization" argument, independent of the mechanism that produces the deformation, and to show that overall relativistic effects can be important. We have, therefore, integrated a set of source free equations, analogous to those in [84], with the deformation as a boundary condition. It would, however, be important to understand the physical

processes that cause the deformation and integrate the same equations with a source, such as the temperature or composition variations used in [144]. Another important effect we are neglecting is that of the magnetic field. It is well known that the equilibrium shape of a star will not be spherical in the presence of a magnetic field and, even though crustal effects may be dominant early on during accretion, the process of magnetic burial could make the field locally strong enough for the magnetic deformations to become important. This effect was recently studied in [85] and [109], who were the first to perform globally self-consistent MHD calculations of magnetic mountains on accreting NS as gravitational wave sources. These calculations did not include crustal effects (as this would make the problem much less tractable), nevertheless it is important to note here that if one were to solve the full inhomogeneous problem, including the magnetic source terms (or terms due to other physical process we have neglected), one could obtain deformations larger than the crustal maximum we have calculated.

It would also be of some interest to consider the full problem in a relativistic formulation of elasticity, such as that in [65], as we have shown that the perturbations of the core can be important, especially in determining the dependence of the maximum quadrupole on the stellar parameters.

Chapter 6

Magnetic mountains

It is clear from the previous chapters that a distorted neutron star can be a very interesting source of gravitational waves. Especially in LMXBs, an accreting neutron star can be rapidly rotating, and if it were distorted this would lead to the emission of gravitational waves, thus potentially explaining the spin equilibrium distribution of these systems [18]. Although it is not necessary to invoke gravitational waves to explain the spin equilibrium of LMXBs [9], the various emission mechanisms are still viable and these systems are likely to be interesting sources. In chapter 5 we have examined one of the main processes that could lead to gravitational wave emission: a "mountain" sustained by the elastic crust that leads to a quadrupolar deformation. There are, however, another two main emission mechanisms; one is the possibility of unstable r-modes being excited [6], the other is a strong magnetic field deforming the star. This chapter will be devoted to exploring this last possibility. The idea that this process could be active in LMXBs was first suggested by Cutler [26], who pointed out that if a star has a strong internal toroidal field it will become prolate and, if the magnetic axis is inclined with respect to the rotation axis, the system will be unstable and the star will become an orthogonal rotator on the viscous timescale, thus becoming an optimal gravitational wave source. The fact that a strongly magnetised star could emit gravitational waves, however, is not new. Heyl [51] has suggested that magnetised white dwarfs may be an interesting source of gravitational waves and several numerical studies have been directed at understanding the GW emission of magnetically distorted neutron stars [20], [85]. In the following we shall review the processes that lead to magnetic deformations and investigate some special cases.

6.1 Magnetic fields in stellar interiors

Chandrasekhar and Fermi [23] where the first to realise that a star would not remain spherical in presence of a strong magnetic field. They calculated the deformation of an incompressible star with a constant dipolar field by minimising the energy of the configuration. The case of a constant density star with an internal poloidal field matched to an external dipole was later considered by Ferraro [32] and by Goosens [45], by solving the Euler equations. The same results can be obtained with the method illustrated in chapter 2 for slow rotation. First of all let us consider the magnetic field in the star. The equations of hydrostatic equilibrium are:

$$\frac{\nabla P}{\rho} = -\nabla\Phi + \frac{(\nabla \times H) \times H}{4\pi\rho} \tag{6.1}$$

where H is the magnetic field, P is the pressure, ρ the density and Φ the gravitational potential which obeys Poisson's equation

$$\nabla^2\Phi = 4\pi G\rho. \tag{6.2}$$

The magnetic field must also obey, from Maxwell's equations

$$\nabla \cdot H = 0 \tag{6.3}$$

and we shall take a polytropic equation of state

$$P = K\rho^{1+1/n}. \tag{6.4}$$

Following [117] let us take the curl of equation (6.1); this leaves us with an equation for the magnetic field

$$\nabla \times \left(\frac{H \times (\nabla \times H)}{\rho} \right) = 0. \tag{6.5}$$

This equation now contains the density, so it should be solved simultaneously with equation (6.1). We will however assume that the magnetic field only produces small deviations from the background spherically symmetric model (we can for example assume that the ratio of magnetic to gravitational energy is small). This allows us to expand all our variables in the form

$$\psi(r,\theta) = \psi_0(r) + \psi_1(r)P_l \tag{6.6}$$

where P_l are the standard Legendre polynomials and ψ_1 is a small perturbation of $O(H^2)$. We can then first of all solve the structure equations in

the absence of a magnetic field and obtain the background model; we can then feed this into equation (6.5) and solve for H, which we will need to solve equation (6.1) and (6.2) to first order for the quantities ρ, P and Φ. Restricting ourselves to axisymmetry, the ϕ component of the magnetic force must be zero, as there is nothing to balance it in equation (6.1), hence

$$[H \times (\nabla \times H)]_\phi = 0 \tag{6.7}$$

Let us then examine some general magnetic field solutions for various background models. If one now splits the magnetic field into to components, a poloidal one $H_p = (H_r, H_\theta, 0)$ and a toroidal one $H_t = (0, 0, H_\phi)$, and introduces a stream function $S(r, \theta)$ such that

$$\begin{aligned} H_r &= \frac{1}{r^2 \sin\theta} \frac{\partial S}{\partial \theta} \\ H_\theta &= \frac{-1}{r \sin\theta} \frac{\partial S}{\partial r} \end{aligned} \tag{6.8}$$

then equations (6.7) and (6.3) reduce to [117]:

$$H_p \cdot \nabla (r \sin\theta H_\phi) = 0 \tag{6.9}$$

which gives

$$H_\phi = \frac{\beta(S)}{r \sin\theta} \tag{6.10}$$

Where β is some function of r and θ. Equation (6.5) then takes the form

$$\begin{aligned} &\frac{\partial}{\partial r}\left\{\frac{1}{\rho r \sin\theta}\frac{\partial S}{\partial \theta}\left(\frac{1}{r\sin\theta}\frac{\partial^2 S}{\partial r^2} + \frac{1}{r^3}\frac{\partial}{\partial\theta}\left(\frac{1}{\sin\theta}\frac{\partial S}{\partial\theta}\right)\right)\right. \\ &\left. + \frac{\beta}{\rho r^2 \sin^2\theta}\frac{\partial \beta}{\partial \theta}\right\} - \frac{\partial}{\partial\theta}\left\{\frac{1}{\rho r \sin\theta}\frac{\partial S}{\partial r}\left(\frac{1}{r\sin\theta}\frac{\partial^2 S}{\partial r^2}\right.\right. \\ &\left.\left. + \frac{1}{r^3}\frac{\partial}{\partial\theta}\left(\frac{1}{\sin\theta}\frac{\partial S}{\partial\theta}\right)\right) + \frac{\beta}{\rho r^2 \sin^2\theta}\frac{\partial\beta}{\partial r}\right\} = 0 \end{aligned} \tag{6.11}$$

In the following we shall be looking for dipole solutions. We can thus take a stream function of the form

$$S(r, \theta) = A(r) \sin^2\theta \tag{6.12}$$

or directly look for solutions in the form:

$$H = \hat{r}\{\Lambda(r)\cos\theta\} + \hat{\theta}\{X(r)\sin\theta\} + \hat{\phi}\{iZ(r)\sin\theta\} \tag{6.13}$$

for this kind of field equation (6.3) gives

$$r\Lambda^{'}(r) + 2\left(\Lambda(r) + X(r)\right) \tag{6.14}$$

We now need to solve equation (6.5) (or equivalently equation (6.11), which depends on the density stratification $\rho(r)$; it is thus necessary for us to prescribe a specific stellar model.

6.2 Uniform density

In a first instance let us take ρ=constant and insert this into equations (6.3) and (6.5). This leads to

$$\Lambda\left(rZ\right)^{'} + 2ZX = 0 \tag{6.15}$$

$$\Lambda\left(r^2Z^{''} - 2Z\right) + 2Z\left(rX^{'} - X\right) = 0 \tag{6.16}$$

$$\Lambda\left[r^2X^{''} - 4\left(\Lambda + X\right)\right] + 2Z\left(rZ^{'} - Z\right) = 0 \tag{6.17}$$

6.2.1 Poloidal fields

Let us restrict our attention to purely poloidal fields. A special case is that of a uniform field for which $\Lambda = -X$ =constant. In this case we can combine equation (6.17) with equation (6.3) to get

$$r^2X^{'''} + 4rX^{''} - 4X^{'} = 0 \tag{6.18}$$

which has the solution

$$X = A + Cr^2 \tag{6.19}$$

with A and C constants and where the $\approx r^{-3}$ solution has been excluded to ensure regularity at the centre. This gives, for Λ,

$$\Lambda = -A - \frac{1}{2}Cr^2 \tag{6.20}$$

Note that for $C = 0$ this corresponds to a uniform dipole field. If we are solving for the stream function it is sufficient to take $S(r, \theta)$ of the form in equation (6.12) and take $\beta = 0$ so that the magnetic field reduces to

$$H = \left(\frac{2A\cos\theta}{r^2}, \frac{-A^{'}\sin\theta}{r}, 0\right) \tag{6.21}$$

Where $A^{'}$ indicates dA/dr. We can now solve equation (6.11) with the boundary conditions that the field must remain finite at the centre. i.e.

$$\frac{A}{r^2}, \frac{A^{'}}{r} \text{ finite at } r = 0 \tag{6.22}$$

and at the surface the field must be continuous with an external curl free dipole field, so that

$$\frac{A}{r} + A^{'} = 0 \tag{6.23}$$

at the surface. An interesting solution was given by Ferraro [32], who considered a constant density star with a current density of the form

$$J = Kr^3 \sin^3\theta \tag{6.24}$$

where K is a constant. In this case equation (6.11) reduces to

$$\Delta S = Kr^2 \sin^2\theta \tag{6.25}$$

which yields for the stream function:

$$S = K\left(\frac{r^4}{10} - \frac{R^2 r^2}{6}\right)\sin\theta^2 \tag{6.26}$$

The magnetic field is then

$$\begin{aligned} H_r &= K\left(-\frac{R^2}{3} + \frac{r^2}{5}\right)\cos\theta \\ H_\theta &= K\left(\frac{R^2}{3} - \frac{2r^2}{5}\right)\sin\theta \end{aligned} \tag{6.27}$$

6.2.2 Toroidal field

For a purely toroidal field, on the other hand, the equations reduce to

$$rZ^{'} = Z \tag{6.28}$$

which gives

$$Z = -iAr \tag{6.29}$$

This corresponds to a uniform current distribution inside the star, i.e. $|\nabla \times B| = 2A$, pointing along the z-axis .

6.2.3 Mixed poloidal/toroidal field

Let us, however, return to the general case. We can formally solve equation (6.14) for X, then equation (6.15) becomes

$$r^2\left(\Lambda Y^{'} - Y\Lambda^{'}\right) = 0 \tag{6.30}$$

where we have defined $Y = Z/r$. Hence, unless $Y = 0$ or $Z = 0$ we have

$$Y = a\Lambda \quad \text{or} \quad Z = ar\Lambda \tag{6.31}$$

Note that equation (6.16) is implied by (6.15) by the use of (6.14); thus the substitutions

$$Z = ar\Lambda \quad \text{and} \quad X = -\Lambda - \frac{r}{2}\Lambda' \tag{6.32}$$

solve equations (6.15) and (6.16). The last equation (6.17) then becomes

$$\frac{1}{2}r\Lambda\left(r^2\Lambda''' + 4r\Lambda'' - r(1+a^2r^2)\Lambda'\right) = 0 \tag{6.33}$$

Disregarding the trivial solution we find that the general solution is

$$\Lambda = \frac{1}{r^3}[C_1(2ar-1)e^{2ar} + C_2(2ar+1)e^{-2ar}] + C_3 \tag{6.34}$$

leading to

$$X = -\frac{1}{2r^3}[C_1(4a^2r^2-2ar+1)e^{2ar} - C_2(4a^2r^2+2ar+1)e^{-2ar}] - C_3 \tag{6.35}$$

In order to assure regularity at the centre we must take $C_1 = C_2$, and the central values of the fields become

$$\Lambda_C = -X_C = \frac{16}{3}C_1a^3 + C_3 \quad \text{and} \quad Z_C = ar\Lambda_C = 0 \tag{6.36}$$

As we can see the parameter a is just a length scale and can be absorbed in the other constants if we define a new dimensionless radial coordinate $x = 2ar$. This allows us to redefine the constants as

$$C_1 = C_1/(2a)^3 \quad \text{and} \quad C_3 = C_3/(2a)^3 \tag{6.37}$$

The free parameters in the regular solution now correspond to the new C_1 and C_3 and are only two (if we exclude the trivial choice of scale or units given by a). Explicitly

$$\begin{aligned}
\Lambda &= \frac{2C_1\cosh(x)}{x^2} - \frac{2C_1\sinh(x)}{x^3} + C_3 \\
X &= \frac{C_1\cosh(x)}{x^2} - \frac{C_1(x^2+1)\sinh(x)}{x^3} - C_3 \\
Z &= \frac{C_1\cosh(x)}{x} - \frac{C_1\sinh(x)}{x^2} + \frac{1}{2}xC_3
\end{aligned} \tag{6.38}$$

We can further interpret the parameters by noting that the central values of the fields are now $\Lambda_C = -X_C = \frac{2}{3}C_1 + C3$ ($Z_C = 0$ still). We can thus use C_1 as an overall scale for the fields and define $\hat{\Lambda} = \Lambda/C_1$ and likewise for the other variables, thus, using $C_3/C_1 = \hat{\Lambda}_C - 2/3$, we obtain

$$\begin{aligned} \Lambda &= \frac{2\cosh(x)}{x^2} - \frac{2\sinh(x)}{x^3} + \hat{\Lambda}_C - 2/3 \\ X &= \frac{\cosh(x)}{x^2} - \frac{(x^2+1)\sinh(x)}{x^3} - \hat{\Lambda}_C + 2/3 \\ Z &= \frac{\cosh(x)}{x} - \frac{\sinh(x)}{x^2} + \frac{1}{2}x(\hat{\Lambda}_C - 2/3) \end{aligned} \tag{6.39}$$

These equations can be solved numerically after imposing boundary conditions at the surface.

Boundary conditions

Let us now focus on the boundary conditions that the magnetic field needs to satisfy at the surface of the star (at the centre it is sufficient to impose regularity). The solenoidal nature of the field requires continuity of the radial component

$$\langle B^r \rangle = 0 \tag{6.40}$$

we shall then require local force balance per unit area. This is the traction $t^a = T^{ab}\hat{n}_b$, i.e. the projection of the total stress tensor along the normal unit vector. Our condition is hence

$$\langle t^a \rangle = 0 \tag{6.41}$$

The stress energy tensor is the sum of a fluid piece and a magnetic piece

$$T^{ab} = -p\delta^{ab} + \frac{1}{4\pi}\left(B^a B^b - \frac{1}{2}B^2\delta^{ab}\right) \tag{6.42}$$

where p is the pressure. Let us consider the projection along the normal to the surface; this will have the form

$$\hat{n}_S = \hat{r} + \hat{n}^1_S \tag{6.43}$$

where $\hat{n}^1_S$ indicates the correction of $O(B^2)$. Projecting T^{ab} along this vector, we obtain

$$-p^0\delta^{ab}\hat{n}^1_{S(a)} - p^1\delta^{ar} + \frac{1}{4\pi}\left(B^a B^r - \frac{1}{2}B^2\delta^{ar}\right) \tag{6.44}$$

Note that the magnetic term is already $O(B^2)$ and one can take $\hat{n}_S = \hat{r}$. At the surface the background pressure p^0 vanishes, so we must impose continuity for

$$t^r = -p^1 + \frac{1}{4\pi}[(B^r)^2 - \frac{1}{2}B^2] \tag{6.45}$$

$$t^\theta = \frac{1}{4\pi}B^r B^\theta \tag{6.46}$$

$$t^\phi = \frac{1}{4\pi}B^r B^\phi \tag{6.47}$$

as we already have $< B^r >= 0$, from the θ and ϕ components of equations (6.47) we also have that $< B^\theta >=< B^\phi >= 0$, which leads to $< B^2 >= 0$. As $p = 0$ in the exterior, it must be that at the surface $p^1 = 0$ (all quantities are now $O(B^2)$ so we can consider the surface of the unperturbed configuration). The conclusion is thus that all components of the magnetic field must be continuous across the interface, i.e. that we have no surface currents. One could of course introduce surface currents and thus have discontinuities in the θ and ϕ components of the field. We feel, however, that, unless there are physical arguments dictating the nature of such currents, the traction conditions above should be used.

Note that if we have a purely toroidal field the conditions in (6.47) are automatically satisfied. The external magnetic field solves

$$\nabla \cdot B = \nabla \times B = 0 \tag{6.48}$$

and the assumption of axisymmetry forces a vanishing toroidal component $B^\phi = 0$. In the case of a purely poloidal field it is sufficient to match with an external curl-free dipole, in the case of a mixed poloidal/toroidal field, however, one must have that

$$Z(S^-) = 0 \tag{6.49}$$

and as we have found that $Z = ar\Lambda$ it must also be the case (provided $a \neq 0$) that $\Lambda = 0$. This means that, under axisymmetry, a mixed poloidal and toroidal dipolar internal field and a general multipolar external field are forced to obey $B^r_{int} = B^r_{ext} = 0$ and $B^\phi_{int} = B^\phi_{ext} = 0$ at the surface. It is thus immediately clear that we cannot match this kind of internal field with an external dipole field. One also has a condition on B^θ, as the exterior solution for a field, which is regular at infinity is of the form

$$B_E = \sum_{l \geq m} \hat{\mathbf{r}}[-(l+1)\frac{A_l}{r^{l+2}}Y_l^m] + \hat{\theta}[\frac{A_l}{r^{l+2}}\partial_\theta Y_l^m] + \hat{\phi}[\frac{imA_l}{r^{l+2}}\sin\theta Y_l^m] \tag{6.50}$$

It is thus clear that if the $\hat{\mathbf{r}}$ component must vanish at the surface, so must the $\hat{\theta}$ component. We thus have that all components of the mixed magnetic field must vanish at the surface.

$$B_r = B_\theta = B_\phi = 0 \tag{6.51}$$

In conclusion one can, therefore, match an interior mixed poloidal/toroidal dipole field only to a vanishing external field. It is thus interesting to note how, as a consequence of the boundary conditions, we are now restricting ourselves to a very limited class of field; notably poloidal or mixed poloidal/toroidal fields that vanish outside the star.

6.3 Non-uniform density

Let us now allow for a non-uniform density stratification. The allowed magnetic field must still satisfy equation (6.5), where the term in ρ is no longer trivial.

6.3.1 Poloidal field

For the case of an $n = 1$ polytrope, following [96], we shall solve equation (6.11), imposing regularity at the centre and matching to an external dipole. The solution for stream function is thus:

$$\begin{aligned} S &= -\frac{2}{3}\frac{(\sin\theta)^2}{rR^2\pi}\left[-r^3\pi^3 - 3\,\sin\left(\frac{r\pi}{R}\right) R\,r^2\pi^2\right. \\ &\quad \left. +6\,R^3\sin\left(\frac{r\pi}{R}\right) - 6\,R^2 r\pi\,\cos\left(\frac{r\pi}{R}\right)\right] \end{aligned} \tag{6.52}$$

which leads to field of the form

$$\begin{aligned} H_r &= \frac{B\cos(\theta)}{\pi R^3}\left[r^3\pi^3 + 3\,\sin\left(\frac{r\pi}{R}\right) R\,r^2\pi^2 - 6\,R^3\sin\left(\frac{r\pi}{R}\right)\right. \\ &\quad \left. +6\,R^2 r\pi\,\cos\left(\frac{r\pi}{R}\right)\right]\frac{1}{(\pi^2-6)} \\ H_\theta &= -\frac{B\sin(\theta)}{2}\frac{}{\pi R^3}\left[2\,r^3\pi^3 - 3\,\sin\left(\frac{r\pi}{R}\right) R\,r^2\pi^2 + 6\,R^3\sin\left(\frac{r\pi}{R}\right)\right. \\ &\quad \left. -6\,R^2 r\pi\,\cos\left(\frac{r\pi}{R}\right) + 3\,r^3\pi^3\cos\left(\frac{r\pi}{R}\right)\right]\frac{1}{(\pi^2-6)} \end{aligned} \tag{6.53}$$

where B is the value of the field at the surface.

6.3.2 Mixed toroidal and poloidal fields

Let us now assume a mixed poloidal and toroidal configuration. We will once again look for dipolar solutions and take a stream function of the form:

$$S(r,\theta) = A(r)\sin^2\theta \tag{6.54}$$

and we shall define β to be

$$\beta = \frac{\lambda}{R}S \tag{6.55}$$

where λ is a constant that describes the strength of the toroidal part of the field compared to the poloidal part. The magnetic field thus takes the form

$$\begin{aligned} H &= (H_r, H_\theta, H_\phi) \\ &= \left(\frac{2A\cos\theta}{r^2}, \frac{-A'\sin\theta}{r}, \frac{\lambda A\sin\theta}{rR}\right) \end{aligned} \tag{6.56}$$

Equation (6.11) can now be written as

$$A\frac{d}{dr}\left[\frac{1}{\rho r^2}\left(\frac{2A}{r^2} - \frac{d^2A}{dr^2}\right) - \frac{\lambda^2 A}{\rho R^2 r^2}\right] = 0 \tag{6.57}$$

We must solve equation (6.57) with the boundary conditions that the field remain finite at the centre, so that

$$\frac{A}{r^2}, \frac{A'}{r} \text{finite at } r = 0 \tag{6.58}$$

and that all the components of the magnetic field be continuous at the surface. As the toroidal field must vanish at the surface this forces the condition

$$A = 0 \tag{6.59}$$

it must also be the case that

$$A' = 0 \tag{6.60}$$

Which derives from the condition that all components of the field must vanish at the surface This justifies the boundary condition

$$A = A' = 0 \tag{6.61}$$

We can thus only consider fields that are vanishing outside the star.

n=1 polytrope

Let us now solve the above equations explicitly, for our case of an $n = 1$ polytrope. We thus need to solve equation (6.57) for $A(r)$ with a background density profile of the kind $\rho(r) = \rho_0 \sin(r\pi/R)R/r\pi$ and impose regularity at the centre and the conditions in (6.61). This leads to the condition

$$\frac{(\cos(\lambda)\lambda^3 - 3\sin(\lambda)\lambda^2 - \cos(\lambda)\lambda\pi^2 + \sin(\lambda)\pi^2)\pi B R^2}{(-\pi+\lambda)^2(\pi+\lambda)^2(-\sin(\lambda)+\cos(\lambda)\lambda)} = 0 \quad (6.62)$$

where B is a constant which parametrises the strength of the magnetic field and λ is the dimensionless parameter $\lambda = C/R$. Equation (6.62) is now an eigenvalue problem for the parameter λ and thus restricts the possible values for the strength of the toroidal field. By taking higher values of λ we can increase the relative strength of the toroidal part of the field compared to the poloidal part. The stream function thus takes the form

$$\begin{aligned} A(r) \;=\; & -\Big[\sin\Big(\frac{r\pi}{R}\Big) r^2\cos(\lambda)\lambda^3 - \sin\Big(\frac{r\pi}{R}\Big) r^2\sin(\lambda)\lambda^2 \\ & -\lambda\sin\Big(\frac{r\pi}{R}\Big) r^2\cos(\lambda)\pi^2 - 2\lambda R\pi\cos\Big(\frac{r\lambda}{R}\Big) r \\ & -2\lambda R\pi r\cos\Big(\frac{r\pi}{R}\Big) + 2\lambda\sin\Big(\frac{r\pi}{R}\Big) R^2\cos(\lambda) \\ & +\sin\Big(\frac{r\pi}{R}\Big) r^2\sin(\lambda)\pi^2 + 2R\pi r\cos\Big(\frac{r\pi}{R}\Big)\sin(\lambda) \\ & -2\sin\Big(\frac{r\pi}{R}\Big) R^2\sin(\lambda) + 2R^2\pi\sin\Big(\frac{r\lambda}{R}\Big)\Big] BR^2 \\ & (-\pi+\lambda)^{-2}(\pi+\lambda)^{-2}(-\sin(\lambda)+\cos(\lambda)\lambda)^{-1} r^{-1} \quad (6.63) \end{aligned}$$

with λ given by equation (6.62). The first three eigenvalues for λ are

$$\begin{aligned} \lambda_1 &= 7.420 \\ \lambda_2 &= 10.706 \\ \lambda_3 &= 13.917 \end{aligned} \quad (6.64)$$

which agree with the values given in [117] with an accuracy of $\approx 0.1\%$.

6.3.3 Purely toroidal fields

In the case of a purely toroidal field equation (6.5) takes the form

$$\frac{\partial}{\partial r}\Big(\frac{H_\phi}{\rho r\sin\theta}\Big)\frac{\partial}{\partial\theta}(H_\phi r\sin\theta) - \frac{\partial}{\partial\theta}\Big(\frac{H_\phi}{\rho r\sin\theta}\Big)\frac{\partial}{\partial r}(H_\phi r\sin\theta) \quad (6.65)$$

The boundary conditions we have to impose are now that the field vanish at the centre of the star and at the surface. We can take a solution of the form

$$H_\phi = A\rho r \sin\theta \tag{6.66}$$

which will satisfy the boundary conditions in equation (6.61) provided that $\rho = \frac{d\rho}{dr} = 0$ at the surface. This means that we can take solutions of the form (6.66) only for polytropic indexes $n > 1$. Note that, for a realistic neutron star equation of state, this condition will be satisfied, as the adiabatic index close to the surface is thought to be $\Gamma \approx 1.33$, giving $n \approx 3$ [28].

6.3.4 Field confined to the crust

It is well known that if the core of a neutron star is a type I superconductor the magnetic field will be expelled from the core and confined to the crust [20]. To discuss this situation one should in principle consider the full equations of hydrostatic equilibrium, including the elastic terms. However, in order to investigate this case, let us consider the case of a fluid with a magnetic field confined to a region close to the surface. Note that this is justified if we assume that the deformed shape is the relaxed configuration of the crust; in this case there are no strains, thus no elastic terms in the equilibrium equations. We shall consider the same field as in the previous section, i.e. of the form in (6.56). We shall, however consider the field to vanish inside a certain radius r_b (which can be considered to be the base of the crust). The boundary conditions for the third order differential equation (6.57) at the surface thus remain

$$A(R) = A^{'}(R) = 0 \tag{6.67}$$

the third condition condition comes from imposing continuity of the B_r component of the magnetic field, i.e. imposing

$$A(r_b) = 0 \tag{6.68}$$

We will again get an eigenvalue problem for the parameter λ, allowing us to calculate the permitted ratios of toroidal to poloidal field strength. It should be noticed that we are not imposing continuity of the tractions; in fact there is a discontinuity in the B^θ component of the field, which will lead to currents at the crust/core interface. In order to simplify the calculation we also take the core to be unperturbed, and simply impose continuity of the perturbation in the gravitational potential $\delta\phi$ and of it's derivative $\delta\phi^{'}$. We shall use this condition in the following to calculate magnetic deformations of stars.

6.4 Magnetic deformations

Now that we have determined the configuration of the magnetic field which is consistent with a chosen stellar interior, we can turn our attention to solving equations (6.1) in order to obtain the new equilibrium shape of the star. As we have already mentioned we shall use the techniques developed in chapter 2 to study slow rotation. We shall define a new variable

$$x(r,\theta) = r\left[1+\varepsilon(r)P_l(\theta)\right] \tag{6.69}$$

where r is the radial variable and P_l is a Legendre polynomial. The perturbed surface thus takes the form

$$x_s(r,\theta) = R\left[1+\varepsilon(R)P_l(\theta)\right] \tag{6.70}$$

where R is the radius of the unperturbed star. We shall also assume that the pressure, density and gravitational potential take the form

$$\psi(r,\theta) = \psi(r) + \delta\psi^l(r)P_l \tag{6.71}$$

where ψ is the background quantity and $\delta\psi$ is a small perturbation of $O(H^2)$. From now on unless there is a risk of confusion we shall write $\delta\psi$ and intend $\delta\psi^l$ Equations (6.1) thus take the form

$$\left(\frac{d\delta p}{dr}+\rho\frac{d\delta\phi}{dr}+\delta\rho\frac{d\psi}{dr}\right)P_l = \frac{\left((\nabla\times H)\times H\right)_r}{4\pi} \tag{6.72}$$

$$\left(\delta p+\rho\delta\phi\right)\nabla P_l = \frac{\left((\nabla\times H)\times H\right)_\theta}{4\pi} \tag{6.73}$$

and they must be solved together with the perturbed Poisson equation

$$\frac{d^2\delta\phi}{dr^2}+\frac{2}{r}\frac{d\delta\phi}{dr}-\frac{6}{r^2}\delta\phi = 4\pi\delta\rho \tag{6.74}$$

Let us first of all tackle the case of an incompressible star.

6.4.1 Deformations of incompressible stars

Poloidal field

In the case of an incompressible star we consider the field in equation (6.27), which gives us for the Lorenz force

$$\frac{\left((\nabla\times H)\times H\right)_r}{4\pi} = \frac{K^2}{4\pi}\left(\frac{R^2r}{3}-\frac{2r^3}{5}\right)\left(\frac{2}{3}-\frac{2}{3}P_2\right) \tag{6.75}$$

$$\frac{\left((\nabla\times H)\times H\right)_\theta}{4\pi} = -\frac{K^2}{4\pi}\left(\frac{R^2r}{6}-\frac{r^3}{10}\right)\left(\frac{1}{3}\frac{dP_2}{d\theta}\right) \tag{6.76}$$

As we have seen for slow rotation, in the case of an incompressible star, there can be no $l = 0$ deformation, as this would not conserve the volume and therefore not conserve the mass of the star. We shall thus only consider the case of $l = 2$. For this case $\delta\phi$ inside the star takes the form (again as in the slow rotation case of chapter 2)

$$\delta\phi = -\frac{4}{5}\pi G\rho\varepsilon(R)r^2 \tag{6.77}$$

inserting this solution into the $\hat{\theta}$ component of equations (6.73) and evaluating at the surface gives

$$\delta p(R) = \frac{4}{5}\pi G\rho\varepsilon(R)R^2 - \frac{2}{15}\frac{K^2R^4}{12\pi} \tag{6.78}$$

If we now remember that

$$\delta p(r) = \delta p(x) - \varepsilon(r)r\frac{dp}{dr}(r) \tag{6.79}$$

we have at the surface

$$\delta p(R) = 0 - \varepsilon(R)R\frac{dp}{dr}(R) \tag{6.80}$$

by using the background pressure from equation (2.60), equation (6.78) gives us

$$\varepsilon(R) = -\frac{1}{48}\frac{K^2R^2}{\pi^2G\rho^2} \tag{6.81}$$

which agrees with the result of [45]. We can also calculate the ellipticity, defined as

$$\epsilon = \frac{I_{zz} - I_{xx}}{I_0} \tag{6.82}$$

where I_0 is the moment of inertia of the spherical star, while I_{jk} is the inertia tensor

$$I_{jk} = \int_V \rho(r)(r^2\delta_{jk} - x_jx_k)dV. \tag{6.83}$$

For a constant density star this definition leads to

$$\begin{aligned} \epsilon &= \frac{1}{2/5MR^2}\int_0^{R(1+\varepsilon P_2)} \rho r^2\sin\theta(x^2 - z^2)drd\theta d\phi \\ &= -\frac{3}{2}\varepsilon = \frac{1}{32}\frac{K^2R^2}{\pi^2G\rho^2} \end{aligned} \tag{6.84}$$

The ellipticity is positive, so the star is oblate, as expected.

6.4.2 n=1 polytrope with a poloidal field

Let us now consider the case of a star with an $n = 1$ polytropic equation of state. The magnetic field appropriate for this case is that in equation (6.53), for which the Lorentz force takes the form (we consider only $l = 2$)

$$\begin{aligned} F_r &= -\frac{1}{2}\left[2\,r^3\pi^3 - 3\sin\left(\frac{r\pi}{R}\right) Rr^2\pi^2 \right. \\ &\quad +6R^3\sin\left(\frac{r\pi}{R}\right) - 6R^2r\pi\cos\left(\frac{r\pi}{R}\right) \\ &\quad \left.+3r^3\pi^3\cos\left(\frac{r\pi}{R}\right)\right]\frac{\pi^2B^2\sin\left(\frac{r\pi}{R}\right)}{r\left(\pi^2-6\right)R}P_2(\theta) \\ F_\theta &= -\frac{1}{2}\pi^2\left(r^3\pi^3 + 3\sin\left(\frac{r\pi}{R}\right) Rr^2\pi^2 - 6R^3\sin\left(\frac{r\pi}{R}\right)\right. \\ &\quad \left.+6R^2r\pi\cos\left(\frac{r\pi}{R}\right)\right]\frac{B^2\sin\left(\frac{r\pi}{R}\right)}{r\left(\pi^2-6\right)R}\frac{dP_2}{d\theta} \end{aligned} \tag{6.85}$$

Having worked out the Lorenz force we can solve the perturbed hydrostatic equilibrium equations (6.73) and Poisson equation (6.74), with the condition that $\delta\phi$ and $\frac{d\delta\phi}{dr}$ be regular at the centre and match the exterior solution at the surface, as we have done in the case of slow rotation. Let us remember that the background quantities we shall need are

$$\rho = \rho_c\sin\left(\frac{r\pi}{R}\right)\frac{R}{r\pi} \tag{6.86}$$

$$\frac{d\phi}{dr} = -\frac{4\,G\rho_c\,R^2}{\pi^2r^2}\left[\pi\,r\cos\left(\frac{\pi\,r}{R}\right) - \sin\left(\frac{\pi\,r}{R}\right)R\right] \tag{6.87}$$

where ρ_c is the central density. From equation (6.73) we then obtain

$$\begin{aligned} \delta\rho &= -1/8\left[B^2r^3\pi^6 + 3\,B^2\sin\left(\frac{\pi\,r}{R}\right)Rr^2\pi^5 + 6\,\pi^4B^2R^2r\cos\left(\frac{\pi\,r}{R}\right)\right. \\ &\quad +2\,\pi^4\rho_c\,\delta\phi\,(r)\,R^2r - 6\,\sin\left(\frac{\pi\,r}{R}\right)B^2R^3\pi^3 - 24\,\rho_c\,\delta\phi\,(r)\,R^2r\pi^2 \\ &\quad \left.+72\,\rho_c\,\delta\phi\,(r)\,R^2r\right]\pi\left(\pi^4 - 12\,\pi^2 + 36\right)^{-1}G^{-1}{\rho_c}^{-1}R^{-4}r^{-1} \end{aligned} \tag{6.88}$$

Inserting this into the right hand side of equation (6.74) we can then solve for $\delta\phi$

$$\begin{aligned} \delta\phi &= 1/4\left[r^5\pi^3\cos\left(\frac{\pi\,r}{R}\right) - 2\,r^5\pi^3 - 12\,\pi^2r^2R^3\sin\left(\frac{\pi\,r}{R}\right)\right. \\ &\quad -3\,r^4\pi^2R\sin\left(\frac{\pi\,r}{R}\right) - 36\,\pi\,rR^4\cos\left(\frac{\pi\,r}{R}\right) \\ &\quad \left.+36\,R^5\sin\left(\frac{\pi\,r}{R}\right)\right]\pi^3B^2\left(\pi^2-6\right)^{-2}r^{-3}R^{-2}{\rho_c}^{-1} \end{aligned} \tag{6.89}$$

We can then evaluate the distortion at the surface:

$$\begin{aligned} \varepsilon &= -\delta\rho/R\frac{d\rho}{dr} \\ &= 1/16\,\frac{\pi^5\left(\pi^2-24\right)B^2}{R^2{\rho_c}^2G\left(\pi^4-12\,\pi^2+36\right)} \end{aligned} \tag{6.90}$$

which for a $1.4M_\odot$ star with $R = 10$km and $B = 10^{12}$G gives

$$\varepsilon \approx -6 \times 10^{-11} \tag{6.91}$$

The ellipticity for an $n = 1$ polytrope is

$$\epsilon = -\frac{11}{32\pi I_0}\int_0^R r^4\delta\rho dr \tag{6.92}$$

which in this case gives

$$\epsilon = -\frac{825}{1024}\,\frac{\pi^2 R\left(\pi^2-12\right)B^2}{\left(\pi^4-12\,\pi^2+36\right)G\rho_c M} \tag{6.93}$$

which for the canonical values defined above gives

$$\epsilon \approx 3 \times 10^{-12} \tag{6.94}$$

so that once again the effect of a poloidal magnetic field is to make the star oblate.

6.4.3 General deformations

Having considered some particular examples, let us now present the formalism for the case of a general field configuration and equation of state. The magnetic field takes the form of equation (6.56), for which the Lorenz force is

$$\begin{aligned} L_r &= \frac{dA}{dr}\frac{(\cos\theta^2-1)}{r^4}\left(\lambda^2Ar^2+\frac{d^2A}{dr^2}-2A\right) \\ L_\theta &= =-\frac{2A}{r^5}\cos\theta\sin\theta\left(\lambda^2Ar^2+\frac{d^2A}{dr^2}-2A\right) \end{aligned} \tag{6.95}$$

which for $l = 2$ reduces to

$$\begin{aligned} L_r(l=2) &= \frac{dA}{dr}\frac{2P_2(\theta)}{3r^4}\left(\lambda^2Ar^2+\frac{d^2A}{dr^2}-2A\right) \\ L_\theta(l=2) &= =\frac{2A}{3r^5}\frac{dP_2}{d\theta}\left(\lambda^2Ar^2+\frac{d^2A}{dr^2}-2A\right) \end{aligned} \tag{6.96}$$

From the angular part of the perturbed hydrostatic equilibrium equations (6.1) we can obtain (for the $l = 2$ case we are considering)

$$\begin{aligned} \delta p &= -\rho\delta\phi + rL_\theta \\ &= -\rho\delta\phi + \frac{2}{3}\frac{A}{r^4}\left(\lambda^2 A r^2 + \frac{d^2A}{dr^2} - 2A\right) \end{aligned} \tag{6.97}$$

which substituted back into the radial part of the equations leads to

$$\begin{aligned} \delta\rho = &-\frac{1}{3r^5\frac{d\phi}{dr}}\left(-3\frac{d\rho}{dr}\delta\phi r^5 + 2\frac{dA}{dr}r^3\lambda^2 A - 4r^2A^2\lambda^2 + 2r^3A\frac{d^3A}{dr^3}\right. \\ &\left.-4r^2A\frac{d^2A}{dr^2} - 4\frac{dA}{dr}Ar + 16A^2\right) \end{aligned} \tag{6.98}$$

where ρ and ϕ are the background density and gravitational potential. This now allows us to compute the source term of the perturbed Poisson equation (6.74), which, for $l = 2$, reads

$$\begin{aligned} &\frac{d^2\delta\phi}{dr^2} + \frac{2}{r}\frac{d\delta\phi}{dr} - \frac{6}{r^2}\delta\phi = -\frac{4\pi G}{3r^5\frac{d\phi}{dr}}\left(-3\frac{d\rho}{dr}\delta\phi r^5 + 2\frac{dA}{dr}r^3\lambda^2 A\right. \\ &\left.-4r^2A^2\lambda^2 + 2r^3A\frac{d^3A}{dr^3} - 4r^2A\frac{d^2A}{dr^2} - 4\frac{dA}{dr}Ar + 16A^2\right) \end{aligned} \tag{6.99}$$

The boundary conditions for this equation remain regularity at the centre and continuity of $\delta\phi$ and its derivative with the external solution, which for $l = 2$ has the form

$$\delta\phi_e = \frac{A}{r^3} \tag{6.100}$$

Having computed $\delta\rho$ in the interior we can obtain $\delta\rho$ from equation (6.98) and thus compute the ellipticity ϵ and the deformation at the surface

$$\varepsilon(R) = -\frac{\delta\rho(R)}{R\frac{d\rho}{dr}(R)} \tag{6.101}$$

What is more, we can assume that the new radial variable x defined in equation (6.69) labels the deformed gravitational equipotential surfaces. This mean that we have to impose that

$$\nabla x \times \nabla\Phi = 0 \tag{6.102}$$

which, if we write

$$\varepsilon(x,\theta) = D_0(x) + D_2(x)P_2(\theta) \tag{6.103}$$

leads to the condition

$$D_2 = -\sqrt{\frac{4\pi}{5}}\frac{\delta\Phi}{r\partial_r\Phi} \tag{6.104}$$

This expression allows us to calculate the quantity D_2 throughout the star and will be of use later, when when discussing oscillations. The $l = 0$ part corresponds simply to a radial perturbation of the star, as is thus not of interest for gravitational waves and will not be considered in this section. This part of the deformation can, however, become necessary in the calculation of the background for oscillations. Let us, therefore, write perturbation equations that need to be solved in the $l = 0$ case, which are the perturbed Euler equation and Poisson equation

$$\begin{aligned}
\frac{d}{dr}\delta\Phi_0 &= \psi_0 \\
\frac{d}{dr}\delta\psi_0 &= 4\pi G\delta\rho_0 - \frac{2}{r}\psi_0 \\
\frac{d}{dr}\delta\rho_0 &= \frac{\rho}{P}\left[L_0(B) - \rho\psi_0 - \left(\frac{d}{dr}\left(\frac{P}{\rho}\right)\Gamma_1 + \frac{d}{dr}\Phi\right)\right]
\end{aligned} \tag{6.105}$$

where we have used the linearised equation of state

$$\frac{\delta P}{P} = \Gamma_1\frac{\delta\rho}{\rho} \tag{6.106}$$

and $L_0(B)$ is the $l = 0$ part of the Lorenz force, which can be calculated once the magnetic field has been specified. These equations can now be integrated, imposing regularity at the centre of the star and imposing that at the surface $\delta\rho_0 = 0$ and matching $\delta\Phi_0$ and $\frac{d\delta\Phi_0}{dr}$ to an exterior solution of the form $\delta\Phi_0^{ext} = A/r$. This will then allow us to calculate

$$D_0 = -\sqrt{4\pi}\frac{\delta\Phi_0}{r\partial_r\Phi} \tag{6.107}$$

6.4.4 $n = 1$ polytrope

For the case of an $n = 1$ polytrope we can use the stream function given in equation (6.63) to determine the magnetic field and the Lorentz force. This allows us to then apply the procedure described above; the result will obviously depend on the value we chose for λ which gives the relative strength of the toroidal part of the field compared to the poloidal part. Results are listed in table 6.1. As expected for low values of λ the effects of the poloidal and toroidal field work against each other and the deformation is small. As λ grows the toroidal field becomes dominant and the star becomes more and more prolate.

λ	ϵ
7.420	-3.6×10^{-13}
10.706	-9.6×10^{-13}
23.433	-4.2×10^{-12}
80.073	-1.2×10^{-11}
183.994	-3.44×10^{-11}
1000.59	-4.3×10^{-9}

Table 6.1: The ellipticity ϵ for various values of λ. We take a star with our typical parameters $M = 1.4M_{\odot}$, $R = 10$km and we take the amplitude of the radial component of the poloidal field, averaged over the radius, to be 10^{12} G. As can be seen, the star starts off with a small deformation as the effects of the poloidal and toroidal components cancel each other out, and becomes more and more prolate as the toroidal component of the field grows. Note that we now have a vanishing exterior field, no longer an external dipole.

6.4.5 n=1 polytrope, field confined to the crust

Let us consider the case when the field is confined to a region close to the surface, which we shall call the "crust", even though we are neglecting its elastic properties. As previously discussed, we shall consider the core to be unperturbed, and use the boundary conditions in equations (6.67) and (6.67)

In this way the deformation is only in the crust and, as the density is low in this region, the quadrupole will in general be much smaller than if we were considering the deformations of the whole star. However it is likely that the field may be confined to the crust after being expelled from a superconducting core. In this case a large number of field lines would be squeezed into a small region close to the surface of the star and would effectively produce a strong field and large deformations. This situation is illustrated in table 6.2, where we have calculated the deformation of the star by assuming that the total magnetic energy in the crust is equal to that of the field extended to the whole star, as calculated in the previous section. As can be seen the ellipticity is larger than in the case of a field extending throughout the star, by up to a factor ≈ 100. This agrees with what was found in [20], where the authors analysed the deformations due to a poloidal field confined to a thin shell close to the surface of a neutron star.

λ	ϵ
103.60	-2.2×10^{-10}
496.39	-6.5×10^{-9}
1008.46	-6.8×10^{-7}

Table 6.2: The ellipticity ϵ for various values of λ. We take a star with our typical parameters $M = 1.4M_{\odot}$, $R = 10$km. We take the field to have the same energy as that, obtained from the previous section, of a field extended to the whole star with $\lambda = 1000.59$. The field is confined to a region close to the surface beginning at a radius $r_b = 9 \times 10^5$ cm, thus roughly corresponding to a crust (1 km thick). The core is taken to be spherical. As can be seen the deformations are larger than in the case of the field extending to the whole star, of up to a factor ≈ 100.

6.5 General deformations: magnetic fields and rotation

The previous framework can easily be extended to the case where the deformation is due not only to a magnetic field, but also to the star's rotation. Following what has been done in chapter 2 we can write the equations of motion as

$$\frac{\nabla p}{\rho} + \nabla\psi = \frac{(\nabla \times H) \times H}{4\pi} \tag{6.108}$$

where

$$\psi = V - 1/2\Omega^2 r^2 \sin\theta^2 \tag{6.109}$$

V is the gravitational potential and Ω the constant rotation rate. As the new term due to rotation is written as the gradient of a scalar function, it's curl will still vanish and the compatibility condition for the magnetic field in equation (6.5) remains the same. We can thus still use the magnetic field from equation (6.56). The equations of hydrostatic equilibrium, for the $l = 2$ case, now take the form

$$\begin{aligned} &\frac{d\delta p}{dr} + \rho\frac{d\delta\phi}{dr} + \delta\rho\frac{d\phi}{dr} + \frac{2}{3}\rho\Omega^2 r = L_r \\ &\delta p + \rho\delta\phi + \frac{\rho\Omega^2 r}{3} = rL_\theta \end{aligned} \tag{6.110}$$

where L_r and L_θ are defined in equation (6.96). We can proceed as in the previous section and use equations (6.110) to obtain $\delta\rho$ as a function

of $\delta\phi$, B and Ω. This allows us to write the perturbed Poisson equation (for $l = 2$) as:

$$\frac{d^2\delta\phi}{dr^2} + \frac{2}{r}\frac{d\delta\phi}{dr} - \frac{6}{r^2}\delta\phi = -\frac{4\pi G}{3r^5\frac{d\phi}{dr}}\left(-3\frac{d\rho}{dr}\delta\phi r^5 + 2\frac{dA}{dr}r^3\lambda^2 A\right.$$
$$-4r^2A^2\lambda^2 + 2r^3A\frac{d^3A}{dr^3} - 4r^2A\frac{d^2A}{dr^2}$$
$$\left.-4\frac{dA}{dr}Ar + 16A^2 + \frac{d\rho}{dr}\Omega^2r^7\right) \tag{6.111}$$

and thus obtain the surface deformation ε and the ellipticity ϵ as defined in equations (6.100) and (6.101).

As an example let us take an $n = 1$ polytrope with the purely poloidal field of equation (6.53). The equations of hydrostatic equilibrium now include the rotation term as in equation (6.110), where now the Lorentz force is that of equation (6.85). We can thus apply exactly the same procedure as we have done previously and solve for the perturbed quantities $\delta\phi$,$\delta\rho$ and δp. This allows us to calculate the deformation at the surface

$$\varepsilon = -\frac{\pi^5B^2\left(24-\pi^2\right)}{16R^2\rho_c^2G\left(\pi^2-6\right)^2} - \frac{5}{4\pi}\frac{\Omega^2}{G\rho_c} \tag{6.112}$$

which for $M = 1.4M_\odot$, $R = 10km$ gives

$$\varepsilon = -6\times10^{-7}\left(\frac{B}{10^{14}G}\right)^2 - 0.2\left(\frac{\Omega}{\Omega_{br}}\right)^2 \tag{6.113}$$

where $\Omega_{br} = \frac{2}{3}\sqrt{\pi G\bar{\rho}}$ is the breakup frequency ($\bar{\rho}$ is the average density). For our values this frequency would be $f \approx 1250$ Hz, which corresponds to a period $P \approx 0.8$ ms. We also calculate the ellipticity $\epsilon = (I_{zz} - Ixx)/I_0$:

$$\epsilon = 3\times10^{-8}\left(\frac{B}{10^{14}G}\right)^2 + 1.5\times10^{-3}\left(\frac{\Omega}{\Omega_{br}}\right)^2 \tag{6.114}$$

6.6 Conclusions

In this chapter we have presented a scheme for calculating the magnetic, together with rotational, deformations of a neutron star. The magnetic field has been taken to be dipolar, with the magnetic axis aligned with the spin axis of the star. We have considered both the case of a purely poloidal field, the effect of which is to make the star oblate, and the case of a mixed poloidal and toroidal field, which makes the star more and

more prolate as the strength of the toroidal component grows. In all the cases considered magnetic deformations are several orders of magnitude smaller than the rotational deformations and would be swamped by the effect of the latter. The situation could, however, become interesting for gravitational wave emission if the magnetic axis were not aligned with the spin axis. In this case the deformation would no longer be axisymmetric and we could have a time varying quadrupole. Rotational deformations, on the other hand, are always axisymmetric and cannot radiate gravitational waves. This conclusion is not altogether new and the emission of gravitational waves had been considered both for the case of magnetised white dwarfs [51] and neutron stars with internal poloidal fields [20], [85]. For neutron stars it has also been suggested that, if the star is made prolate by a strong magnetic field and the magnetic axis is inclined with respect to the spin axis, then the configuration will become unstable on the viscous timescale and the star will become an orthogonal rotator, which is an optimal gravitational wave source [26].

Finally, the calculation of the equilibrium shape of a magnetised neutron star can be used as a background for a mode calculation, which would be of interest for the analysis of data from the giant flares observed from magnetars. This problem shall be the focus of the following chapter.

Chapter 7

Oscillations in Magnetised Neutron Stars

There has been much recent interest in Soft Gamma Repeaters (SGRs), as there exist at least two systems in which quasi-periodic oscillations have been observed during a flare. SGRs are thought to be magnetars, neutron stars with very strong magnetic fields, greater than $B \approx 5 \times 10^{13} G$ [29]. The flares are characterised by a peak in the hard part of the spectrum, followed by a decaying softer tail which lasts for hundreds of seconds. It is a detailed analysis of the tail that has revealed several oscillations with frequencies ranging from a few tenths of Hz to a few hundred Hz [56], [137] and [150]. These oscillations are generally thought to be torsional modes in the crust, excited by fractures in the crust and caused by the evolution of the intense magnetic field [30]. Glampedakis et al. [44] also showed that global modes of the star could, for sufficiently strong fields, play a part in addition to crustal modes. These possibilities have been recently investigated, for the case of a star with a purely poloidal dipole field, in [132] and [133]. It is thus of interest to write the equations for general oscillations on a deformed magnetised background, given by a generic dipolar magnetic field, such as one of the examples calculated in the previous chapter.

7.1 Oscillation equations

We shall write the oscillation equations using the formalism of Saio [120], [119]. We start by considering a uniformly, slowly, rotating and magnetised star. As we have seen in the previous chapter the star will not be

spherical and a distorted potential surface can be written in the form

$$r = a(1+\epsilon) \tag{7.1}$$

where ϵ is a function of a and θ which represents the deformation of the equilibrium structure from the background spherical state. The equilibrium physical quantities are functions only of a. Following [129], we shall write the equations of motion in a frame corotating with the star, denoted by $\{q^i\}$, starting from a static cartesian frame, denoted by $\{x^i\}$. Our coordinates in the rotating frame will be a spherical polar system, where the radial coordinate is taken to be the variable a in equation (7.1). Explicitly

$$x^1 = a(1+\epsilon)\sin\theta\cos(\phi+\Omega t) \tag{7.2}$$
$$x^2 = a(1+\epsilon)\sin\theta\sin(\phi+\Omega t) \tag{7.3}$$
$$x^3 = a(1+\epsilon)\cos\theta \tag{7.4}$$

The metric in the new coordinates will be given by

$$g_{ab} = \delta_{ij}\frac{\partial x^i}{\partial q^a}\frac{\partial x^j}{\partial q^b} \tag{7.5}$$

which, after linearizing with respect to ϵ, leads to

$$g_{ab} = \begin{Bmatrix} 1+2\epsilon+2a\frac{\partial\epsilon}{\partial a} & a\frac{\partial\epsilon}{\partial a} & 0 \\ a\frac{\partial\epsilon}{\partial a} & a^2(1+2\epsilon) & 0 \\ 0 & 0 & a^2(1+2\epsilon)\sin^2\theta \end{Bmatrix} + O(\epsilon^2) \tag{7.6}$$

the connection coefficients, in the coordinate basis

$$\left\{e_a = \frac{\partial}{\partial a}, e_\theta = \frac{\partial}{\partial\theta}, e_\phi = \frac{\partial}{\partial\phi}\right\}, \tag{7.7}$$

can be obtained by

$$\Gamma^a_{bc} = \frac{1}{2}g^{ad}\left(g_{bd,c} + g_{cd,b} - g_{bc,d}\right) \tag{7.8}$$

We shall, however, use a normalised vector basis

$$\{\hat{e}_i\}\left\{\hat{e}_a = \frac{\partial}{\partial a}, \hat{e}_\theta = \frac{1}{a}\frac{\partial}{\partial\theta}, \hat{e}_\phi = \frac{1}{a\sin\theta}\partial\partial\phi\right\}. \tag{7.9}$$

for which the covector basis is

$$\{\hat{\omega}^i\} = \{da, ad\theta, a\sin\theta d\phi\} \tag{7.10}$$

The connection coefficients in this basis are calculated in Appendix A. Having calculated these quantities, and assuming a displacement vector of the form

$$\xi = (\delta a, a\delta\theta, a\sin\theta\delta\phi)\exp(i\sigma t) \tag{7.11}$$

we can write the Euler equations in the form:

$$\sigma^2\left[(1+2\epsilon)\xi^i + a\xi^r\nabla_0^i\epsilon + \delta^{ia}(\xi_k\nabla_0^k\epsilon)\right] - \nabla_0^i\psi' - \frac{1}{\rho}\nabla_0^i P'$$
$$+\frac{\rho'}{\rho^2}\delta^{ia}\frac{dP}{da} + i\sigma C^i + L^i = 0 \tag{7.12}$$

where primes (') denote the Eulerian perturbations and $i\sigma C^i$ represents the Coriolis force and the vector C^i has the following components:

$$C^a = 2\Omega\left(1+2\epsilon+a\frac{\partial\epsilon}{\partial a}\right)\sin\theta\xi^\phi \tag{7.13}$$

$$C^\theta = 2\Omega\left(1+2\epsilon+\tan\theta\frac{\partial\epsilon}{\partial a}\right)\cos\theta\xi^\phi \tag{7.14}$$

$$C^\phi = 2\Omega\left[\xi^a\sin\theta\left(1+2\epsilon+a\frac{\partial\epsilon}{\partial a}\right)+\xi^\theta\left(1+2\epsilon+\tan\theta\frac{\partial\epsilon}{\partial\theta}\right)\right] \tag{7.15}$$

and L^i is the Lorenz force

$$L^i = \frac{1}{4\pi\rho}\left[\nabla_0^i(b_jB_0^j) - (b_j\nabla_0^j)B_0^i - (B_{0j}\nabla_0^j)b^i\right] \tag{7.16}$$

The differential operator ∇_0 is the same as for spherical polar coordinates. The continuity equation reads

$$\rho' + \nabla_0^i(\rho\xi_i) + \rho\xi_i\nabla_0^i\left(3\epsilon + a\frac{\partial\epsilon}{\partial a}\right) = 0 \tag{7.17}$$

and the Poisson equation is

$$\nabla_0^2\psi' = 4\pi G\rho' \tag{7.18}$$

We shall also need the linearized equation of state

$$\frac{P'}{P} = \Gamma_1\frac{\rho'}{\rho} \tag{7.19}$$

The final equation we shall use is the perturbed induction equation, which in vector notation for simplicity, reads

$$\frac{\partial\overline{b}}{\partial t} = \overline{\nabla}_0\times(\overline{v}\times\overline{B}_0) \tag{7.20}$$

where v is the velocity of the fluid relative to the rotating frame. The terms in the previous equations include magnetic and rotational terms, and must be computed to $O(\epsilon)$ where, depending on the process that is causing the deformation $\epsilon = O(B^2, \Omega^2)$. We shall decompose the fluid displacement vector and the perturbed magnetic field in vector spherical harmonics

$$\xi/a = \sum_{l\geq m} \left[S_{lm} Y_l^m, \left(\frac{mK_{lm}}{\sin\theta} + H_{lm} \frac{\partial}{\partial\theta} \right) Y_l^m, \left(iK_{lm} \frac{\partial}{\partial\theta} + \frac{imH_{lm}}{\sin\theta} \right) Y_l^m \right] \tag{7.21}$$

$$b = \sum_{l\geq m} \left[M_{lm} Y_l^m, \left(m\frac{T_{lm}}{\sin\theta} + N_{lm} \frac{\partial}{\partial\theta} \right) Y_l^m, \left(+iT_{lm} \frac{\partial}{\partial\theta} + \frac{imN_{lm}}{\sin\theta} \right) Y_l^m \right] \tag{7.22}$$

The background magnetic field will be taken to be, as in the previous chapter, dipolar

$$B_0 = [\Lambda(r)\cos\theta, X(r)\sin\theta, iZ(r)\sin\theta] \tag{7.23}$$

The functions $\Lambda(r)$, $X(r)$ and $Z(r)$ specify the background field and could be, for example, any of those described in chapter 6. By using the expansions in equations (7.21) and (7.22) in equations ((7.17), the a-component of (7.12), (7.18) and (7.19), we can obtain the following relations (where summation over $l \geq m$ is implicit):

$$\begin{aligned} a\frac{dS_{lm}}{da} Y_l^m = & \left[\left(\frac{V}{\Gamma_1} - 3 \right) S_{lm} + \frac{V}{\Gamma_1} (\Psi_{lm} - \zeta_{lm}) + l(l+1) H_{lm} \right] Y_l^m \\ & + \Delta_2 \left(mK_{lm} \cos\theta Y_l^m + H_{lm} \sin\theta \cos\theta \partial_\theta Y_l^m \right) - D\Delta_0 S_{lm} Y_l^m + \\ & + \frac{1}{2} D\Delta_2 S_{lm} Y_l^m - \frac{3}{2} D\Delta_2 S_{lm} \cos^2\theta Y_l^m \end{aligned} \tag{7.24}$$

$$
\begin{aligned}
&a\frac{d\zeta_{lm}}{dA}Y_l^m = [aAS_{lm} + (1-U-aA)\zeta_{lm} + aA\Psi_{lm}]\,Y_l^m + \\
&+\omega^2 c_1\left[(1-D_2)S_{lm}Y_l^m + 3D_2 S_{lm}\cos^2\theta Y_{lm}\right. \\
&+2a\frac{dD_2}{dr}(3S_{lm}\cos^2\theta Y_l^m - S_{lm}Y_l^m) - 3amK_{lm}D_2\cos\theta Y_l^m \\
&\left.-3aH_{lm}D_2\sin\theta\cos\theta\partial_\theta Y_l^m\right] - 2x_1\omega\varpi\,(K_{lm}\sin\theta\partial_\theta Y_l^m + mH_{lm}Y_l^m) \\
&+c_b\left[\frac{d}{da}(M_{lm}\Lambda)\cos\theta Y_l^m + \frac{d}{da}(N_{lm}X)\sin\theta\partial_\theta Y_l^m + m\frac{d}{da}(T_{lm}X)Y_l^m\right. \\
&-m\frac{d}{dr}(N_{lm}Z)Y_l^m - \frac{d}{dr}(T_{lm}Z)\sin\theta\partial_\theta Y_l^m - \Lambda\frac{dM_{lm}}{da}\cos\theta Y_l^m \\
&-\frac{XM_{lm}}{a}\sin\theta\partial_\theta Y_l^m + m\frac{ZM_{lm}}{a}Y_l^m + M_{lm}\frac{d\Lambda}{da}\cos\theta Y_l^m \\
&+\frac{N_{lm}\Lambda}{a}\sin\theta\partial_\theta Y_l^m + m\frac{T_{lm}\Lambda}{a}Y_l^m - (T_{lm}Z - N_{lm}X)\frac{\sin\theta}{a}\partial_\theta Y_l^m \\
&\left.-\frac{m}{a}(N_{lm}Z - T_{lm}X)Y_l^m\right] \qquad (7.25)
\end{aligned}
$$

$$
a\frac{d\Psi_{lm}}{da} = (1-U)\Psi_{lm} + \langle\Psi\rangle_{lm} \qquad (7.26)
$$

$$
\begin{aligned}
a\frac{d\langle\Psi\rangle_{lm}}{da} &= -aAUS_{lm} + \frac{UV}{\Gamma_1}\zeta_{lm} + \left[l(l+1) - \frac{UV}{\Gamma_1}\right]\Psi_{lm} \\
&\quad -U\langle\Psi\rangle_{lm} \qquad (7.27)
\end{aligned}
$$

where the variables ζ_{lm}, Ψ_{lm} and $\langle\Psi\rangle_{lm}$ are defined as

$$
\zeta_{lm}Y_l^m = \frac{1}{g}\left(\frac{P'}{\rho} + \psi'\right) \qquad (7.28)
$$

$$
\Psi_{lm}Y_l^m = \frac{\psi'}{ga} \qquad (7.29)
$$

$$
\langle\Psi\rangle_{lm} = = \frac{1}{g}\frac{\partial\psi'}{\partial a} \qquad (7.30)
$$

The deformation ϵ is written as

$$
\epsilon = D_0(a) + D_2(a)P_2(\cos\theta) \qquad (7.31)
$$

and

$$\begin{aligned}
&\omega = \sigma(\tfrac{R^3}{GM})^{1/2}, && \varpi = \Omega(\tfrac{R^3}{GM})^{1/2}, && c_1 = (\tfrac{a}{R})^3 \tfrac{M}{M_r} \\
&A = \tfrac{d\ln\rho}{da} - \tfrac{1}{\Gamma_1}\tfrac{d\ln P}{da}, && M_r = 4\pi \textstyle\int_0^a \rho a^2 da, && g = \tfrac{M_r}{Ga^2} \\
&U = \tfrac{d\ln M_r}{d\ln a}, && V = \tfrac{ga\rho}{P} && c_b = \tfrac{1}{4\pi\rho g} \\
&\Delta_0 = 3D_0 + a\tfrac{dD_0}{da}, && \Delta_2 = 3D_2 + a\tfrac{dD_2}{da}
\end{aligned} \tag{7.32}$$

These equations can be simplified by using the relations

$$\cos\theta Y_l^m = Q_{l+1}\, Y_{l+1}^m + Q_l\, Y_{l-1}^m \tag{7.33}$$

$$\sin\theta\partial_\theta Y_l^m = lQ_{l+1}\, Y_{l+1}^m - (l+1)\, Q_l\, Y_{l-1}^m \tag{7.34}$$

$$\begin{aligned}
\cos\theta\, \sin\theta\partial_\theta Y_l^m = {} & [\, lQ_{l+1}^2 - (l+1)Q_l^2\,]\, Y_l^m + lQ_{l+1}Q_{l+2}Y_{l+2}^m \\
& -(l+1)Q_lQ_{l-1}Y_{l-2}^m
\end{aligned} \tag{7.35}$$

$$\begin{aligned}
\cos^2\theta\, Y_l^m = {} & [\, Q_{l+1}^2 + Q_l^2\,]\, Y_l^m + Q_{l+1}Q_{l+2}Y_{l+2}^m \\
& +Q_lQ_{l-1}Y_{l-2}^m
\end{aligned} \tag{7.36}$$

where

$$Q_l = \left(\frac{l^2 - m^2}{(2l+1)(2l-1)}\right)^{1/2} \tag{7.37}$$

With the use of relations (7.34) and (7.36) equations (7.24)-(7.27) take the form:

$$\begin{aligned}
a\frac{dS_l}{da} = {} & \left[\left(\frac{V}{\Gamma_1} - 3\right) S_l + \frac{V}{\Gamma_1}(\Psi_{lm} - \zeta_l) + l(l+1)H_l\right] \\
& +\Delta_2\left[mK_{l-1}Q_l + mK_{l+1}Q_{l+1} + \left(lQ_{l+1}^2 - (l+1)Q_l^2\right) H_l\right. \\
& +(l-2)Q_{l-1}Q_lH_{l-2} - (l+3)Q_{l+2}Q_{l+1}H_{l+2}] - D\Delta_0 S_l \\
& +\frac{1}{2}D\Delta_2 S_l - \frac{3}{2}D\Delta_2\left[\left(Q_{l+1}^2 + Q_l^2\right) S_l + Q_{l-1}Q_l S_{l-2}\right. \\
& \left.+Q_{l+2}Q_{l+1}S_{l-2}\right]
\end{aligned} \tag{7.38}$$

$$
\begin{aligned}
a\frac{d\zeta_l}{dA} = & [aAS_l + (1-U-aA)\zeta_l + aA\Psi_l] + \omega^2 c_1 \left[(1-D_2)S_l\right. \\
& +3D_2\left[\left(Q_{l+1}^2 + Q_l^2\right)S_l + Q_{l-1}Q_l S_{l-2} + Q_{l+2}Q_{l+1}S_{l-2}\right] \\
& +6a\frac{dD_2}{da}\left[\left(Q_{l+1}^2 + Q_l^2\right)S_l + Q_{l-1}Q_l S_{l-2} + Q_{l+2}Q_{l+1}S_{l-2}\right] \\
& -a\frac{dD_2}{da}S_l - 3amD_2\left(Q_l K_{l-1} + Q_{l+1}K_{l+1}\right) \\
& +3aD_2\left[\left(lQ_{l+1}^2 - (l+1)Q_l^2\right)H_l + (l-2)Q_{l-1}Q_l H_{l-2}\right. \\
& \left.-(l+3)Q_{l+2}Q_{l+1}H_{l+2})\right] - 2x_1\omega\varpi\left[((l-1)Q_l K_{l-1} - (l+2)Q_{l+1}K_{l+1})\right. \\
& \left.+mH_l\right] + c_b\left[\frac{d}{da}\left[\Lambda\left(Q_l M_{l-1} + Q_{l+1}M_{l+1}\right)\right] + m\frac{d}{da}(T_l X)\right. \\
& +\frac{d}{da}\left[X\left((l-1)Q_l N_{l-1} - (l+2)Q_{l+1}N_{l+1}\right)\right] - m\frac{d}{dr}(N_l Z) \\
& -\frac{d}{dr}\left[Z\left((l-1)Q_l T_{l-1} - (l+2)Q_{l+1}T_{l+1}\right)\right] + m\frac{T_l\Lambda}{a} \\
& -\Lambda\frac{d}{da}\left(Q_l M_{l-1} + Q_{l+1}M_{l+1}\right) + \frac{d\Lambda}{da}\left(Q_l M_{l-1} + Q_{l+1}M_{l+1}\right) \\
& -\frac{m}{a}(N_l Z - T_l X) - \frac{X}{a}\left((l-1)Q_l M_{l-1} - (l+2)Q_{l+1}M_{l+1}\right) \\
& +m\frac{ZM_l}{a} + \frac{(\Lambda+X)}{a}\left((l-1)Q_l N_{l-1} - (l+2)Q_{l+1}N_{l+1}\right) \\
& \left.-\frac{Z}{a}\left((l-1)Q_l T_{l-1} - (l+2)Q_{l+1}T_{l+1}\right)\right] \qquad (7.39)
\end{aligned}
$$

$$
a\frac{d\Psi_l}{da} = (1-U)\Psi_l + \langle\Psi\rangle_l \qquad (7.40)
$$

$$
\begin{aligned}
a\frac{d\langle\Psi\rangle_l}{da} = & -aAUS_l + \frac{UV}{\Gamma_1}\zeta_l + \left[l(l+1) - \frac{UV}{\Gamma_1}\right]\Psi_l \\
& -U\langle\Psi\rangle_l \qquad (7.41)
\end{aligned}
$$

where for simplicity we have omitted the index m from all quantites, such that $F_l = F_{lm}$.

We shall now apply a similar procedure to the angular part of the

Euler equations (7.12)

$$\begin{aligned}
&\omega^2 c_1 \left[(1+2D_0+2D_2P_2)\left\{mK_lY_l^m + H_l\sin\theta\partial_\theta Y_l^m\right\}\right.\\
&\left.+3D_2S_l(\cos^2\theta-1)\cos\theta Y_l^m\right] + \zeta_l\sin\theta\partial_\theta Y_l^m\\
&-2c_1\omega\varpi\left[mH_l\cos\theta Y_l^m + K_l\sin\theta\cos\theta\partial_\theta Y_l^m\right]\\
&-c_bL^\theta = 0
\end{aligned} \tag{7.42}$$

$$\begin{aligned}
&\omega^2 c_1(1+2D_0+2D_2P_2)\left[mH_lY_l^m + K_l\sin\theta\partial_\theta Y_l^m\right] + m\zeta_lY_l^m\\
&+2c_1\omega\varpi\left[S_lY_l^m - S_l\cos^2\theta Y_l^m + mK_l\cos\theta Y_l^m + H_l\sin\partial_\theta Y_l^m\right]\\
&-c_bL^\phi = 0
\end{aligned} \tag{7.43}$$

where

$$\begin{aligned}
L^\theta &= \frac{M_l}{a}\frac{d}{da}(aX)\left[1-\cos^2\theta\right]Y_l^m + 3T_lZ\cos\theta\sin\theta\partial_\theta Y_l^m\\
&+(X+\Lambda)\left[N_l\sin\theta\cos\theta\partial_\theta Y_l^m + mT_l\cos\theta Y_l^m\right] + mN_lZ\cos\theta Y_l^m\\
&+\frac{\Lambda}{a}\frac{d}{da}(aN_l)\cos\theta\sin\theta\partial_\theta Y_l^m + \frac{\Lambda}{a}\frac{d}{da}(aT_l)\cos\theta Y_l^m + m^2ZT_lY_l^m\\
&+XM_l(1-\cos^2\theta)Y_l^m - l(l+1)ZT_lY_l^m + mZN_l\cos\theta Y_l^m\\
&-m^2ZT_lY_l^m + ZT_l\sin\theta\cos\theta\partial_\theta Y_l^m - \Lambda M_l\sin\theta\cos\theta\partial_\theta Y_l^m\\
&-mXT_l\cos\theta Y_l^m + \Lambda M_l(1-\cos^2\theta)Y_l^m - XN_l\sin\theta\cos\theta\partial_\theta Y_l^m\\
&+ZT_ll(l+1)\cos\theta^2Y_l^m
\end{aligned} \tag{7.44}$$

and

$$\begin{aligned}
L^\phi &= \frac{M_l}{a}\frac{d}{da}(aZ)(1-\cos^2\theta)Y_l^m + 3ZN_l\sin\theta\cos\theta\partial_\theta Y_l^m\\
&+3ZT_l\cos\theta Y_l^m + m(\Lambda+X)N_l\cos\theta Y_l^m + (\Lambda+X)T_l\sin\theta\cos\theta Y_l^m\\
&+m\frac{\Lambda}{a}\frac{d}{da}(aN_l)\cos\theta Y_l^m + \frac{\Lambda}{a}\frac{d}{da}(aT_l)\cos\theta\sin\theta\partial_\theta Y_l^m - m^2N_lZY_l^m\\
&-l(l+1)XT_l(1-\cos\theta^2)Y_l^m - m\Lambda M_l\cos\theta Y_l^m - mXT_lY_l^m\\
&+ZM(1-\cos^2\theta)Y_l^m
\end{aligned} \tag{7.45}$$

with the use of relations (7.34) and (7.36), equations (7.42) and (7.43)

give

$$\begin{aligned}
&\omega^2 c_1 \left[(1+2D_0-D_2)\left\{mK_l+(l-1)Q_lH_{l-1}-(l+2)Q_{l+1}H_{l+1}\right\}\right.\\
&+3D_2\left[(l-1)Q_l(Q_{l+1}^2+Q_l^2)H_{l-1}+(l-3)Q_lQ_{l-1}Q_{l-2}H_{l-3}\right.\\
&+(l+1)Q_{l+2}^2Q_{l+1}H_{l+1}-(l+2)Q_{l+1}(Q_{l+1}^2+Q_l^2)H_{l+1}\\
&\left.-lQ_{l-1}^2Q_lH_{l-1}-(l+4)Q_{l+3}Q_{l+2}Q_{l+1}H_{l+3}\right]+3mD_2\left[Q_{l-1}Q_lK_{l-2}\right.\\
&\left.+(Q_{l+1}^2+Q_l^2)K_l+Q_{l+2}Q_{l+1}K_{l+2}\right]-3D_2\left[Q_{l-1}Q_lS_{l-2}\right.\\
&\left.+(Q_{l+1}^2+Q_l^2)S_l+Q_{l+2}Q_{l+1}S_{l+2}\right]+3D_2\left[Q_l(Q_{l+1}^2+Q_l^2)S_{l-1}\right.\\
&+Q_{l-2}Q_{l-1}Q_lS_{l-3}+Q_{l+2}^2Q_{l+1}S_{l+1}+Q_{l+1}(Q_{l+1}^2+Q_l^2)S_{l+1}\\
&\left.\left.+Q_{l-1}^2Q_lS_{l-1}+Q_{l+3}Q_{l+2}Q_{l+1}S_{l+3}\right]\right]+(l-1)Q_l\zeta_{l-1}-(l+2)Q_{l+1}\zeta_{l+1}\\
&+2c_1\omega\varpi\left[mQ_lH_{l-1}+mQ_{l+1}H_{l+1}+(l-1)Q_lK_{l-1}+(l+2)Q_{l+1}K_{l+1}\right]\\
&-c_bL_l^\theta=0
\end{aligned}\tag{7.46}$$

for the θ component of the Euler equations, while for the ϕ component we have

$$\begin{aligned}
&\omega^2 c_1\left[(1+2D_0-D_2)\left\{mH_l-(l-1)Q_lK_{l-1}+(l+2)Q_{l+1}K_{l+1}\right\}\right.\\
&-3D_2\left[(l-1)Q_l(Q_{l+1}^2+Q_l^2)K_{l-1}+(l-3)Q_lQ_{l-1}Q_{l-2}K_{l-3}\right.\\
&+(l+1)Q_{l+2}^2Q_{l+1}K_{l+1}-(l+2)Q_{l+1}(Q_{l+1}^2+Q_l^2)K_{l+1}\\
&\left.-lQ_{l-1}^2Q_lK_{l-1}-(l+4)Q_{l+3}Q_{l+2}Q_{l+1}K_{l+3}\right]+3mD_2\left[Q_{l-1}Q_lH_{l-2}\right.\\
&\left.\left.+(Q_{l+1}^2+Q_l^2)H_l+Q_{l+2}Q_{l+1}H_{l+2}\right]\right\}+m\zeta_l+2c_1\omega\varpi\left[S_l\right.\\
&\left.-(Q_{l+1}^2+Q_l^2)S_l-Q_{l-1}Q_lS_{l-2}-Q_{l+2}Q_{l+1}S_{l+2}+mQ_lK_{l-1}\right.\\
&\left.+mQ_{l+1}K_{l+1}+(l-1)Q_lH_{l-1}-(l+2)Q_{l+1}H_{l+1}\right]-c_bL_l^\phi=0
\end{aligned}\tag{7.47}$$

The quantities L_l^θ and L_l^ϕ are

$$
\begin{aligned}
L_l^\theta &= \frac{M_l}{a}\frac{d}{da}(aX) - \frac{1}{a}\frac{d}{da}(aX)\left[(Q_{l+1}^2+Q_l^2)M_l + Q_{l+1}Q_lM_{l-2}\right.\\
&\left.+Q_{l+2}Q_{l+1}M_{l+2}\right] + 3Z\left[\left\{lQ_{l+1}^2-(l+1)Q_l^2\right\}T_l + (l-2)Q_{l-1}Q_lT_{l-2}\right.\\
&\left.-(l+3)Q_{l+2}Q_{l+1}T_{l+2}\right] + m(X+\Lambda)\left[Q_lT_{l-1}+Q_{l+1}T_{l+1}\right]\\
&+(X+\Lambda)\left[\left\{lQ_{l+1}^2-(l+1)Q_l^2\right\}N_l + (l-2)Q_{l-1}Q_lN_{l-2}\right.\\
&\left.-(l+3)Q_{l+2}Q_{l+1}N_{l+2}\right] + mZ\left[Q_lN_{l-1}+Q_{l+1}N_{l+1}\right] + XM_l\\
&+\frac{\Lambda}{a}\frac{d}{da}\left\{a\left[\left\{lQ_{l+1}^2-(l+1)Q_l^2\right\}N_l + (l-2)Q_{l-1}Q_lN_{l-2}\right.\right.\\
&\left.\left.-(l+3)Q_{l+2}Q_{l+1}N_{l+2}\right]\right\} + \frac{\Lambda}{a}\frac{d}{da}\left[a\left\{Q_lT_{l-1}+Q_{l+1}T_{l+1}\right\}\right]\\
&-X\left[(Q_{l+1}^2+Q_l^2)M_l + Q_{l-1}Q_lM_{l-2} + Q_{l+2}Q_{l+1}M_{l+2}\right] + \Lambda M_l\\
&+mZ\left(Q_lN_{l-1}+Q_{l+1}N_{l+1}\right) - m^2ZT_l - mX\left(Q_lT_{l-1}+Q_{l+1}T_{l+2}\right)\\
&-\Lambda\left[\left((l+1)Q_{l+1}^2-lQ_l^2\right)M_l+(l-1)Q_{l-1}Q_lM_{l-2}-(l+2)Q_{l+2}Q_{l+1}M_{l+2}\right]\\
&-X\left[(lQ_{l+1}^2-(l+1)Q_l^2)N_l+(l-2)Q_{l-1}Q_lN_{l-2}-(l+3)Q_{l+2}Q_{l+1}N_{l+2}\right]\\
&+l(l+1)Z\left[(Q_{l+1}^2+Q_l^2)T_l + Q_{l-1}Q_lT_{l-2} + Q_{l+2}Q_{l+1}T_{l+2}\right]\\
&+(m^2-l(l+1))ZT_l
\end{aligned}
\tag{7.48}
$$

$$
\begin{aligned}
L_l^\phi &= \frac{M_l}{a}\frac{d}{da}(aZ) - \frac{1}{a}\frac{d}{da}(aZ)\left[(Q_{l+1}^2+Q_l^2)M_l + Q_{l+1}Q_lM_{l-2}\right.\\
&\left.+Q_{l+2}Q_{l+1}M_{l+2}\right] + 3Z\left[\left\{lQ_{l+1}^2-(l+1)Q_l^2\right\}N_l + (l-2)Q_{l-1}Q_lN_{l-2}\right.\\
&\left.-(l+3)Q_{l+2}Q_{l+1}N_{l+2}\right] + 3Z\left(Q_lT_{l-1}+Q_{l+1}T_{l+1}\right) + m(\Lambda+X)\left[Q_lN_{l-1}\right.\\
&\left.+Q_{l+1}N_{l+1}\right] + (\Lambda+X)\left[\left(lQ_{l+1}^2-(l+1)Q_l^2\right)N_l + (l-2)Q_{l-1}Q_lN_{l-2}\right.\\
&\left.-(l+3)Q_{l+2}Q_{l+2}N_{l+2}\right] + m\frac{\Lambda}{a}\frac{d}{da}\left[a\left(Q_lN_{l-1}+Q_{l+1}N_{l+1}\right)\right]\\
&+\frac{\Lambda}{a}\frac{d}{da}\left[a\left\{\left(lQ_{l+1}^2-(l+1)Q_l^2\right)T_l + (l-2)Q_{l-1}Q_lT_{l-2}\right.\right.\\
&\left.\left.-(l+3)Q_{l+2}Q_{l+1}T_{l+2}\right\}\right] + l(l+1)XT_l - l(l+1)X\left[(Q_{l+1}^2+Q_l^2)T_l\right.\\
&\left.+Q_{l-1}Q_lT_{l-2} + Q_{l+2}Q_{l+2}T_{l+2}\right] - m\Lambda\left(Q_lM_{l-1}+Q_{l+1}M_{l+1}\right)\\
&-Z\left[(Q_{l+1}^2+Q_l^2)M_l + Q_{l-1}Q_lM_{l-2} + Q_{l+2}Q_{l+2}M_{l+2}\right] + ZM_l
\end{aligned}
\tag{7.49}
$$

Finally we can use the induction equation (7.20) to provide the magnetic eigenfunctions K_{lm}, N_{lm} and T_{lm} in terms of the fluid eigenfunctions

S_{lm}, K_{lm} and H_{lm}. In detail

$$a^2 M_l = m[\,\Lambda K_l - Z S_l\,] + Q_l(l+1)\,[\,(l-1)\Lambda H_{l-1} + X S_{l-1}\,] + Q_{l+1}\,l\,[\,(l+2)\Lambda H_{l+1} - X S_{l+1}\,] \tag{7.50}$$

$$a^2 l(l+1) N_l = m[\,a\frac{d}{da}(\Lambda K_l) - a\frac{d}{da}(Z S_l)\,] + Q_l(l+1)\,[\,a\frac{d}{da}(X S_{l-1}) + (l-1)a\frac{d}{da}(\Lambda H_{l-1})\,] + l\,Q_{l+1}\,[\,(l+2)a\frac{d}{da}(\Lambda H_{l+1}) - a\frac{d}{da}(X S_{l+1})\,] \tag{7.51}$$

$$a^2 l(l+1) T_l = m[\,r(\Lambda H_l)' - a(X S_l)' + l(l+1)(X H_l - Z K_l)\,] + Q_l(l+1)\,[\,(l-1)a\frac{d}{da}(\Lambda K_{l-1}) + a\frac{d}{da}(Z S_{l-1}) + l(l-1)(X K_{l-1} - Z H_{l-1})\,] + l\,Q_{l+1}\,[\,(l+2)a\frac{d}{da}(\Lambda K_{l+1}) - a\frac{d}{da}(Z S_{l+1})' + (l+1)(l+2)(Z H_{l+1} - X K_{l+1})\,] \tag{7.52}$$

Together with relations (7.50), (7.51) and (7.52), equations (7.38), (7.39), (7.40), (7.41), (7.46) and (7.38) form a set of coupled ODEs for the fluid displacementsS_l, K_l, H_l together with the variables $\zeta_l, \Psi_l, \langle\Psi\rangle_l$ and allow to recover the magnetic eigenfunctions M_l, N_l and T_l. These equations reduce to those of Saio [120] in the case of no magnetic field.

7.1.1 The exterior problem

The exterior vacuum is assumed current-free,

$$\nabla \cdot \hat{b} = \nabla \times \hat{b} = 0 \tag{7.53}$$

which has the solution $\hat{b} = \nabla\Pi$ with,

$$\Pi = \sum_{l \geq m} \frac{c_l}{r^{l+1}} Y_l^m(\theta, \phi) \tag{7.54}$$

Then

$$\hat{\mathbf{b}} = \sum_{l \geq m} \left[\hat{\mathbf{r}} \left\{ -(l+1)\frac{c_l}{r^{l+2}} Y_l^m \right\} + \hat{\theta} \left\{ \frac{c_l}{r^{l+2}} \partial_\theta Y_l^m \right\} + \hat{\phi} \left\{ \frac{imc_l}{r^{l+2}\sin\theta} Y_l^m \right\} \right] \tag{7.55}$$

Continuity at the surface, i.e $\langle b \rangle = 0$ results in the following pair of surface boundary conditions for the interior field:

$$T_l(R^-) = 0 \qquad \text{and} \qquad K_l(R^-) = -(l+1)N_l(R^-) \tag{7.56}$$

7.2 Conclusions

We have presented a set of ODEs for the most general oscillation mode of a magnetized star with a background dipolar magnetic field. Once one has picked an equation of state and a background magnetic field, the equations must be integrated from the centre of the star to the surface, with suitable boundary conditions, such as regularity of the eigenfunctions at the centre of the star and continuity of the tractions at the surface of the star. Some simplifying assumptions, such as neglecting coupling to $l \pm 2$ or higher, will be necessary to make the equations more tractable.

Such an integration is, however, beyond the scope of the present investigation. We have derived the equations governing the oscillations as an application of the deformed backgrounds calculated in chapter 6 and believe that they can be of great use for future applications, such as those in [132] and [133], allowing us to explore various background field configurations for the neutron star.

Much more work is obviously needed, to make the general equations tractable for numerical integration and elastic effects in the crust should be included. We are, however, confident that, in the near future, comparison between observed QPO frequencies in the tail of magnetar flares and theoretical calculations will provide precious information on the equation of state and internal field configuration of neutron stars.

Appendix A

Curvilinear Coordinates

A.1 Curvilinear Coordinates

Let us define a set of coordinates (q_1, q_2, q_3) in a three dimensional space where we have already defined Cartesian coordinates. This consists then of supplying the relations

$$\begin{aligned} q_1 &= q_1(x, y, z) \\ q_2 &= q_2(x, y, z) \\ q_3 &= q_3(x, y, z) \end{aligned} \tag{A.1}$$

or the inverse relations

$$\begin{aligned} x &= x(q_1, q_2, q_3) \\ y &= y(q_1, q_2, q_3) \\ z &= z(q_1, q_2, q_3) \end{aligned} \tag{A.2}$$

This allows us to write the distance between to neighboring points as

$$ds^2 = dx^2 + dy^2 + dz^2 = \sum_{i,j} h_{ij}^2 dq^i dq^j \tag{A.3}$$

thus defining the metric

$$h_{ij}^2 = \frac{\partial x}{\partial q_i}\frac{\partial x}{\partial q_j} + \frac{\partial y}{\partial q_i}\frac{\partial y}{\partial q_j} + \frac{\partial z}{\partial q_i}\frac{\partial z}{\partial q_j} \tag{A.4}$$

If we now limit ourselves to orthogonal coordinate systems we have

$$h_{ij} = 0, \text{ if } i \neq j \tag{A.5}$$

and by defining the **Scale Factors**

$$h_{ii} = h_i = \sqrt{\sum_{k=1}^{n} \frac{\partial x_k}{\partial q_i}} \tag{A.6}$$

we can write

$$\begin{aligned} ds^2 &= (h_1 dq_1)^2 + (h_2 dq_2)^2 + (h_3 dq_3)^2 \\ ds_i &= h_i dq_i \end{aligned} \tag{A.7}$$
$$\tag{A.8}$$

With each family of surface q_i =constant, we can now associate a unit vector a_i, perpendicular to the q_i =constant surface and in the direction of increasing q_i.

A.1.1 Differential Vector Operations

We can now move on to defining some differential vector operators. Let us start with the gradient of a scalar function. This is a vector having the magnitude and direction of the maximum space rate of change of the function. From this interpretation the component of $\nabla\Psi(q_1, q_2, q_3)$ in the direction normal to the family of surfaces q_1 =constant is

$$\nabla\Psi^1 = \frac{\partial\Psi}{\partial s_1} = \frac{\partial\Psi}{h_1 \partial q_1} \tag{A.9}$$

This is the component in the direction of increasing q_1, i.e. along the unit vector a_1. By repeating the same procedure for q_2 and q_3 we can write

$$\begin{aligned} \nabla\Psi(q_1, q_2, q_3) &= a_1 \frac{\partial\Psi}{\partial s_1} + a_2 \frac{\partial\Psi}{\partial s_2} + a_3 \frac{\partial\Psi}{\partial s_3} \\ &= a_1 \frac{\partial\Psi}{h_1 \partial q_1} + a_2 \frac{\partial\Psi}{h_2 \partial q_2} + a_3 \frac{\partial\Psi}{h_3 \partial q_3} \end{aligned} \tag{A.10}$$

Without presenting the derivation, which can be found in [11], we shall present the formulae for divergence,laplacian and curl

$$\nabla \cdot V(q_1, q_2, q_3) = \frac{1}{h_1 h_2 h_3} \left[\frac{\partial}{\partial q_1}(V_1 h_2 h_3) + \frac{\partial}{\partial q_2}(V_2 h_3 h_1) + \frac{\partial}{\partial q_3}(V_3 h_1 h_2) \right] \tag{A.11}$$

$$\nabla^2\Psi(q_1,q_2,q_3) = \frac{1}{h_1h_2h_3}\left[\frac{\partial}{\partial q_1}\left(\frac{h_2h_3}{h_1}\frac{\partial\Psi}{\partial q_1}\right)+ +\frac{\partial}{\partial q_2}\left(\frac{h_3h_1}{h_2}\frac{\partial\Psi}{\partial q_2}\right)+\frac{\partial}{\partial q_3}\left(\frac{h_1h_2}{h_3}\frac{\partial\Psi}{\partial q_3}\right)\right] \quad \text{(A.12)}$$

$$\nabla\times V = \frac{1}{h_1h_2h_3}\begin{vmatrix} a_1h_1 & a_2h_2 & a_3h_3 \\ \frac{\partial}{\partial q_1} & \frac{\partial}{\partial q_2} & \frac{\partial}{\partial q_3} \\ h_1V_1 & h_2V_2 & h_3V_3 \end{vmatrix} \quad \text{(A.13)}$$

A.2 Spherical Polar Coordinates

Let us now examine in some detail the case of spherical polar coordinates. We shall relabel (q_1,q_2,q_3) as (r,θ,ϕ), where:

$$\begin{aligned} r &= (x^2+y^2+z^2) \\ \theta &= \arccos\frac{z}{(x^2+y^2+z^2)^{1/2}} \\ \phi &= \arctan\frac{y}{x} \end{aligned} \quad \text{(A.14)}$$

or

$$\begin{aligned} x &= r\sin\theta\cos\phi \\ y &= r\sin\theta\sin\phi \\ z &= r\cos\theta \end{aligned} \quad \text{(A.15)}$$

for $0\le r<\infty$, $0\le\theta\le\pi$ and $0\le\phi\le 2\pi$. The scale factors are

$$\begin{aligned} h_1 &= h_r = 1 \\ h_2 &= h_\theta = r \\ h_3 &= h_\phi = r\sin\theta \end{aligned} \quad \text{(A.16)}$$

(A.17)

and the unit vectors are

$$\begin{aligned} \mathbf{r} &= \mathbf{i}\sin\theta\cos\phi+\mathbf{j}\sin\theta\sin\phi+\mathbf{k}\cos\theta \\ \theta &= \mathbf{i}\cos\theta\cos\phi+\mathbf{j}\cos\theta\sin\phi-\mathbf{k}\sin\theta \\ \phi &= -\mathbf{i}\sin\phi+\mathbf{j}\cos\phi \end{aligned} \quad \text{(A.18)}$$

and therefore vary in direction as the angles θ and ϕ vary. This gives us:

$$\nabla\Psi = \mathbf{r}\frac{\partial\Psi}{\partial r} + \theta\frac{1}{r}\frac{\partial\Psi}{\partial\theta} + \phi\frac{1}{r\sin\theta}\frac{\partial\Psi}{\partial\phi} \tag{A.19}$$

$$\nabla\cdot\mathbf{V} = \frac{1}{r^2\sin\theta}\left[\sin\theta\frac{\partial}{\partial r}\left(r^2V_r\right) + r\frac{\partial}{\partial\theta}\left(\sin\theta V_\theta\right) + r\frac{\partial V_\phi}{\partial\phi}\right] \tag{A.20}$$

$$\nabla\cdot\nabla\Psi = \frac{1}{r^2\sin\theta}\left[\sin\theta\frac{\partial}{\partial r}\left(r^2\frac{\partial\Psi}{\partial r}\right) + \frac{\partial}{\partial\theta}\left(\sin\theta\frac{\partial\Psi}{\partial\theta}\right) + \frac{1}{\sin\theta}\frac{\partial^2\Psi}{\partial\phi^2}\right] \tag{A.21}$$

$$\nabla\times V = \frac{1}{r^2\sin\theta}\begin{vmatrix} \mathbf{r} & r\theta & r\sin\theta\phi \\ \frac{\partial}{\partial r} & \frac{\partial}{\partial\theta} & \frac{\partial}{\partial\phi} \\ V_r & rV_\theta & r\sin\theta V_\phi \end{vmatrix} \tag{A.22}$$

A.2.1 Covariant derivatives

It is important to point out that the basis we are working in is orthonormal, but to obtain this we have to pay the price of it not being a "coordinate basis", i.e. the commutators of the basis vectors do not vanish. For example

$$\begin{aligned}[\hat{e}_r,\hat{e}_\theta]f &= \left(e_r\frac{1}{r}e_\theta - \frac{1}{r}e_\theta e_r\right)f \\ &= \left(\frac{\partial}{\partial r}\frac{1}{r}\frac{\partial}{\partial\theta}f - \frac{1}{r}\frac{\partial}{\partial\theta}\frac{\partial}{\partial r}f\right) = -\frac{1}{r^2}\frac{\partial f}{\partial\theta} \neq 0\end{aligned} \tag{A.23}$$

This means that the metric in this base will be flat, but the connection coefficients will NOT vanish. From the definition of the unit vectors

(A.19) we can calculate:

$$\begin{aligned}
\nabla_r \hat{r} &= 0 \\
\nabla_r \hat{\theta} &= 0 \\
\nabla_r \hat{\phi} &= 0 \\
\nabla_\theta \hat{r} &= \frac{1}{r}\hat{\theta} \\
\nabla_\theta \hat{\theta} &= -\frac{1}{r}\hat{r} \\
\nabla_\theta \hat{\phi} &= 0 \\
\nabla_r \hat{r} &= \frac{1}{r}\hat{\phi} \\
\nabla_\theta \hat{\theta} &= \frac{\cot\theta}{r}\hat{\theta} \\
\nabla_\phi \hat{\phi} &= -\frac{\cot\theta}{r}\hat{\phi} - \frac{1}{r}\hat{r}
\end{aligned} \tag{A.24}$$

If we now wish to calculate the connection coefficients we can use the definition, for a coordinate basis

$$\Gamma^a_{bc} = \frac{1}{2} g^{ad} \left(g_{bd,c} + g_{cd,b} - g_{bc,d} \right) \tag{A.25}$$

We can thus compute these coefficients on the coordinate basis

$$\{e_i\} = \left\{ e_r = \frac{\partial}{\partial r}, e_\theta = \frac{\partial}{\partial \theta}, e_\phi = \frac{\partial}{\partial \phi} \right\}, \tag{A.26}$$

and then pass to the orthonormal basis

$$\{\hat{e}_i\} \left\{ \hat{e}_r = \frac{\partial}{\partial r}, \hat{e}_\theta = \frac{1}{r}\frac{\partial}{\partial \theta}, \hat{e}_\phi = \frac{1}{r\sin\theta}\frac{\partial}{\partial \phi} \right\}. \tag{A.27}$$

for which the covector basis is

$$\left\{ \hat{\omega}^i \right\} = \{ dr, r d\theta, r \sin\theta d\phi \} \tag{A.28}$$

The connection coefficients in this basis are now given, using the notation of [94], by

$$\hat{\Gamma}^i_{jk} = < \hat{\omega}^i, \hat{\nabla}_k \hat{e}_j > \tag{A.29}$$

where quantities denoted as $\hat{q}$ are calculated in the new basis, and

$$< \omega^i, \nabla_k e_j > = \Gamma^i_{jk}. \tag{A.30}$$

The only non vanishing components are

$$\hat{\Gamma}^{\theta}_{r\theta} = \Gamma^{\phi}_{r\phi} = -\Gamma^{r}_{\theta\theta} = -\Gamma^{r}_{\phi\phi} = 1/r \tag{A.31}$$

$$\Gamma^{\phi}_{\theta\phi} = -\Gamma^{\theta}_{\phi\phi} = \cot\theta/r. \tag{A.32}$$

With the above expressions we can compute

$$A_{j;k} = \frac{1}{g_{kk}}\frac{\partial A_j}{\partial x_k} - \Gamma^{i}_{jk}A_i \tag{A.33}$$

Thus for example proving that, if the basis is orthonormal,

$$\nabla_i \hat{r}_j = g_{ij} - \hat{r}_i\hat{r}_j \tag{A.34}$$

an expression that is useful when deriving the perturbation equations for the crust.

A.3 Deformed background

Let us calculate the metric and the connection coefficients in a basis adapted to a deformed background, such as that of chapters 6 and 7. The metric is now

$$g_{ab} = \begin{Bmatrix} 1+2\epsilon+2a\frac{\partial\epsilon}{\partial a} & a\frac{\partial\epsilon}{\partial a} & 0 \\ a\frac{\partial\epsilon}{\partial a} & a^2(1+2\epsilon) & 0 \\ 0 & 0 & a^2(1+2\epsilon)\sin^2\theta \end{Bmatrix} + O(\epsilon^2) \tag{A.35}$$

And our normalised vector basis is

$$\{\hat{e}_i\}\left\{\hat{e}_a = \frac{\partial}{\partial a}, \hat{e}_\theta = \frac{1}{a}\frac{\partial}{\partial\theta}, \hat{e}_\phi = \frac{1}{a\sin\theta}\frac{\partial}{\partial\phi}\right\}. \tag{A.36}$$

for which the covector basis is

$$\{\hat{\omega}^i\} = \{da, ad\theta, a\sin\theta d\phi\} \tag{A.37}$$

First of all we can calculate the connection coefficients on the coordinate basis

$$\left\{e_a = \frac{\partial}{\partial a}, e_\theta = \frac{\partial}{\partial\theta}, e_\phi = \partial\partial\phi\right\}, \tag{A.38}$$

using equation (A.25). The result is

$$\Gamma^1_{11} = 2\frac{\partial\epsilon}{\partial a} + a\frac{\partial^2\epsilon}{\partial a^2} + O(\epsilon^2) \tag{A.39}$$

$$\Gamma^1_{12} = a\frac{\partial^2\epsilon}{\partial a\partial\theta} + O(\epsilon^2) \tag{A.40}$$

$$\Gamma^1_{22} = -a + a^2\frac{\partial\epsilon}{\partial a} + a\frac{\partial^2\epsilon}{\partial\theta^2} + O(\epsilon^2) \tag{A.41}$$

$$\Gamma^1_{33} = a\sin\theta\left[\cos\theta\frac{\partial\epsilon}{\partial\theta} - \sin\theta\left(1 - a\frac{\partial\epsilon}{\partial a}\right)\right] + O(\epsilon^2) \tag{A.42}$$

$$\Gamma^2_{12} = \frac{1}{a}\left(1 + a\frac{\partial\epsilon}{\partial a}\right) + O(\epsilon^2) \tag{A.43}$$

$$\Gamma^2_{22} = 2\frac{\partial\epsilon}{\partial\theta} + O(\epsilon^2) \tag{A.44}$$

$$\Gamma^2_{33} = -\sin\theta\cos\theta + O(\epsilon^2) \tag{A.45}$$

$$\Gamma^3_{13} = \frac{1}{a}\left(1 + a\frac{\partial\epsilon}{\partial a}\right) + O(\epsilon^2) \tag{A.46}$$

$$\Gamma^3_{23} = \frac{1}{\sin\theta}\left(\cos\theta + \frac{\partial\epsilon}{\partial\theta}\right) + O(\epsilon^2) \tag{A.47}$$

We can now calculate the coefficients for the new basis, which we shall denote $\hat{\Gamma}^i_{jk}$, using equation (A.29), thus obtaining

$$\hat{\Gamma}^1_{11} = 2\frac{\partial\epsilon}{\partial a} + a\frac{\partial^2\epsilon}{\partial a^2} + O(\epsilon^2) \tag{A.48}$$

$$\hat{\Gamma}^1_{12} = \frac{\partial^2\epsilon}{\partial a\partial\theta} + O(\epsilon^2) \tag{A.49}$$

$$\hat{\Gamma}^1_{22} = -\frac{1}{a} + \frac{\partial\epsilon}{\partial a} + \frac{1}{a}\frac{partial^2\epsilon}{\partial\theta^2} + O(\epsilon^2) \tag{A.50}$$

$$\hat{\Gamma}^1_{33} = \frac{1}{a}\left[\cos\theta\frac{\partial\epsilon}{\partial\theta} - \sin\theta\left(1 - a\frac{\partial\epsilon}{\partial a}\right)\right] + O(\epsilon^2) \tag{A.51}$$

$$\hat{\Gamma}^2_{12} = \frac{1}{a}\left(1 + a\frac{\partial\epsilon}{\partial a}\right) + O(\epsilon^2) \tag{A.52}$$

$$\hat{\Gamma}^2_{22} = \frac{2}{a}\frac{\partial\epsilon}{\partial\theta} + O(\epsilon^2) \tag{A.53}$$

$$\hat{\Gamma}^2_{33} = -\frac{\cot\theta}{a} + O(\epsilon^2) \tag{A.54}$$

$$\hat{\Gamma}^3_{13} = \frac{1}{a}\left(1 + a\frac{\partial\epsilon}{\partial a}\right) + O(\epsilon^2) \tag{A.55}$$

$$\hat{\Gamma}^3_{23} = \frac{\cot\theta}{a}\left(1 + \cos\theta\frac{\partial\epsilon}{\partial\theta}\right) + O(\epsilon^2) \tag{A.56}$$

Bibliography

[1] Abbot B. et al. (LIGO Scientific Collaboration), 2005, P.R.L., 94, 181103

[2] Alecian E., Morsink S.M., 2004, Ap.J., 614, 914

[3] Alpar M.A., Langer S.A., Sauls J.A., 1984, Ap.J., 282, 533

[4] Alpar M.A., Sauls J.A., 1988, Ap.J., 327, 723

[5] Anderson V.J., Terentjev E.M., Eur.Phys.J. E 4,21-28 (2001)

[6] Andersson N., 1998, Ap.J., 502, 708

[7] Andersson N., Jones D.I., Kokkotas K.D., Stergioulas N., 2000, Ap.J., 534, 75

[8] Andersson, N., C.Q.G., 2003, 20, R105

[9] Andersson N., Glampedakis K., Haskell B., Watts A.L., 2005, MNRAS, 361, 1153

[10] Andersson N., Sidery T., Comer G.L. 2006, MNRAS, 368, 162

[11] Arfken G., Mathematical Methods for Physicists, Second edition 1970, Accademic Press

[12] Astone P. et al., 2002, C.Q.G., 19, 1911

[13] Baade W., Zwicky F., 1934, PNAS, 20(5), 259

[14] Baym G., Pethick C., Sutherland P., 1971, Ap.J. 170, 299

[15] Berti E., Gravitational Waves from Perturbed Stars, PhD Thesis, Universitá di Roma "La Sapienza"

[16] Bildsten L.,Cutler C., 1992, Ap.J.,400,175-180

[17] Bildsten, L. et al.,1997,Ap.J. Suppl.,113,367

[18] L. Bildsten,Ap.J. Lett.,1998,501,89-93

[19] Boirin L. et al., 2000, A&A, 361, 121

[20] Bonazzola S., Gourgoulhon E., 1996, A&A, 312, 675

[21] Campbell, C.G. and Heptinstall, P.M.,1998, MNRAS,301,558

[22] Chakrabary D. et al., 2003, Nature, 424, 42

[23] Chandrasekhar S., Fermi E., 1953, Ap.J., 118, 116

[24] Chandrasekhar A., Lebovitz N.R., 1962, Ap.J. 136, 1082

[25] Cumming A., Zweibel E., Bildsten L., 2001, Ap.J., 557, 958

[26] Cutler C., 2002, Phys.Rev.D, 66, 084025

[27] Cutler C., Ushomirsky G., Link B., 2003,Ap.J. 588, 975-991

[28] Douchin F., Haensel P., 2001, A&A, 380, 151-167

[29] Duncan R.C., Thompson C., 1992, Ap.J., 292, L9

[30] Duncan R.C., 1998, Ap.J., 498, L45

[31] Elsner R.F. and Lamb F.K., 1977, Ap.J.,215,897

[32] Ferraro V.C.A, 1954, Ap.J. 119, 407

[33] Ford, E. C. et al.,Ap. J.,537,368-373

[34] Ford E.C. et al., 1998, Ap.J. Letters, 508, L155

[35] Frank J., King A., Raine D, 1985, Accretion Power in Astrophysics, Cambridge University Press

[36] Galloway D.K. et al., 2005, Ap.J. Letters, 622, L45

[37] Galloway D.K., Cumming A., Chakrabarty D., 2004, American Astronomical society HEAD meeting, 8 25.01, Bull. Am.Ast.Soc. 36, 954

[38] Galloway D.K. et al., 2001, Ap.J. Letters, 549, L85

[39] Galloway D.K., private communication

[40] Ghosh P., Lamb F., 1991, in J.Ventura D.Pines eds, , Neutron stars: theory and observation. Kluwer Academic Publishers, pp 363–444

[41] Ghosh P., Lamb F., 1992, in van den Heuvel E., Rappaport S., eds, X-ray binaries and recycled pulsars. Kluwer Academic Publishers, pp 487–510

[42] Giles A.B., et al., 2002, Ap.J., 568, 279

[43] Glampedakis, K., Kennefick, D., 2002, Phys.Rev.D, 66,044002

[44] Glampedakis, K., Samuelsson L., Andersson N, 2006, MNRAS, 371, L74

[45] Goosens M., 1972, Ap&SS, 16, 286

[46] Haensel P., Zdunik J.L, 1990, A&A 229, 117-122

[47] Haensel P., 1995,"Astrophysical Sources of Gravitational Radiation", Les Houches 1995, eds. J.A.Marck and J.P.Lasota

[48] Haensel P., 2001, "Neutron Star Crusts", D.Blaschke, N.K.Glendenning and A.Sedrakian (Eds.): LNP 578, 127-174, Springer-Verlag

[49] Hartman J.M. et al., 2003, American Astronomical society HEAD meeting, 7 17.38, Bull. Am.Ast.Soc. 35, 865

[50] Haskell B., Jones D.I., Andersson N., 2006, MNRAS, 373 (4), 1423

[51] Heyl J.S., 2000, MNRAS, 317, 310

[52] Homan J. et al., 2002, Ap.J., 568, 878

[53] Homan J. et al., 1999, Ap.J., 513, 419

[54] Hughs, S., 2000, Phys.Rev.D, 61,084004

[55] Hulse R.A., Taylor J.H., 1975, Ap.J. 195 L51

[56] Israel G. et al., 2005, Ap.J., 628, L53

[57] Jaranowski P.,Krolak A., 1992, Ap.J.,194:586-591

[58] Jones D.I., 2004, Phys.Rev.D 70, 042002

[59] Jones P.B., 2004, MNRAS, 251, 3, 956

[60] Jonker P.G. et al., 2002, MNRAS, 336, L1

[61] Jonker P.G. et al. 2002, MNRAS, 333, 665

[62] Jonker P.G. et al., 2000, Ap.J., 537, 374

[63] Kaaret P. et al., 2003, Ap.J., 598, 481

[64] Kaaret P. et al., 2002, Ap.J., 575, 1018

[65] Karlovini M., Samuelsson L., 2003, C.Q.G. 20, 3613-3648

[66] Krauss M., Chakrabarty D., 2004, American Astronomical Society HEAD meeting, 8

[67] Lamb F.K., Pines D., 1978, Ap.J., 224, 969

[68] Lamb F.K., Pines D., 1978, Ap.J., 225, 582

[69] Lyne A.G. et al., 2004, Science, 303, 1153

[70] Landau L.D. and Lifshitz E.M, 1986,"Theory of Elsticity, 3rd Edition", Pergamon Press

[71] Lattimer J.M., Prakash M., Phys.Rep.333-334,121-146 (2000)

[72] Lightman, A. P. and Eardley, D. M., 1974,,Ap. J. Letters, 187, L1

[73] Lavagetto G., Burderi L., D'Antona F., Di Salvo T., Iaria R., Robbia N.R., 2005, MNRAS, 359, 734L

[74] Lindblom L., 1992, Ap.J. 398, 569-573

[75] Liu, Q. Z. and van Paradijs, J. and van den Heuvel, E. P. J. , 2001, A&A, 368, 1021

[76] Manchester, R. N., Hobbs, G. B., Teoh, A. & Hobbs, M., 2005, AJ, 129, 1993-2006

[77] Markwardt C.B., Swank J.H, Strohmayer T., 2004, The Astronomer's Telegram, 353

[78] Markwardt C.B., Swank J.H., 2003, IAU circ., 8144, ed. Green D.W.E.

[79] Markwardt C.B., Smith E., Swank J.H., 2003, IAU circ., 8080, ed. Green D.W.E.

[80] Markwardt C.B. et al., 2002, Ap.J. Letters, 575,1, L21

[81] Markwardt C.B., Strohmayer T., Swank J.H., 1999, Ap.J. Letters, 505, L23

[82] Markwardt C.B., private communication

[83] Marsh T.R, Nelemans G., Steeghs D., 2004, MNRAS, 350, 113

[84] McDermott P.N., Van Horn H.M., Hansen C.J., 1988, Ap.J., 325, 725

[85] Melatos A., Payne D.J.B., 2005, Ap.J., 623, 1044

[86] Mendez M., van der Klis M., 2000, MNRAS, 318, 938

[87] Mendez M. et al., 1998, Ap.J. Letters, 622, L45

[88] Mestel, L., 2004, "Stellar magnetism", Oxford University Press

[89] Migliari S., van der Klis M., Fender A.P., 2003, MNRAS, 245, L35

[90] Miller, M. C., 2003, "Interpreting QPOs from Accreting Neutron Stars", in proceedings of X-Ray Timing 2003: Rossi and Beyond, preprint astro-ph/0312449

[91] Miller, G. S., 1990, Ap.J., 356, 572

[92] Miller M., Lamb F., Psaltis D., 1998, Ap.J., 508, 791

[93] Miniutti G., Neutron Star Oscillations in General Relativity and Emission of Gravitational Waves, PhD Thesis, Universitá di Roma "La Sapienza"

[94] Misner C.W., Thorne K.S., Wheeler J.A., 1973, *Gravitation*, Freeman & Co., San Francisco

[95] Mitra, A., 1992, A.&A., 257, 807

[96] Monaghan J.J., 1966, MNRAS, 134, 275

[97] Muno M.P., 2004,X-ray timing 2003: Rossi and beyond: AIP Conference Proceedings, 714, 239, Eds. Kaaret P., Lamb F.K., Swank J.H. Melville NY, American Institute of Physics

[98] Narayan R., Yi I., , 1994, Ap.J. Letters ,428, 13

[99] Narayan R., Yi I., , 1995, Ap.J. , 444, 231

[100] Narayan R., Yi I., , 1995, Ap.J. , 452, 710

[101] Natalucci L. et al., 1999, Ap.J. Letters, 523, L45

[102] Nelson R.W. et al, , 1997, Ap.J. Letters, 488, 117

[103] Nelson, R. W. et al. 1997, Ap.J. Lett., 488, L117

[104] Ogata S., Ichimaru S., 1990, Phys.Rev.A 42, 4867

[105] Paczynski B., 1967, Acta Astronomica 17,3

[106] Pandharipande V.R., Pines D., Smith R.A., 1976, Ap.J. 208, 550-566

[107] Park, M. and Miller, G. S., 1991, Ap. J., 371, 708

[108] Papaloizou, J. and Pringle, J. E., 1978, MNRAS, 184, 501

[109] Payne D.J.B., Melatos A., 2004, MNRAS, 351, 569

[110] Perna R., Bozzo E., Stella L., 2006, Ap.J. 639, 363

[111] Phinney E.S., Pulsars as probes of globular cluster dynamics, Structure and dynamics of globular clusters, 1993, 141, S.G. Djorkovski and G. Meylan, 50,ASP

[112] Poisson, E., Phys.Rev.D, 47,4 (1993)

[113] Press W.H., Teukolsky S.A., Vetterling W.T., Flannery B.P., 1992, "Numerical Recipies, Fortran 77, second edition", Cambridge University Press

[114] Psaltis D., Chakrabarty C., 1999, Ap.J., 521, 332

[115] Ravenhall D.G., Bennett C.D., Pethick C.J., 1972, P.R.L., 28,978

[116] Remillard R.A., Swank J., Strohmeyer T., 2002, IAU circ., 7893, ed. Green D.W.E.

[117] Roxburgh I.W., 1966, MNRAS, 132, 347

[118] Ruderman M., 1992,in Pines D., Tamagaki R., Tsuruta S. (Eds.), Proc.Conf. SENS'90, Structure and Evolution of Neutron Stars, Addison-Wesley, Redwood City CA, p.353

[119] Saio H., 1981, Ap.J., 244, 299

[120] Saio H., 1982, Ap.J., 256, 717

[121] Sato K., 1979, Prog.Theor.Phys. 62, 957

[122] Schutz, B.F., Am.J.Phys, 52, 5 (1984)

[123] Shapiro S.L., Teukolsky, S.A., 1993, Phys.Rev.D, 47,4

[124] Sedrakian A.D., Sedrakian D.M., 1995, Ap.J., 447, 305

[125] Shapiro,S. and Teukolsky,S., 1983, "Black Holes, White Dwarfs and Nutron Stars", John Wiley and Sons

[126] Shakura, N. I. and Sunyaev, R. A., 1973, A.&A., 24, 337

[127] Shapiro, S. L. and Lightman, A. P. and Eardley, D. M., 1976, Ap.J., 204, 187

[128] Smale A.P. et al., 1988, MNRAS, 232, 647

[129] Smeyers P., Denis J., 1971, A&A, 14, 311S

[130] Smith D.A., Morgan E.H., Bradt H., 1997, Ap.J., 486, 355

[131] Sood N.K., Trehan S.K., 1970, Ap&SS 8, 422

[132] Sotani H., Kokkotas K.D., Stergioulas N., 2006, astro-ph/0608626v1

[133] Sotani H., Kokkotas K.D., Stergioulas N., Vavoulidis M., 2006, astro-ph/0611666v1

[134] Stroeer A., Vecchio A., Nelemans G., 2005, Ap.J., 633, L33

[135] Strohmayer T.E., Ogata S., Iyetomi H., Ichimaru S., Van Horn H.M.,1991, Ap.J. 375, 679

[136] Strohmayer T.E. et al., 2003, Ap.J. Letters, 596, L67

[137] Strohmayer T.E., Watts A.L., 2005, Ap.J., 632, L111

[138] Strohmayer T.E. et al., 1996, Ap.J. letters, 496, L9

[139] Swank J., 2003 Quasi-periodic oscillations ffrom low-mass X-ray binaries with neutron stars, RXTE meeting,

[140] Takatsuka T., Tamagaki R., 1988, Prog.Theor.Phys 79(2)

[141] Tassoul J.L., 1978, "Theory of Rotating Stars", Princeton University Press

[142] Titarchuk L., Cui W., Wood K., 2002, Ap.J.Lett., 576, L49

[143] Tomsick J.A. et al., 1999, Ap.J., 521, 341

[144] Ushomirsky, G. and Cutler, C. and Bildsten, L., 2000, MNRAS, 319, 902

[145] van Strateen S., van der Klis M., Mendez M., 2003, Ap.J., 596, 1155

[146] Wagoner, R. V., 1984, Ap.J., 278, 345-348

[147] Wang Y.M., 1987, A.&A., 183, 257-264

[148] Wang Y.M., 1991, A.&A., 102, 36-44

[149] Y.-M. Wang, 1995 , Ap.J. Lett., 449, 153-156

[150] Watts A.L., Strohmayer T.E., 2006, Ap.J., 637, L117

[151] Weinberg S., 1972, *Gravitation and Cosmology:Principles and Applications of the General Theory of Relativity*, John Wiley & Sons

[152] White N.E., Stella L., 1988, MNRAS, 231, 325

[153] White N.E and Zhang W., , 1997, Ap.J. Lett., 490, 87-90

[154] White, N. E. and Stella, L., 1988, "The radius of a magnetosphere in the radiation pressure dominated region of an accretion disk", MNRAS, 231,

[155] Wijnands R., 2003 An observational review of accretion driven X-ray pulsars, astro-ph/0309347 325

[156] Wijnands R. et al., 2003, Nature, 424, 44

[157] Wijnands R., Strohmayer T., Franco L.M., Ap.J. Letters, 549, L71

[158] Wijnands R., van der Klis M., 1998, Nature, 394, 344

[159] Wijnands R. et al., 1998, Ap.J. Letters, 493, L87

[160] Wijnands R., van der Klis M., 1997, Ap.J. Letters, 482, L65

[161] Yi I. and Grindlay J., 1998 Ap.J., 505,828

[162] Yi I. and Wheeler J.C. and Vishniac E.T., 1997 Ap.J. Lett., 481,51

[163] Yi I. and Wheeler J.C., 1998, Ap.J.,498, 802

[164] Zhang W. et al., 1998, Ap.J. Letters, 495, L9

[165] Zhang W. et al., 1998, Ap.J. Letters, 500, L171

[166] Zhang W., Strohmayer T., Swank J., Ap.J. Letters, 500, L167